University of Parma
University of Bologna
University of Brescia
University of Ferrara

Ph.D. Degree in Geotechnical Engineering (XVII)
January 2005

IMPLEMENTATION AND USE OF CONSTITUTIVE MODELS IN GEOMECHANICS: ANALYSIS OF SHALLOW FOOTINGS ON SAND

Martino Leoni

Thesis director: *Prof. Lorella Montrasio*
Head of the Ph.D. Programme in Geotechnical Engineering: *Prof. Gian Paolo Giani*

Table of Contents

1 Introduction

This thesis work deals with the resolution of boundary value problems via Finite Element (FE) analyses. Since powerful computers have come to be accessible to the common users, the use of FE methods to solve engineering problems has been stimulated. Many FE codes have been developed, both for professional and for research purposes.

The standard FE method has been widely developed starting from the pioneering work carried out in the last century by many researcher in both mathematics and engineering fields.

A geometrical representation of the boundary value problem, object of the study allowing the decomposition of the geometry for a complex domain in simpler sub-domains, has to be provided by the user; the sub-domains are the *elements*, which are defined as *finite* since they are bounded by polygons so that each one occupies a finite area, and the entire set of elements forms a *mesh* of finite elements.

Each element is characterized by a finite number of integration points (Gauss points) in which the governing equations are formulated. The overall solution, in terms of nodal displacements, is achieved in a variational form by enforcing the solution of an energy function typically formulated in an integral form, the so called "weak form" of the Virtual Work Theorem.

Because of the discrete nature of the formulation, the integration operation becomes a finite sum over the Gauss points of the whole domain. Once the general solution is achieved, enforcing the fulfilment of the boundary conditions, the state of stress is determined for each Gauss point from the stress-strain relations, and the local solution is extended to the vertices of the elements (nodes) and then to the whole domain.

The resolution of a boundary value problem via FE analyses requires the assumption of a constitutive model in order to simulate the stress-strain behaviour at Gauss point level for each material involved in the analysis.

For some of the materials commonly used in civil and industrial engineering, relatively simple constitutive laws are able to describe and to model the real mechanical behavior: for example, as for steel structures, a linear elastic relation is able to well capture the material behaviour for loading levels far from the yielding load.

If we complete the former relation with a yield criterium aiming to predict the overall behaviour when the yielding load is approached, we obtain a more complex law but now able to predict the mechanical behaviour for a wider loading range.

For more complex materials, such as concrete or granular materials, the need of constitutive laws more realistic than a simple Young elastic relation is nowadays commonly acknowledged..

Moreover, the availability of higher-performance CPUs has encouraged an intense development of complex constitutive laws starting first within the framework of the elastoplasticity, and then following even different mathematical structures.

As for the geomaterials, the work of the Cambridge group, and mainly by Schofield and Wroth, has brought to the development of the Cam-Clay model (Schofield and Wroth, 1967), that is a milestone in the world of elastoplasticity.

Most of the constitutive models nowadays available for the resolution of BVP involving geomaterials, such as the extensions or modifications proposed by many researchers (see e.g.(Nova, 1977),(Nova, 1988),(Borja and Tamagnini, 1998),(Lade, 1977)) stem from Cam-Clay pioneer model.

Besides, many other constitutive models have been developed outside the framework of elastoplasticity: in the recent past a new family of constitutive laws has been proposed coming from the studies of two separate research groups, the former in Karslruhe, which brought to the K-hypoplasticity, the latter in Grenoble, with the CLoE hypoplastic model.

The predictive capabilities of the hypoplastic models for the resolution of BVPs have been investigated in many papers (e.g.(Viggiani and Tamagnini, 2000),(Leoni and Montrasio, 2003),(Leoni et al., 2003)) for different classes of geotechnical engineering problems involving rather different stress paths.

Whatever constitutive model is chosen for the soil, the best confirmation of its predictive capacity comes from the comparison with measurements on real structures, since the more complex a constitutive law is, the larger is the set of parameters involved in its definition.

A higher number of parameters to be calibrated brings to an higher level of uncertainty on the final results: one can therefore understand the importance of a reliable set of experimental measurements allowing to perform a comparison between FE predictions and real data, in order to assess the reliability of the FE model for a particlar class of BVP.

Nevertheless, it must be pointed out how hard is to have a good set of experimental measurements available due to the intrinsic difficulties for which special equipments are required, and to their consequent high cost.

In this thesis work, two different constitutive models have been implemented: an elastoplastic model (SSC) which is a simplified version of the original “Sinfonietta Classica” (Nova, 1988), and the hypoplastic CLoE model (Chambon et al., 1994).

We have chosen to make some simplifications in the original SC mainly because of its formulation: the original SC has a complicated definition for the constitutive functions, so that their mathematical formulation has been restricted to the first and second invariant of stress tensor, thus neglecting the dependence on the Lode’s angle.

Moreover, while the hardening law, which relates the evolution of the hardening parameter to the plastic deformations, has been implemented in differential form, in the original SC an integrated formula is given.

The commercial FE code chosen for the implementation is Abaqus, by Hibbitt, Karlssonn and Sorensen, due to its wide diffusion in both research and applied engineering domains and the possibility given to the user to implement its own constitutive relations.

A large set of experimental measurements was available coming from the work by Montrasio and Nova (Montrasio and Nova, 1997), thus the laboratory tests have been simulated via FE analyses in order to compare the numerical results with the experimental ones and to evaluate the predictive capabilities of the two models.

In the next paragraphs of Chapter 1, an overview on the resolution techniques for the problem of shallow foundations followed by some details about the FE method will be given, together with a description of the experimental set-up and the laboratory tests.

In Chapter 2 a wide description of the two models will be given, while in Chapter 3 full details of the implementation process are depicted, along with the description of the validation tests performed in order to assess the reliability of the two implementations.

In Chapter 4 the BVP of a rigid shallow foundation on sand is studied, and the results are compared to those obtained in the laboratory tests, aiming to assess the capability of the models to capture the real behaviour of the footing during loading tests.

In addition to the complex constitutive models, an extended version of a more simple well-known Mohr-Coulomb model, already implemented in the FE code, is used.

Its description is given in the next introductory pages; moreover, after a discussion about the obtained results, some conclusions are drawn in Chapter 5.

1.1 Modelling of shallow foundations

The study of the behaviour of the soil on which a shallow foundation is built is both a classical academic and an applied engineering problem that has been studied from many different points of view.

Many conferences have been and continue to be organized about this topic, and many researchers and practising engineers give their contribution with case histories and studies of academical problems.

Mainly the problems on which it has been investigated in the past are the determination of the bearing capacity and the prediction of the settlements experienced by the foundation during the construction stages and the whole life of the structure.

To this end, many methods have been developed in the field of analytical methods and physical modelling, and the recent development of high performance calculators has stimulated the use of numerical methods.

Within the framework of physical modelling, many Authors have performed experimental tests on scaled problems, by reproducing the real problem reducing the dimensions of the foundation by a scale factor.

Many theoretical methods have been developed in order to extend the results obtained on the scaled models to the real cases, and in this framework must be regarded the macro-element approach proposed by Montrasio and Nova (Montrasio and Nova, 1997). In the same framework, some other models have also been recently proposed (Nova and Di Prisco, 2003),(Cremer et al., 2002),(Cremer et al., 2001),(Butterfield and Gottardi, 2003).

The common assumption of these approaches is the substitution of infinitesimal variables, like stress and strain variables, with external loads and displacements by considering them as generalised stress and strain variables, respectively.

In other cases, according to the Buckingham theorem about model scaling, the weight of the soil has been suitably increased making use of a geotechnical centrifuge in order to directly transpose the experimental data as a solution to the real problem.

About this last approach many papers have been written using a variety of centrifuges which differ from a dimensional point of view and from the maximum tangential velocity they can reach. The use of such a technique has been used for studying many problems, from the physical modelling of piles (Colombi, 2005) to the bearing capacity of offshore structures (Allersma, 2003).

Another “classical” approach to the problem of shallow foundations is based on the theoretical models proposed for the determination of the limit load and for the prediction of the settlements experienced by the structure.

Among the methods taken into consideration are the simplified schemes in which the soil is considered rigid and perfectly plastic for the determination of the limit load, and perfectly elastic for the evaluation of the settlements.

Other approaches,that are different but can still be included in this family of methods, have been developed using the principle of overposition of effects (Terzaghi, 1943) which have brought to many subsequent studies in which many different aspects, like the load inclination or eccentricity, have been taken into account by multiplying by empyrical factors the terms of the general expression proposed by Terzaghi (Brinch Hansen, 1967),(Vesic, 1975).

In all these methods the most important parameter is the friction angle of the soil, since the range of variability of the bearing capacity of a shallow foundation is strongly influenced by the value assumed for the shear resistance angle.

For evaluating the settlements for a shallow foundation, in most cases the elastic solutions proposed by Boussinesq (Boussinesq, 1885) or their extension of the simple point-load case (Poulos and Davis, 1974) have been and are still used.

A strong limitation of such an approach is the use of elastic parameters, directly related to the Young modulus E and to the Poisson ratio ν, since the experimental behaviour of granular and soft soils is far away from being elastic. The numerical evaluation of such parameters, which play a fundamental role in the computation of the settlements, is not therefore straightforward.

In recent years, thanks to the availability of high-performance CPUs at low cost, many advanced numerical models have been developed to solve the systems of differential equations involved in the resolution of many engineering problems.

In particular, in geomechanics and geotechnical engineering, many numerical methods have been proposed: the most important are the Finite Difference (FD) method, the Boundary Element Method (BEM) and the Finite Element Method (FEM), which is nowadays a well-established solution technique widely used for the resolution of many different kinds of problems.

In addition, in the last decade another approach was proposed: the Discrete Element Method (DEM), has come to light thanks to the theory mainly developed by Cundall (Cundall and Strack, 1979) however, due to the high computational cost of the method, the application for the resolution of complex geothechnical engineering problems seems still far from being accessible to the common user.

Among the methods cited above, the FEM is undoubtedly the most used both in research and in practical applications.

During the last years many aspects have been studied about this method, which requires the definition of a mechanical behaviour for the soil through the choice of a constitutive model.

Many constitutive models have been developed, within the framework of elastoplasticity, starting from the pioneering Cam-Clay model by Schofield and Wroth (Schofield and Wroth, 1967) and following other theoretical models, like for example, hypoplasticity.

After their implementation in FE codes, they have come to be available to researchers and practising engineers for the resolution of boundary value problems.

Nowadays, many studies and researches are carried out about mathematical problems involved in the application of the FE model (e.g. (Tamagnini et al., 2000),(Borja et al.,

2001)), about implementation algorithms (e.g. (Leoni, 2004),(Fellin and Ostermann, 2002)) and the application of the method for the resolution of geotechnical engineering problems.

Since this work mainly focuses on the use of the FE method for the modelling of shallow foundations on sand, some further details about the method will be given in the next Section 1.2, while in Section 1.3 a description of the laboratory tests which have been chosen as reference for the evaluation of the predictive capacity of the constitutive models considered, will be given.

1.2 The FE method

Since this work focuses on the numerical modelling of the loading tests described in Point 1.3, a brief description of the finite element (FE) method will be given.

While this introduction aims to give an outline of the main characteristics of the method, some further details will be given in Chapter 3, focusing on the implementation of the constitutive routines.

The basic principle behind the FE method is the decomposition of a *continuum* problem, controlled by an *infinite* number of variables, in an assembly of a *finite* number of sub-domains to form a *discrete* system, in which only the definition of a finite number of variables is necessary. The solution of a complicated problem is obtained by approximating the solution over each sub-domain (element) by a simple function. The functions used to represent the behaviour of the solution within an element are called *shape* (or *interpolation*) *functions*, and they are usually chosen as polynomial functions.

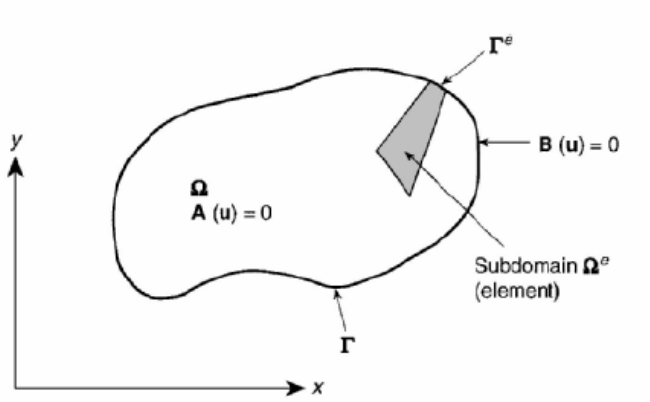

Fig. 1.1 Problem domain Ω and boundary Γ (Zienkievicz and Taylor, 2000).

The general problem of continuum mechanics is to find a displacement function u so that a set of differential equations, say the differential equilibrium equations, is satisfied over the domain Ω, together with the boundary conditions specified on Γ (Fig. 1.1).

In order to solve the system of differential equilibrium equations, we follow a *variational* approach, in the sense that a *test function* is introduced and the differential equations, multiplied by such a function, are integrated over the domain Ω.

Being the FE method an approximated one, we can freely take the test function δu as shape function N multiplied by an arbitrary function δa, and the global solution u can be

expressed as function of the nodal displacements a_i and of the shape functions N_i which depend on the interpolation chosen for the elements (Eq. 1.1). Global shape functions N_i are therefore written as *local* shape functions over each element, and then suitably assembled into an *incidence matrix* Z_e, which reflects the topology of the discretization and makes possible the transition from the local nodal displacements u to the global displacements a_i.

$$\delta u = N \delta a; \quad u = \sum N_i a_i; \quad a_i = Z_e a \tag{1.1}$$

From the fulfilment of the differential equations governing the physical process and of the boundary conditions, stems that the virtual work statement 1.2 which represents the so-called *weak form* of the equilibrium equations, has to be zero.

$$\underbrace{\int_\Omega \delta \varepsilon^T \sigma d\Omega}_{f_{int}} - \underbrace{\int_\Omega \delta u^T b d\Omega + \int_\Gamma \delta u^T t d\Gamma}_{f_{ext}} = 0 \tag{1.2}$$

It can be observed how the first term of the LHS accounts for the internal forces acting on the body, while the other terms depend on the external (known) forces.

Moreover, the integral accounting of the internal forces can be worked out introducing 1.3, and 1.4:

$$\delta \varepsilon = S \delta u, \quad S^T = \left\{ \frac{\partial}{\partial x} \; \frac{\partial}{\partial y} \; \frac{\partial}{\partial z} \; \cdots \right\} \tag{1.3}$$

$$B = \frac{\partial}{\partial x_i} N_i \tag{1.4}$$

Simplifying equation 1.2 we obtain:

$$Z_e^T \int_\Omega B^T \sigma d\Omega \; + \; f_{ext} = 0 \tag{1.5}$$

The resolution of the problem can be carried out via an iterative procedure: starting from an equilibrated configuration, computed for the n^{th} step of the analysis, a displacement increment is imposed and a load increment is consequently applied onto the body. Our task is to find a solution, i.e. a displacement u such that:

- The body is equilibrated at $(n+1)^{th}$ step:

$$Z_e^T \int_\Omega B^T \sigma_{n+1} d\Omega \; + \; f_{n+1}^{ext} = 0 \tag{1.6}$$

- The stress update is compatible with the constitutive assumption given for the material.

1.2.1 The equilibrium iteration

After a general description of the FE method, it is worth going deeper into the description of the general procedure to be followed for its application: a displacement increment is given starting from the equilibrated body with the known nodal displacements a_n:

$$a_{n+1} = a_n + \Delta a_n \tag{1.7}$$

The strain in the element at the end of the increment is

$$\varepsilon_{n+1} = SNa = Ba \tag{1.8}$$

The element is therefore deformed by the strain increment

$$\Delta\varepsilon_n = \varepsilon_{n+1} - \varepsilon_n \tag{1.9}$$

wherein ε_n is known. By means of the constitutive law, the stress increment is computed starting from the strain increment. Hence, the new state of stress is computed and the internal forces are evaluated. Equation 1.6 is therefore solved by Newton-Raphson iterations, that requires the evaluation of the derivative of the LHS of equation 1.6, which is the *residual* $R(d_{n+1})$ of the iteration.

$$Z_e^T \int_\Omega B^T \sigma_{n+1} d\Omega + f_{n+1}^{ext} = R(d_{n+1}) \tag{1.10}$$

The solution is accepted when the residual approaches zero, thus meaning the equivalence between internal ant external forces. The derivative of the residual is the so-called *consistent tangent operator* of the k^{th} iteration, because it is consistent with Newton's method.

1.2.2 Consistent tangent operator

To evaluate the consistent tangent operator of the k^{th} equilibrium iteration, equation 1.10 has to be differentiated with respect to d_{n+1}. Provided that the system of external forces is independent from d_{n+1}, the derivative of the residual can be written as

$$Z_e^T \underbrace{\left(\int_\Omega B^T \frac{\partial \sigma_{n+1}}{\partial \varepsilon_{n+1}} B d\Omega \right)}_{\text{element tangent stiffness}} Z_e = R'(d_{n+1}) \tag{1.11}$$

The material information on the element level to build the consistent tangent operator is the so-called Jacobian:

$$\frac{\partial \sigma_{n+1}}{\partial \varepsilon_{n+1}} = \frac{\partial (\sigma_{n+1} - \sigma_n)}{\partial (\varepsilon_{n+1} - \varepsilon_n)} \tag{1.12}$$

The general strategy used by Abaqus and many other FE packages, is the *cosolution*: the FE code solves the equilibrium problem, while the constitutive law is solved by a solver for ordinary differential equations.

In particular, the solver must provide the FE code with both the updated stress and the consistent tangent operator (Hibbitt et al., 2003).

Another possibility supplied by Abaqus is the possibility to make use of user defined constitutive models, in addition to the models already embedded in the library of constitutive routines of the program. In this case, the routine must fulfill the tasks which would have to be accomplished by the numerical solver, i.e. for each equilibrium iteration, stresses have to be updated, as well as the Jacobian of the $(n+1)^{th}$ iteration.

A fundamental role is played by the constitutive assumption for the material, since it is directly involved in the computation of the element tangent stiffness. A non-linearity in the formulation of the constitutive model provokes a non-linearity in the internal force vector and a suitable integration strategy has to be developed in order to get the solution in terms of stress and Jacobian updating at the end of each time increment. Some further details about the integration strategies will be given in Chapter 3, dealing with the implementation of the constitutive models.

1.3 Laboratory tests on shallow foundations on sand

The experimental testswere performed at ISMES Laboratory in Bergamo (Italy) and are widely described in (Montrasio, 1994). The main purpose of the experiments was the modelling of the behaviour of rigid shallow foundations on sand.

As far as the materials used and the testing procedures is concerned, an accurate description will be given in the following paragraphs.

1.3.1 Description of the granular material

The experimental tests were carried out using an homogeneous layer of dense Ticino sand, which is widely studied and used for laboratory tests. Physical characteristics of the material are summarized in Table 1.1 and Fig. 1.2.

As for the density, although three different values for the relative density were obtained by pluvial deposition (D_R=0.45, 0.70 and 0.96), in this work only the denser material has been chosen as reference, that is to say the one with D_R=0.96.

In Fig. 1.3 the shear strength values are plotted versus the confining pressure, for a relative density within the range 0.80-0.90. (Bellotti et al., 1985)

γ_{max} (kN/m^3)	γ_{min} (kN/m^3)	D_{10} (mm)	D_{50} (mm)	D_{60} (mm)	Gs
16.68	13.65	0.29	0.47	0.51	2.649

Table 1.1 Physical and geometric characteristic of Ticino sand.

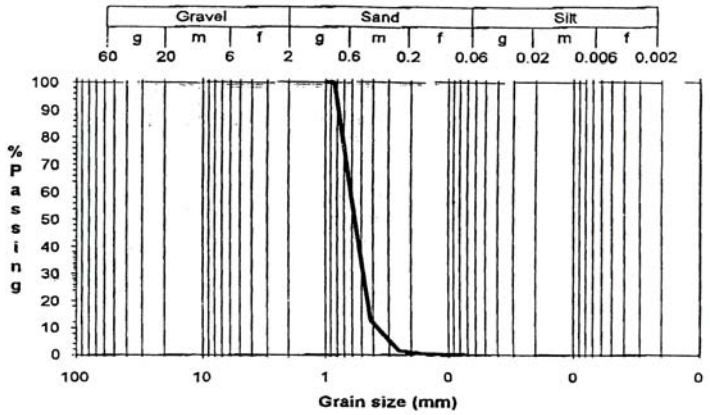

Fig. 1.2 Granulometric curve of Ticino sand.

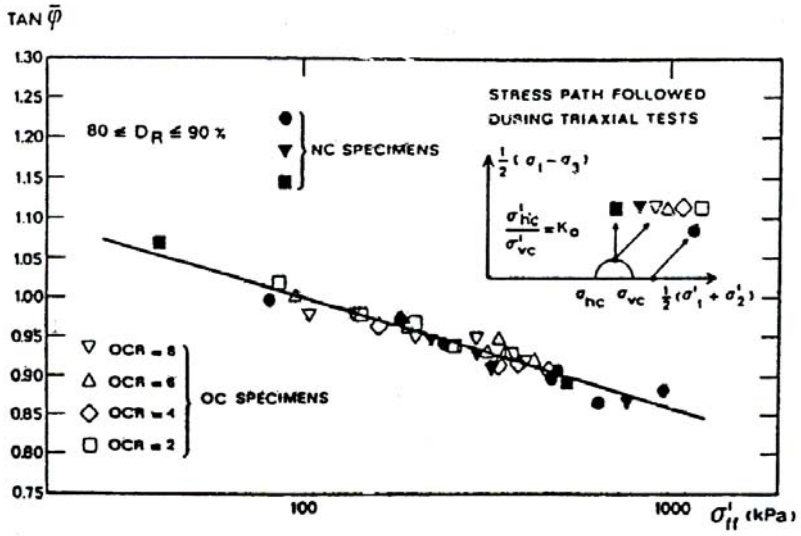

Fig. 1.3 Shear strength for Ticino sand (Bellotti et al., 1985).

1.3.2 Experimental apparatus

The homogeneous sand layer was set into a 0.8 m high cylindrical metallic caisson with a diameter of 1.2 m.

A pluvial deposition technique was chosen in order to obtain the desired relative densities of 0.45,0.70 and 0.96. As a support for the tools allowing the application of vertical loads, a steel frame was applied to the container and pulleys to the side bars in order to apply the horizontal loads, if required by the testing procedure. An overall image of the experimental apparatus is given in Fig. 1.4.

The model foundations were modelled using 0.08 m wide metallic plates with three different lengths of 0.08, 0.016 and 0.024 m so that three different shape ratios (length/width) a=1, a=2 and a=3 were considered.

Due to the plate's thickness and particular shape it can be considered to be perfectly rigid with respect to the stiffness of the soil. Moreover, the foundation has several grooves fitting with the loading blade (Fig. 1.5) to make possible the application of eccentric and inclied loads with negligible spurious overturning moments

For all series of tests of interest, sand was glued to the foundation base to assure a perfect roughness of the base, but some preliminary tests were carried out in which the base of the metallic plate was smooth, in order to check the influence of the friction on the final results.

The loading ram (Fig. 1.6) is a servo-controlled oleo-dynamic piston by means of which a constant load rate can be imposed on the foundation.

In order to perform tests in which the vertical load is constant but the horizontal load and/or overturning moment increases, a different loading system is used: a horizontal steel wire was connected to a vertical stick.

Horizontal load and overturning moment were given by applying a dead weight to the wire which pulls the foundation via a pulley. A load cell was used to quantify the frictional loss of the pulley.

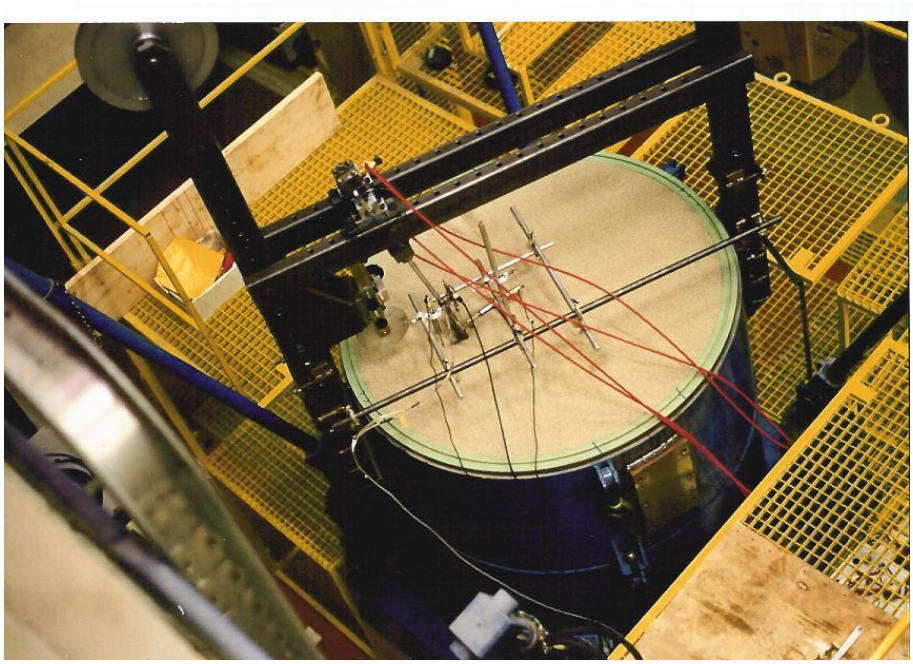

Fig. 1.4 Experimental set-up (Montrasio and Nova, 1997).

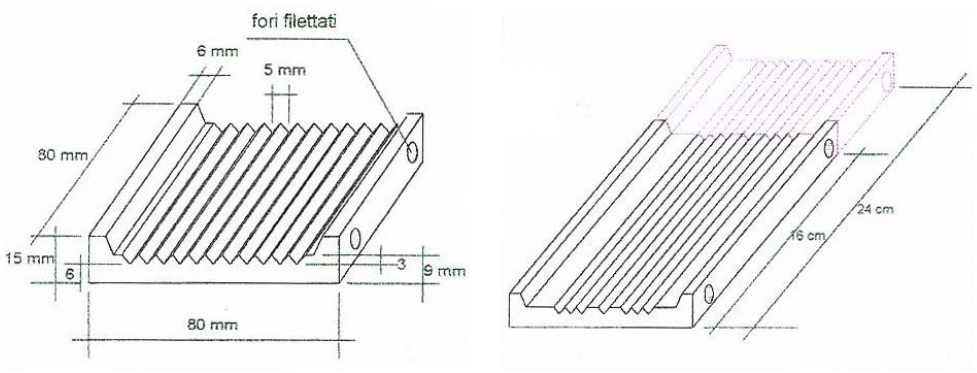

Fig. 1.5 Geometry of the foundations (Montrasio and Nova, 1997).

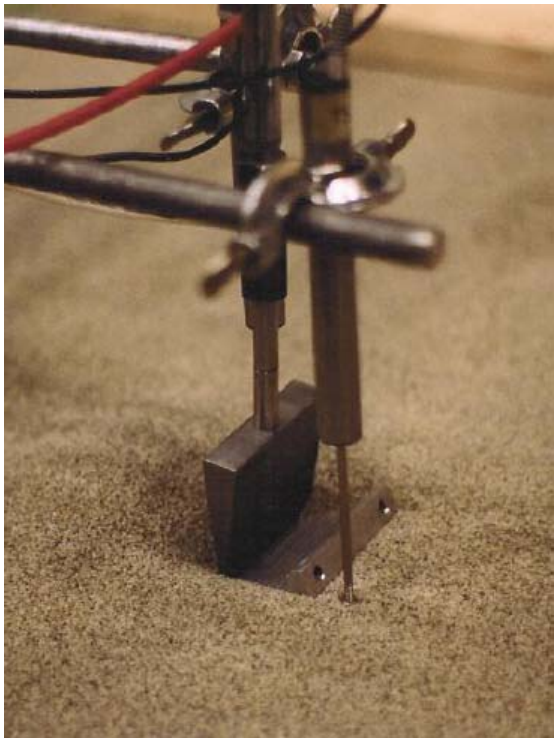

Fig. 1.6 Loading ram (Montrasio and Nova, 1997).

1.3.3 Test procedures and data collection

By applying loads to the metallic plate, six different cases were analyzed on the foundations with different aspect ratios (a=1,2 and 3):

- centered vertical loading;
- inclined loading (with no overturning moment) from zero to failure;
- eccentric loading (with no horizontal load) from zero to failure;
- application of a horizontal load and overturning moment at constant centred vertical load, from zero to failure;
- application of a horizontal load at constant;
- eccentric vertical load.

A total of 90 tests were performed, some of them aiming to check the repeatability of the tests and the influence of some factors, like the distance from the border of the caisson or the roughness of the base of the metallic plate. In addition, some tests were performed also on foundations set at different depths in order to study the influence of the lateral weight of the soil on the predicion of the limit load.

As far as the measurement procedure is concerned, horizontal loads were known since directly applied as dead loads, while load cells between the piston tip and the foundation gave the measure of the applied vertical load.

After their calibration, three linear variable differential transducers (LVDT) were placed in a suitable way (not aligned) on the metallic foundation and 3 on the sides of the plate (2 on the longer side) in order to measure vertical and horizontal displacements of the plate, while rotations in three independent directions can be easily computed knowing the displacements and distances between the LVDTs. The presence of spurios moments and rotations would have requested a larger number of LVDTs to be placed in order to measure such out-of-plane movements.

The particular loading technique, however, has assured the reasonable absence of such components, thus allowing to limit the number of transducers required.

The LVDTs were connected to a data logger allowing a continuous data acquisition, so that the measurement system allowed to know horizontal and vertical loads, horizontal displacement and vertical settlement, applied momentum and the rotation of the foundation.

All the colleced data were plotted in graphs using a common spreadsheet which played a fundamental role since they have been the reference for further comparisons between numerical and experimental results, as will be described in Section 4.2.

2 Constitutive models for the soil

When the resolution of a geotechnical engineering problem is solved via FE analyses, the most crucial step is the choice of the constitutive model for the soil.

As long as computer capabilities were limited, due to both the CPUs' low clock speed and by the limited storage capacities of the mass storage memories, one had to deal with the computational cost of each analysis, since it was the bottleneck of the whole process.

Only simple constitutive models could be used, and the behaviour of soils was often modelled by a simple linear elastic law; even the implementation of a Mohr-Coulomb failure criterium could be cumbersome as regards the computational time required for the analysis.

Nowadays, that powerful CPUs are available at low costs and the data storage is no more a problem, researchers have pushed themselves towards more complicated models aiming to a better reproduction of the mechanical behaviour of materials, in general, and particularly of geomaterials.

The last part decades have seen the birth of a large quantity of constitutive models starting from the first Cam-Clay model, developed in the '60s by Schofield and Wroth (Schofield and Wroth, 1967) within the framework of elastoplasticity.

Perhaps the problem is exactely the opposite: in these last years a huge quantity of constitutive models has been developed, so that when the geotechnical engineer has to "pick" a suitable constitutive model for the soil, he could be a little bewildered.

Two are the questions to be answered when choosing a costitutive model, and particularly for geomaterials:

1. Is it accurate enough in reproducing the mechanical behaviour, considering the particular class of engineering problem I am studying?
2. Am I able to carry out a satisfactory calibration of the material parameters of the model with the available experimental data?

For answering to the former question a systematic study on different classes of engineering problems would be required. In technical literature is not easy to find such a studies, and in the last years some analyses have been performed in order to assess the capability of many classes of constitutive models to predict ground movements around excavations (Viggiani and Tamagnini, 2000),(Leoni et al., 2003) and retaining structures (Tejchman and Herle, 1999).

The latter question is much more difficult, because it involves specific know-how: not always we agree, for example, on the definition of *simple* laboratory or in situ tests. Due to the cost of experimental tests, it is often difficult to have reliable measurements or test data

available for the FE analyst in order to carry out a proper identification of the constitutive parameters.

In this work the problem of shallow foundations on a dense Ticino sand is studied.

Three different constitutive models have been used: the Advanced Mohr Coulomb model (Ménetrey and Willam, 1995) already present in the library of constitutive models of ABAQUS FE code; a simplified version of "Sinfonietta Classica" (modified from (Nova, 1988)) and the hypoplastic CLoE constitutitve model which has been developed in Grenoble over the last 20 years (Chambon et al., 1994).

The last two models have been implemented by the Author as user-defined models exploiting the possibility given by ABAQUS to implement user-defined models through the *umat* routine.

In the next paragraphs a description of the models will be given, first defining the main features of the families of constitutive model considered.

2.1 Elastoplasticity

Two of the three models used, namely the Extended Mohr Coulomb and the Simplified Sinfonietta Classica, have been developed within the framework of elastoplasticity. The plasticity theory has been primarly introduced for modelling the mechanical behaviour of steel, and it has therefore extended to other materials such as soils.

The basic assumption of plasticity, and in particular of elastoplasticity, is the tensorial decomposition of the total strain tensor in an elastic and a plastic part:

$$\varepsilon = \varepsilon_{el} + \varepsilon_{pl} \tag{2.1}$$

It is worth noting that equation 2.1 is often formulated in rate form. Main features of plasticity are:

- Yield criterion (defined through a function *f*): is a boundary between admissible and impossible states of stress, usually formulated in terms of deviatoric and mean stress. By definition, only points inside the domain bounded by *f* or on the boundary *f* itself can represent a possible state of stress. In particular, in elastoplastic models, the area inside *f* is the so-called *elastic domain* since the behaviour inside the yield function is purely elastic and completely reversible.
- Plastic potential *g*. The essential feature that characterizes plastic flow is the concept of *irreversibility*: the direction of plastic strains is defined through the gradient of plastic potential *g* and its norm is given by the flow rule (Eq. 2.2):

$$\dot{\varepsilon}_{pl} = \lambda \frac{\partial g}{\partial \sigma} \tag{2.2}$$

- Hardening law (Eq. 2.3), which defines the evolution of the hardening parameter(s) q with respect to the scalar λ and function *h*:

$$\dot{q} = \lambda h(\sigma, q) \tag{2.3}$$

g and *h* are prescribed functions which define the direction of plastic flow and the type of hardening. The parameter λ is a nonnegative parameter, called *consistency parameter* (Simo and Hughes, 1997), which is assumed to be constrained by the Kuhn-Tucker complementarity conditions:

$$\lambda \geq 0, \quad f(\sigma, q) \leq 0, \quad \lambda f(\sigma, q) = 0 \tag{2.4}$$

In addition to conditions 2.4, equation 2.5 has to be fulfilled:

$$\lambda \dot{f}(\sigma, q) = 0 \tag{2.5}$$

In the scientific literature, conditions 2.4 are the *loading/unloading conditions*, while equation 2.5 goes by the name of *consistency condition*.

To better understand the role played by the Kuhn-Tucker conditions, let us consider the unloading/reloading case: by definition, $f(\sigma,q)<0$, so that λ must be equal to zero to have the 3rd equation of 2.4 fulfilled.

From the flow rule (2.2) and the hardening law (2.3) it follows that $\dot{\varepsilon}_{pl}=0$ and $\dot{q}=0$, thus the process is perfectly elastic, and $\dot{\varepsilon}=\dot{\varepsilon}_{el}$.

Now suppose that the actual state of stress is located on the boundary surface *f*, so that $f(\sigma,q)=0$. Two different situations can arise:

Case 1) $$\lambda\dot{f}=0 \quad \text{and} \quad \dot{f}<0 \;\Rightarrow\; \lambda=0 \tag{2.6}$$

It follows again that $\dot{\varepsilon}_{pl}=0$, $\dot{q}=0$ and $\dot{\varepsilon}=\dot{\varepsilon}_{el}$. This type of response is called *unloading from a plastic state*;

Case 2) $$\lambda\dot{f}=0 \quad \text{and} \quad \dot{f}=0 \tag{2.7}$$

In Case 2, equation 2.5 is automatically satisfied, but two further cases are possible:

I. if $\lambda=0$, (in addition to $\dot{f}=0$) we have the so-called *neutral loading*, since no plastic strains arise even if we are in a plastic state;

II. if $\lambda>0$ plastic strains arise and we have both $\dot{\varepsilon}_{pl}\neq 0$ and $\dot{q}\neq 0$; this latter case is called *plastic loading*.

It is worth noting how any situation in which $f(\sigma,q)>0$ would violate conditions 2.4, so this possibility has not been considered.

From the consistency condition 2.5 we can write the time derivative of f using the chain rule:

$$\begin{aligned}\dot{f} &= \frac{\partial f}{\partial\sigma}:\dot{\sigma}+\frac{\partial f}{\partial q}\cdot\dot{q}\\ &= \frac{\partial f}{\partial\sigma}:C:\left[\dot{\varepsilon}-\dot{\varepsilon}_{pl}\right]+\frac{\partial f}{\partial q}\cdot\dot{q}\\ &= \frac{\partial f}{\partial\sigma}:C:\dot{\varepsilon}-\lambda\left[\frac{\partial f}{\partial\sigma}:C:\frac{\partial g}{\partial\sigma}+\frac{\partial f}{\partial q}\cdot h\right]\le 0\end{aligned} \tag{2.8}$$

Assuming that $\left[\frac{\partial f}{\partial\sigma}:C:\frac{\partial g}{\partial\sigma}+\frac{\partial f}{\partial q}\cdot h\right]>0$, it follows:

$$\dot{f} = 0 \;\Leftrightarrow\; \lambda = \frac{\left\langle \frac{\partial f}{\partial \sigma} : C : \dot{\varepsilon} \right\rangle}{\frac{\partial f}{\partial \sigma} : C : \frac{\partial g}{\partial \sigma} + \frac{\partial f}{\partial q} \cdot h} \tag{2.9}$$

where $\langle x \rangle := \left[x + |x| \right] / 2$ denotes the ramp function, equal to zero if x is negative, otherwise equal to x itself.

This gives a mathematical explanation of the neutral condition: λ is zero if and only if the numerator of 2.9 is equal to zero, i.e. if the scalar product defined by the elastic tensor C between the normal to f and the strain rate is zero, thus implying a 90° angle between the normal to f and the $\dot{\varepsilon}$ tensor.

Assembling 2.1 and 2.2 we obtain:

$$\dot{\sigma} = C : \left[\dot{\varepsilon} - \dot{\varepsilon}_{pl} \right] = C : \left[\dot{\varepsilon} - \lambda \frac{\partial g}{\partial \sigma} \right] \tag{2.10}$$

Substituting in 2.10 the expression of λ obtained in Eq. 2.9, we can express the increment of stress in rate form in terms of total strain rate as:

$$\dot{\sigma} = C^{ep} : \dot{\varepsilon} \tag{2.11}$$

where C^{ep} is the so-called tensor of *tangent elastoplastic moduli* given by the expression:

$$C^{ep} = \begin{cases} C & \text{if } \lambda = 0 \\ C - \dfrac{C : \dfrac{\partial g}{\partial \sigma} \otimes C : \dfrac{\partial f}{\partial \sigma}}{\dfrac{\partial f}{\partial \sigma} : C : \dfrac{\partial g}{\partial \sigma} + \dfrac{\partial f}{\partial \sigma} \cdot h} & \text{if } \lambda > 0 \end{cases} \tag{2.12}$$

Note that C^{ep} is in general unsymmetric, but comes to be symmetric if:

$$\frac{\partial g}{\partial \sigma} = \frac{\partial f}{\partial \sigma} \tag{2.13}$$

that is referred as *associative flow rule*, i.e. the normal to the plastic potential has the same direction than the normal to the yielding surface.

2.1.1 Extended Mohr Coulomb (EMC)

Considering the outline of elastoplasticity given in Section 2.1, we are now ready to describe the main features of the elastoplastic models used in this work.

The first consitutive model stems from the well known Mohr-Coulomb (MC) failure criterium: the Extended Mohr-Coulomb elastoplastic model has been developed by considering a yielding surface similar to the general MC line in addition to a flow rule and a hardening law.

As it is well known, MC model assumes that failure occurs when tangential stress in a point reaches a limit value expressed in terms of normal stresses. The classical formulation of the model is given by Equation 2.14, and in plane τ, σ as: (Fig. 2.1)

$$\tau = \sigma \tan\varphi + c \tag{2.14}$$

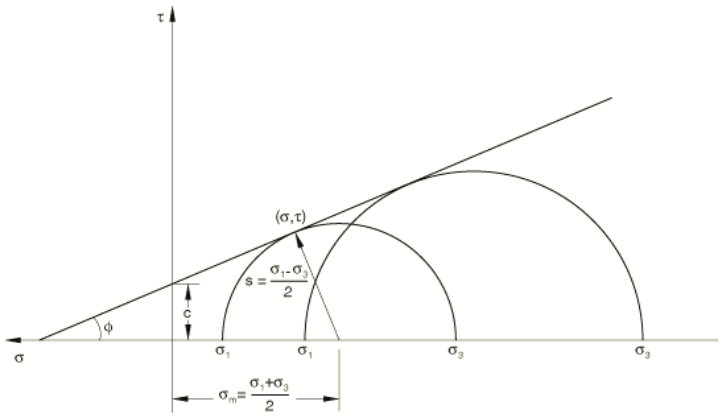

Fig. 2.1 Mohr-Coulomb failure criterium (Hibbitt et al., 2003).

In EMC, the failure surface is given by the equation: (Fig. 2.2)

$$F = R_{mc}\left(\Theta,\phi\right)q - p\tan\varphi - c = 0 \tag{2.15}$$

with:

$$R_{mc}\left(\Theta,\phi\right) = \frac{1}{\sqrt{3}\cos\phi}\sin\left(\Theta + \frac{\pi}{3}\right) + \frac{1}{3}\cos\left(\Theta + \frac{\pi}{3}\right)\tan\phi \tag{2.16}$$

where Θ is the deviatoric polar angle (Chen and Han, 1988), ϕ Is the slope of the failure line in $p / R_{mc} \cdot q$ plane and c soil cohesion.

Variables q and p are, respectively, stress deviator and effective mean stress, as commonly defined in soil mechanics.

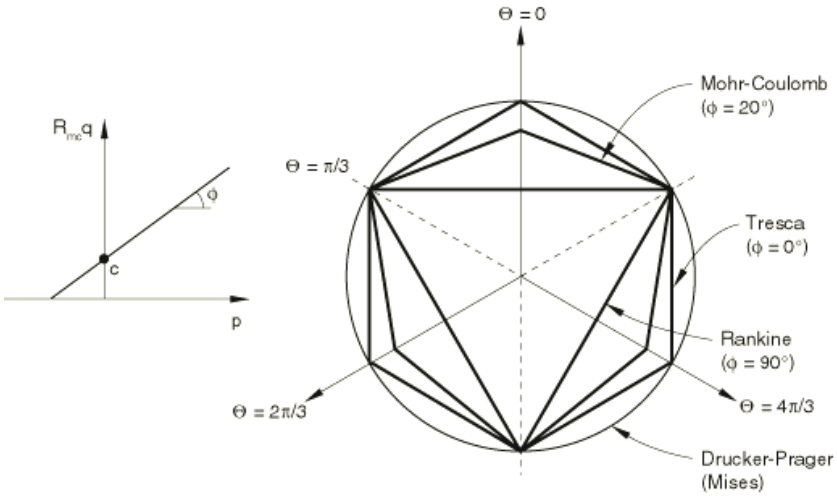

Fig. 2.2 Mohr Coulomb yield surface in meridional and deviatoric planes (Hibbitt et al., 2003).

Plastic potential function is a smooth elliptic function given by: (Ménetrey and Willam, 1995)

$$G = \sqrt{\left(\varepsilon c_{|0} \tan\varphi\right)^2 + \left(R_{mw} q\right)^2} - p \tan\psi \qquad 2.17$$

in which R_{mw} is a function of Lode's angle and of a out-of-roundness parameter influencing the shape of the failure surface in the deviatoric plane; ψ is the dilatancy angle; $c_{|0}$ is the initial cohesion yield stress; ε is a parameter, referred to as the eccentricity, that defines the rate at which the function approaches the asymptote, provided that the flow potential tends to a straight line as the eccentricity tends to zero.

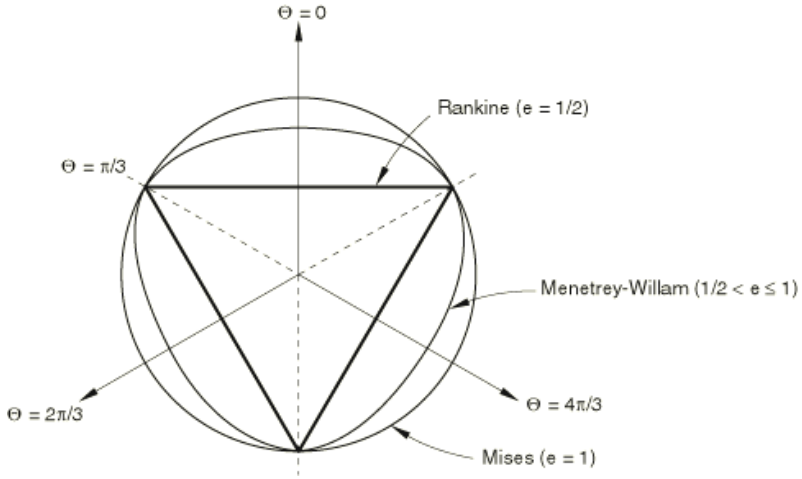

Fig. 2.3 Menétrey-Willam flow potential in the deviatoric plane.

This flow potential, which is continuous and smooth in the meridional stress plane, ensures that the flow direction is uniquely defined in this plane (Fig. 2.3). The function asymptotically approaches a linear flow potential at high confining pressure stress and intersects the hydrostatic pressure axis at 90°. A family of hyperbolic potentials in the meridional stress plane is shown in Fig. 2.4.

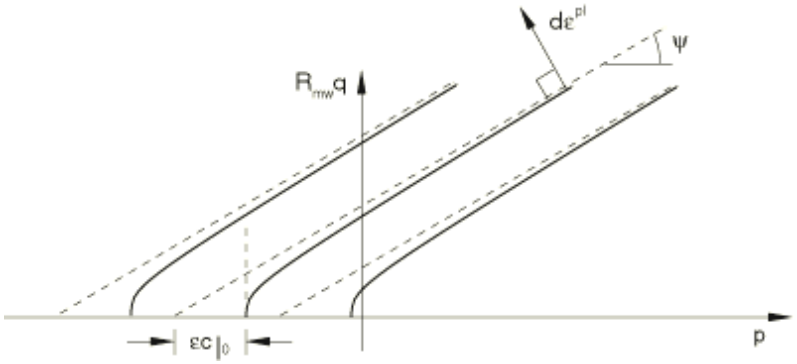

Fig. 2.4 Family of hyperbolic flow potentials in the meridional plane (Hibbitt et al., 2003).

The hardening law has to be provided by the user as tabular data in the input file, and the unique hardening parameter is the cohesion yield stress, which is assumed to be dependent, by default, only on the equivalent plastic strain, defined as:

$$\dot{\varepsilon}_{pl} = \int \frac{1}{c} \sigma : d\varepsilon_{pl} \qquad 2.18$$

In the elastoplastic model a linear elastic behaviour of the soil is assumed until the critical line is reached, so that an estimate of the values of Young's modulus and Poisson ratio, E and ν, have to be provided by the user.

The use of EMC model requires therefore the identification of six parameters:

ϕ : slope of the failure curve in p - $R_{mc} \cdot q$ plane (classical friction angle);

ψ : dilatancy angle;

$c_{|0}$: initial cohesion stress, corresponding to zero plastic strains;

E : Young's modulus;

ν : Poisson ratio.

Other constitutive parameters, like ε and the out-of-roundness parameter are not calibrated but the default value proposed by ABAQUS is accepted, due to their minor influence and the difficulties in their identification without carrying out specific tests.

2.1.2 Simplified Sinfonietta Classica (SSC)

The second elastoplastic model considered for this study is derived form the model "Sinfonietta Classica" proposed in the '80s in (Nova, 1988) and particularly suitable for modeling the mechanical behaviour of sands and clays.

Main ingredients of the original model are the constitutive functions, the yield function f (Eq. 2.19) and the plastic potential g (Eq. 2.20):

$$f = 3\beta(\gamma - 3)\ln\frac{p'}{p_c} + \frac{9}{4}(\gamma - 1)\cdot J2\eta - \gamma \cdot J3\eta \qquad 2.19$$

$$g = 9(\gamma - 3)\ln\frac{p'}{p_g} + \frac{9}{4}(\gamma - 1)\cdot J2\eta - \gamma \cdot J3\eta \qquad 2.20$$

where p' is proportional to the first invariant of the effective stress tensor; the preconsolidation pressure p_c is the hardening parameter, the unique internal variable of the model; p_g is the parameter corresponding to p_c for the plastic potential whose identification is unnecessary since the plastic potential g is involved in the calculations only through its derivatives; $J2\eta$ and $J3\eta$ are, respectively, the second and the third invariant of the stress ratio tensor, defined by the ratio between the effective stress deviator and the first invariant of the effective stress tensor; γ is a parameter related to M, the slope of the limit surface in q/p' plane and to the critical friction angle ϕ'_{CV}.

It can be observed that, in general, the normality rule ($f \equiv g$) applies only if $\beta = 3$.

The evolution law of p_c is ruled by the full plastic strain tensor, and is given in integrated form by:

$$p_c = p_{c0}\exp\left[\frac{tr(\varepsilon^p_{rs}) + \xi\sqrt{J2e} + \psi\sqrt[3]{J3e}}{B_p}\right] \qquad 2.21$$

where p_{c0} is the initial value of p_c, and $J2e$, $J3e$ are the second and third invariants of the plastic strain deviator; B_p is the plastic logarithmic volumetric compliance, and ξ, ψ are parameters involved in the determination of the friction angle in both compression and extension, and in the definition of dilatancy at failure.

The elastic behavior is modeled in a non-linear rate form introducing an hypoelastic law that relates stress and strain in rate form by mean of a stress depending compliance matrix.

A simplified version of Sinfonietta Classica has been herein proposed: only the dependance on second and third invariant is kept, so that functions f and g become:

$$f = 3\beta(\gamma - 3)\ln\frac{p'}{p_c} + \frac{9}{4}(\gamma - 1)\cdot J2\eta \qquad 2.22$$

$$g = 9(\gamma - 3)\ln\frac{p'}{p_g} + \frac{9}{4}(\gamma - 1)\cdot J2\eta \qquad 2.23$$

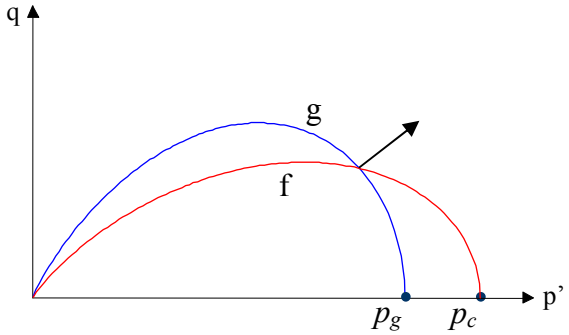

Fig. 2.5 Shape of *f* and *g* in q/p' plane.

The evolution of the hardening parameter p_c is expressed in differential form by:

$$\dot{p}_c = \frac{p_{c0}}{B_p}\left(tr(\dot{\varepsilon}^p_{rs}) + \xi\sqrt{\dot{e}_{rs} : \dot{e}_{rs}}\right) \qquad 2.24$$

where $\dot{e}_{rs}$ is the rate form of the plastic strain deviator, defined as:

$$e_{rs} = \varepsilon - tr(\varepsilon)\cdot \mathrm{I}_{3x3} \qquad 2.25$$

This kind of formulation will be helpful when integrating the mathematical model in the framework of implicit methods in order to obtain the stress update within each iteration.

With these assumptions in mind, the relation between γ above defined and M, slope of the limit surface in q-p' plane, is given by:

$$\gamma = \frac{9 - M^2}{3 - M^2} \qquad 2.26$$

Equation 2.26 stems from the differentiation of the plastic potential with respect to the variables of stress, so that:

$$\frac{\partial g}{\partial \sigma_1} + \frac{\partial g}{\partial \sigma_2} + \frac{\partial g}{\partial \sigma_3} = 0 \qquad 2.27$$

which corresponds to the critical state, as determined by Schofield and Wroth.

In equation 2.27 the increment of plastic volumetric strains is therefore set to zero, according to the definition of plastic strains with respect to the gradient of the plastic potential.

The limit conditions in triaxial compression and extension are then given by:

$$3(\gamma-3)-(\gamma-1)\eta^2+\frac{\xi}{\sqrt{6}}\frac{\varepsilon_{pl}}{|\varepsilon_{pl}|}\left(3(\gamma-1)-\frac{2}{3}\gamma\eta\right)\eta=0 \qquad 2.28$$

The SSC model allows to take into account a value of dilatancy at failure d_{f}, which can be derived from the limit condition:

$$d_{\mathrm{f}}=-3\frac{\xi}{\sqrt{6}}\frac{\varepsilon_{pl}}{|\varepsilon_{pl}|} \qquad 2.29$$

the value of d_{f} is therefore related to the constitutive parameter ξ which, in addition to γ, governs the value of the limit stress ratio and thus the apparent friction angle.

From equations 2.28 and 2.29 it is evident thet neither the limit stress ratio, i.e. the friction angle, nor the dilatancy at failure are affected by the confining pressure.

The elastic behaviour of the model is supposed to be hypoelastic. This assumption derives from the original SC model, togheter with its incremental formulation:

$$\dot{\varepsilon}_{el}=D_e(\sigma)\dot{\sigma}' \qquad 2.30$$

As it is well known, this kind of formulation, which is very convenient for its simplicity and its capability to model the unloading behaviour in triaxial tests, has serious shortcomings due, from a mathematical point of view, to the need of an integration of the law for each loading/unloading step.

From a theoretical point of view, since hypoelasticity is not based on the definition of an elastic potential, by choosing a convenient stress cycle it is possible to obtain energy from the sample, which is evidently a nonsense. We can therefore assume that the model would not be able to model any cyclic behaviour.

To overcome both this shortcomings, the solution could be the choice of a different approach for the elastic phase of the model, like hyperelasticity (e.g.(Borja et al., 1997)) in which the stress/strain relation is given through the derivatives of a *free energy function*, thus allowing both the fast resolution of the elastic step (derivatives can be given in closed form) and the preservation of the physical constraints.

Moreover, a hyperelastic behaviour has been already assumed with good results in more advanced models derived from SC ((Tamagnini et al., 2002),(Nova et al., 2003)). In this work, the original hypoelastic relation has been kept because only monothonic loading schemes will be studied.

2.2 Hypoplasticity

A particular class of incrementally non–linear models which has received special attention in recent times is the so–called theory of hypoplasticity, as defined in (Kolymbas, 1991).

A general outline of the theory was laid down by Kolymbas (1991), and several review papers followed thereafter, the most recent of which are (Wu and Kolymbas, 1999) and (Tamagnini et al., 2000). The constitutive equation of an inviscid hypoplastic material is characterized by the following standard functional form:

$$\dot{\sigma} = \mathbf{A}(\sigma, k)\dot{\varepsilon} + \mathbf{b}(\sigma, k)\left|\dot{\varepsilon}\right| \qquad 2.31$$

where the fourth–order tensor $\mathbf{A}(\sigma, k)$ and the second–order tensor $\mathbf{b}(\sigma, k)$ are suitable tensor–valued functions of the current stress state σ and, possibly, of a set of additional (internal) state variables k, accounting for the effects of previous loading history.

The first term on the right hand side of equation 2.31 is linear in the strain rate, and is formally equivalent to the hypoelasticity theory proposed in (Truesdell, 1956). The incremental non-linearity of the constitutive equation is concentrated in the second term, where the rate of deformation appears only through its norm.

The particular structure of the basic constitutive equation 2.31 of hypoplastic models allows a simple and effective graphical illustration of incremental non–linearity.

This can be done by employing the so–called stress response envelopes (SRE), first proposed by (Gudehus, 1979) as a tool for visualizing the properties of a given constitutive equation in rate–form.

A stress response envelope is defined as the image in the stress rate space of the unit sphere in the strain rate space, under the map defined by the constitutive equations.

In the general case, a SRE is a "surface" in a six–dimensional space.

However, in the particular case of axisymmetric (triaxial) loading, the number of independent stress and strain variables reduces to two, and a convenient graphical representation of the SRE can be given in the so–called Rendulic plane of stress rates: $\dot{\sigma}_a : \sqrt{2}\dot{\sigma}_r$, where $\dot{\sigma}_a, \dot{\sigma}_r$ are the axial and radial (principal) stresses, respectively (Fig. 2.6)

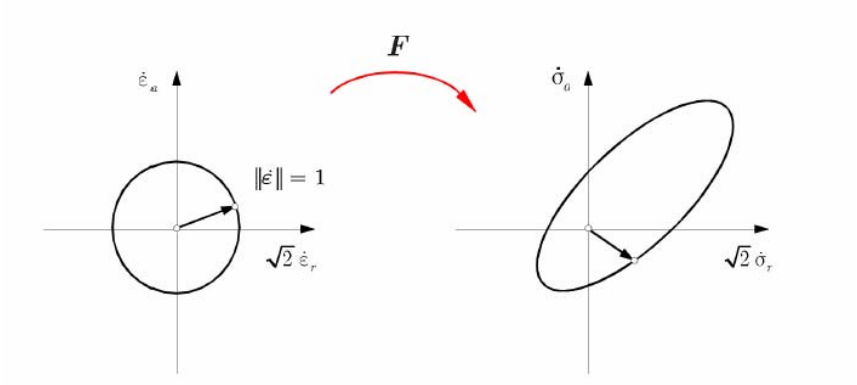

Fig. 2.6 Stress Response Envelope for axysimmetric loading.

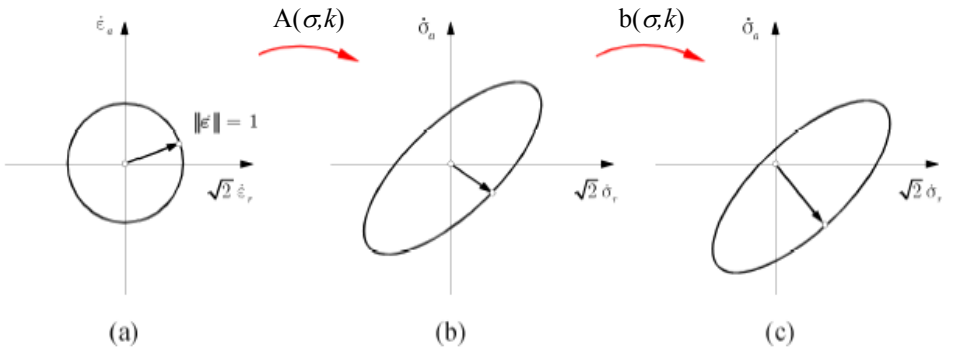

Fig. 2.7 Graphical interpretation of hypoplastic constitutive equation: a) unit circle in the strain rate plane; b) effect of the linear term; c) effect of the non–linear term.

Upon the map defined by equation 2.31, the SRE of a hypoplastic material is obtained as sketched in Fig. 2.7. The effect of the linear operator A is to transform the unit circle into an ellipse centred at the origin of the stress rate plane. The subsequent application of the nonlinear term $\mathbf{b}(\sigma,k)\left|\dot{\varepsilon}\right|$, in which only the strain rate norm is involved, results in a translation of the ellipse along the direction defined by tensor $\mathbf{b}(\sigma,k)$. In its final configuration, the SRE is non–symmetric with respect to the origin of the stress rate space. This lack of symmetry expresses in graphical terms the concept of incremental non–linearity, as expressed by equation 2.31: in fact, choosing $\dot{\varepsilon}_1 = \dot{\varepsilon}^*, \dot{\varepsilon}_2 = -\dot{\varepsilon}^*$, incremental non-linearity requires that:

$$F(\dot{\varepsilon}^*) \neq -F(-\dot{\varepsilon}^*) \qquad 2.32$$

i.e., a full reversal of strain rate does not correspond to a complete reversal of stress rate. Clearly, this is possible only when the SRE is non–symmetric with respect to the origin of the stress rate space.

Starting from the basic mathematical structure of equation 2.31, two different formulations of hypoplasticity have been developed over the last decade, with the specific objective of modeling the behavior of granular, coarse–grained materials.

The first one, referred to in the following as K–hypoplasticity, was developed in Karlsruhe after the pioneer work of Kolymbas, see e.g. (Kolymbas and Wu, 1993). The second originated in Grenoble from the work of Chambon and Desrues under the general name of CLoE hypoplasticity (Chambon et al., 1994).

Although these two approaches share a number of similarities, the motivations for their independent development were different in various respects. As a result, some important differences are apparent in their original formulation, as well as in their respective subsequent developments.

2.2.1 CLoE–hypoplasticity

The origins of CLoE hypoplasticity — where the acronym CLoE stands for ***C****onsistance et* ***Lo****calisation* ***E****xplicite* — can be traced back to the researches by Chambon and Desrues on strain localization in incrementally non–linear materials ((Desrues, 1984),(Chambon and Desrues, 1985),(Desrues and Chambon, 1989)). In the development of CLoE model, the following basic assumptions have been introduced to derive specific functional forms for the tensors **A** and **b** in equation 2.31:

1) To keep the formulation as simple as possible, the set of state variables is limited to the Cauchy stress tensor.

2) According to the experimentally observed behavior of granular materials, the domain of admissible stress states is bounded by a surface S, called limit surface, formally defined by means of a scalar function $\psi(\sigma)$, as function of the set of stress state σ for which:

$$\psi(\sigma) = 0 \qquad 2.33$$

3) The constitutive equation 2.31 is invertible at all the stress states inside the limit surface. Due to assumption (1), tensors **A** and **b** admit the following representation as a 6x6 matrix and a six–components column vector in the reference frame of the principal stress directions:

$$A = \begin{bmatrix} A_{1111} & A_{1122} & A_{1133} & 0 & 0 & 0 \\ A_{2211} & A_{2222} & A_{2233} & 0 & 0 & 0 \\ A_{3311} & A_{3322} & A_{3333} & 0 & 0 & 0 \\ 0 & 0 & 0 & A_{1212} & 0 & 0 \\ 0 & 0 & 0 & 0 & A_{1313} & 0 \\ 0 & 0 & 0 & 0 & 0 & A_{2323} \end{bmatrix} \quad b = \begin{bmatrix} b_{11} \\ b_{22} \\ b_{33} \\ 0 \\ 0 \\ 0 \end{bmatrix} \qquad 2.34$$

Assumptions (1) and (2) imply that for any stress state on S, the stress rate predicted by equation 2.31 is directed inside the limit surface, regardless of the direction of the rate of deformation:

$$\frac{\partial \psi}{\partial \sigma} \cdot \dot{\sigma} = 0 \qquad 2.35$$

The above condition has a direct geometrical interpretation in terms of response envelopes: the response envelope corresponding to a stress state on the limit surface must be tangent to $\psi(\sigma) = 0$. This condition represents a fundamental constraint in the development of functional forms for the tensors **A** and **b**, known as *consistency condition* (Chambon et al., 1994).

The strategy adopted to develop specific functional forms for the constitutive tensors **A** and **b** in the first generation of CLoE models is based on the interpolation procedure described in the next paragraph.

A number of special loading paths, known as basic paths, are defined along which the material response to particular loading conditions is described via suitable response functions interpolating experimentally observed data.

For each stress state, a set of image points is then defined along the basic paths, for which **A** and **b** can be easily determined by differentiating the response functions (Fig. 2.8).

The actual values of **A** and **b** are then evaluated by interpolating the corresponding tensors at the image points, based on the current values of Lode angle and normalized deviatoric stress $q/q_{L,}$ being q_L the deviator stress on the limit surface for the current values of mean stress and Lode's angle.

In performing the interpolation, the consistency condition at the limit surface, equation 2.35, has to be enforced through a suitable rotation of tensor **A**. To ease the calibration procedure and to link material constants to commonly observed features of soil behavior, the basic paths are selected among those which are experimentally accessible by means of standard laboratory equipments i.e., triaxial compression and extension; isotropic compression starting from isotropic and anisotropic stress states.

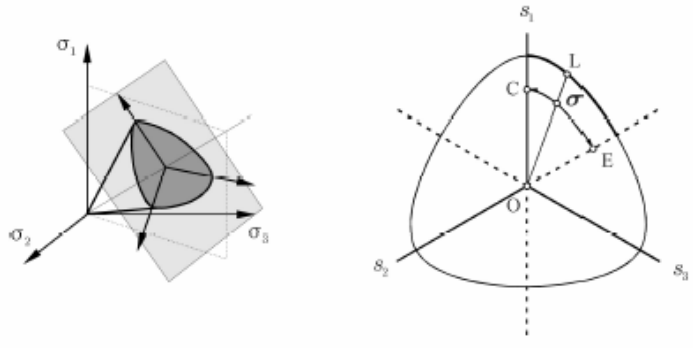

Fig. 2.8 Limit surface and image points for CLoE models.

These routine laboratory tests can provide informations on all the unknown components of the constitutive tensors except for the so–called *out–of axis* shear moduli A_{1212}, A_{1313} and A_{2323} of the representation in equations 2.34.

This approach presents the advantage of directly linking the constitutive functions to the observed material behaviour along an as large as possible set of loading paths, in contrast with common practice in the development of elastoplastic constitutive models, where the mathematical formulation of the constitutive equations is generally based on experimental investigation on a much more limited number of stress–paths.

However, this advantage is paid in terms of a relatively large number of parameters required to describe the response functions, and complexity of the interpolation procedure, which does not allow to define an explicit form for the functions $\mathbf{A}(\sigma)$ and $\mathbf{b}(\sigma)$.

3 Implementation of the models

Since computers have become more and more powerful, researchers have been developing analysis techniques to take benefit of computational capabilities of modern computers.

In particular, in engineering, the FE method has been developed, thus allowing practising engineers as well as researchers to solve even complex boundary value problems.

The reliability of the results obtained through FE analyses is strongly influenced by the choice of the constitutive model for the materials involved in the problem.

In geotechnics the main material involved is the soil. Unlike in structural or mechanical engineering, where materials are often clearly identified by more or less simple constitutive relations, the "soil" material is very complex and can be studied under many points of view, depending on the particular aspects involved in the specific analysis.

For example, soils can show a completely different behaviour depending on their physical characteristics (e.g. grain size) or their particular state (denser or looser).

The formulation of the constitutive relation for the soil is therefore influenced by the characteristics of the material to be modelled. Along last decades, a high quantity of constitutive models as well as algorithms have been developed, in order to make possible the use of such mathematical laws in FE analyses.

In most cases, the implementation of a constitutive law requires the resolution of systems of differential equations, thus requiring robust numerical integration algorithms which stems from the theory of differential calculus.

Such numerical methods can be summarized in *explicit* and *implicit* methods: each one of the two methods has its advantages and shortcomings: in particular, for the integration of the elastoplastic model, the return mapping algorithm was formulated following an implicit scheme, while the integration of the CLoE model was carried out in an explicit framework.

Since the third constitutive model (EMC model) used for the soil was already embedded in the library of constitutive models of the ABAQUS code, it will not be considered within this chapter, completely devoted to the description of the implementation strategies followed for SSC and CLoE models.

3.1 Implementation of the SSC model

In the classical elastoplastic formulations, total strains are typically splitted into elastic and plastic deformations.

Furthermore, main ingredients of every elastoplastic formulations, are the yield function (Eq. 2.22), which allows to distinguish between elastic and elastoplastic domain, the plastic potential (Eq. 2.23) whose gradient is proportional to the plastic deformations through the scalar λ and the flow rule, which relates the hardening parameter p_c to plastic strains as defined in equation 2.24.

The implementation has been carried out within the well-established *elastic predictor* **(EP)** – *plastic corrector* **(PC)** framework: starting from the initial state of strain and stress, given a strain increment, the stresses are updated, for each Gauss-point, assuming that the first step is perfectly elastic, i.e. the increment of plastic strains is set to zero, so that the hardening parameter is left unchanged in this first step.

If the trial state is inside the yield function *f*, the stress is updated to the trial stress and the routine ends, while if the final state is outside or on the yield function (i.e. $f \geq 0$), the plastic corrector procedure is initialized, passing as initial state (trial state) the results of the elastic predictor.

The whole EP process is summarized in Box 3.1.

1. *Increment of total (elastic) strain* ε^{n+1} *starting from equilibrated* n^{th} *state:*
   $\sigma^{n}, \varepsilon^{n} \rightarrow \dot{\varepsilon}^{n+1}, \dot{\varepsilon}_{pl} = 0$
2. *Evaluation of trial state of stress* $\sigma_{tr}{}^{n+1}$ *through elastic relation*

$$TEST: \text{ if } f(\sigma_{tr}{}^{n+1}, p_c{}^{n}) < 0$$
$$\sigma^{n+1} = \sigma_{tr}{}^{n+1}, p_c{}^{n+1} = p_c{}^{n} \rightarrow \text{END}$$

else PLASTIC CORRECTOR ($\dot{\varepsilon} = 0$)

Box 3.1 Elastic Predictor (EP).

It is worth noting how, due to the hypoelastic nature of the elastic relation of the model, as described in Chapter 2, an integration procedure is necessary even for the resolution of a simple elastic step.

For integrating the hypoelastic equation 2.30, a general scheme has been used, that is the Generalized Midpoint Method (GMM-α), as described in (Tamagnini et al., 2000), and briefly summarized below.

The general scheme of GMM-α method can be written as:

$$\sigma^{n+1} = \sigma^{n} + (D_e^{-1})^{n+\alpha} \Delta\varepsilon^{n+1} \tag{3.1}$$

where

$$\begin{aligned} \sigma^{n+\alpha} &:= (1-\alpha)\sigma^{n} + \alpha\sigma^{n+1} \\ (D_e)^{n+\alpha} &:= D_e(\sigma^{n+\alpha}) \end{aligned} \tag{3.2}$$

with $\alpha \in [0,1]$. If $\alpha = 0$ the method degenerates into the weel-known Euler explicit method, while, if $\alpha = 1$ we obtain the classical backward Euler method.

In the present case it has been chosen a value $\alpha = 0.5$, which corresponds to the Crank-Nicolson method, which is proven to be second order accurate. A rigorous non-linear accuracy and stability analysis of the GMM-α algorithms for hardening plasticity and viscoplasticity has been presented in (Simo and Govindjee, 1986)

For any given α, the evaluation of the stress increment requires an iterative procedure to determine the generalized midpoint stress. In order to improve the algorithm accuracy, a substepping scheme is adopted in which the given strain increment is subdivided in substeps.

In this case, a simple substepping scheme with a constant substep size is employed, thus $\Delta T_k = 1/n_s$. A complete description of the GMM-α algorithm is given in (Hairer and Wanner, 1991), and is summarized in Box 3.2.

At the beginning of first substep ($k = 1$), the stress is initialized to the converged value at time station t_n.

Then, at the j^{th} iteration of the generic substep $k \in [1, n_s]$, the generalized midpoint stress $\sigma_{k+\alpha}^{(j)}$ is evaluated according to step 4.

Note that if $j = 1$ the update of the midpoint stress is based on the stress increment $\Delta\sigma_{k-1}$ at the end of previous substep, while the stress increment at the previous iteration $\Delta\sigma_{k-1}^{(j-1)}$ is used otherwise.

A new value of the stress increment is therefore computed in step 5, starting from the values of the elastic tensor at $\sigma_{k+\alpha}^{(j)}$.

The iteration process is repeated until a relative norm of the residual $r^{(j)}$, defined as in step 6, is less then a prescribed tolerance *TOL*, or the iteration counter j is equal to a prescribed maximum number of iterations JMAX.

1. Initialize substep counter, stress and stress increment:
$$k=1 \quad \sigma_k\big|_{k=1}=\sigma_n \quad \Delta\sigma_0=0$$

2. Compute substep size: $\Delta T_k=\dfrac{1}{n_s}$

3. Initialize iteration counter: $j=1$

4. Compute generalized midpoint stress:
$$\sigma_{k+\alpha}^{(j)}=\begin{cases}\sigma_k+\alpha\Delta\sigma_{k-1} & \text{if } j=1\\ \sigma_k+\alpha\Delta\sigma_{k-1}^{(j-1)} & \text{otherwise}\end{cases}$$

5. Compute stress increment according to equation (3.1):
$$\Delta\sigma_k^{(j)}=\Delta T_k(D_e)_{k+\alpha}^{(j)}\Delta\varepsilon_{n+1}$$

6. Compute residual for current iteration:
$$r^{(j)}:=\begin{cases}\Delta\sigma_k^{(j)}-\Delta\sigma_{k-1} & \text{if } j=1\\ \Delta\sigma_k^{(j)}-\Delta\sigma_k^{(j-1)} & \text{otherwise}\end{cases}$$

7. Check for convergence:
$$(\|r^{(j)}\|/\|\Delta\sigma_k^{(j)}\|<TOL).\text{OR.}(j=\text{JMAX})?$$
$$\begin{cases}yes: \ \Delta\sigma_k=\Delta\sigma_k^{(j)}, \ \text{GOTO 8}\\ no: \ \ j=j+1, \ \text{GOTO 4}\end{cases}$$

8. Update stress tensor:
$$\sigma_{k+1}=\sigma_k+\Delta\sigma_k$$

9. Check for the end of the substepping:
$$k=n_s?\begin{cases}yes: \ \sigma_{n+1}=\sigma_{k+1}, \ \text{END}\\ no: \ \ k=k+1, \ \text{GOTO 3}\end{cases}$$

Box 3.2 Genetalized Midpoint Method (GMM-α) (Tamagnini et al., 2000).

At the end of the integration of the elastic relation, the elastic predictor ends with the test at point 2 in Box 3.1. If necessary, the PC routine is initialized: with the hypotheses of constant total strain, the trial state of stress is mapped back to the yielding surface, which is changed

by updating the value of the hardening parameter accordingly to the evolution of plastic strains.

The actualization of stress and strains is achieved by means of *return mapping equations*, which consist in the definition of a residual vector and a Jacobian matrix within a local Newton-Raphson iterative process. In this work, while always the same procedure has been chosen for the resolution of the EP, that is a Generalized Midpoint Method (GMM) (Tamagnini et al., 2000), two different strategies have been adopted and compared for the formulation of the PC problem. The description of the two strategies will be the object of next paragraphs.

Regardless the specific strategy chosen for the return mapping equations, the general scheme for the resolution of the problem is the discretization of the following system of differential equations, which governs the PC problem:

$$\begin{cases} \varepsilon_{el} = \varepsilon - \varepsilon_{pl} & \text{(a)} \\ \dot{\sigma} = D_e^{-1}\dot{\varepsilon}_{el} & \text{(b)} \\ \dot{\varepsilon}_{pl} = \lambda \dfrac{\partial g}{\partial \sigma} & \text{(c)} \\ \dot{p}_c = \dfrac{p_{c0}}{B_p}\left(tr(\dot{\varepsilon}_{rs}^{p}) + \xi\sqrt{\dot{e}_{rs} : \dot{e}_{rs}} \right) = \lambda h(\sigma, p_c) & \text{(d)} \\ f(\sigma, p_c) = 0 & \text{(e)} \end{cases} \qquad 3.3$$

Equation (a) states the decomposition of total strain in elastic and plastic part, while (b) is the hypoplastic relations (see 2.1.2 for the description of the SSC model).

Equation (c) and (d) are the evolution of plastic strains and of the hardening parameter, respectively. In (d) the evolution of p_c is expressed both in terms of evolution of plastic strains and in terms of plastic multiplier λ and hardening function h; (e) comes from the Kuhn-Tucker conditions 2.4 for the PC problem, where λ is different from zero.

Due to the strongly non-linear nature of the system 3.3, the integration of the return mapping equations is performed by an implicit Backward Euler scheme, formulated in terms of stress (approach #1) and strain (approach #2) components.

For both the formulations, however, the return mapping equations require the vanishing of a residual vector R via a full Newton-Raphson iterative scheme represented in Box 3.3.

A difficulty in applying the scheme is the necessity to formulate the tangent matrix for the local problem, since it involves the partial derivatives of the equations f, g and h with respect to the unknowns of the problem, which are the four components of stress (only the plane state is here considered), the hardening parameter and the increment of the plastic multiplier $\Delta\lambda$.

In scientific literature many examples can be found about return mapping schemes formulated in terms of stress (e.g. (Lourenço, 1995)) or strain (e.g.(Tamagnini et al., 2002)) components.

(Initial state of stress from the solution of the EP – see *Box 3.1*)

...3. DO WHILE *(*CONV $\neq$ *true):*

a. Evaluate the Jacobian $J = \dfrac{\partial R}{\partial x}$

b. J^{th} *increment of the unknown vector:*

$$\delta x_{n+1}^{j} = \left(\frac{\partial R}{\partial x}\right)^{-1} R_{n+1}^{j}; \quad x = x + \delta x$$

c. Convergence check (tolerance tolRETM=1.10^{-12}*):*

CONV = *true*

IF $R(k)^{n+1}(x + \delta x) > tolRETM$

THEN CONV = *false*

Box 3.3 Plastic Corrector (PC).

3.1.1 Formulation F#1: integration in terms of stress

System 3.4 describes the discretization of the plastic corrector problem in terms of stresses:

$$\begin{cases} \sigma^{n+1} = \sigma_{tr}^{n+1} - D^{e}(\sigma^{n+1})\Delta\lambda^{n+1}Q^{n+1} \\ p_c^{\,n+1} = p_{ctr}^{\,n+1} + \Delta\lambda^{n+1}h^{n+1} \\ f(\sigma^{n+1}, p_c^{\,n+1}) = 0 \end{cases} \qquad 3.4$$

The unknowns of the problem at time t_{n+1} are the stress components, the value of p_c and the plastic multiplier $\Delta\lambda$, while the trial stress components σ_{tr} (as results of the elastic predictor) and the value of the hardening parameter (unchanged during the elastic predictor) are known quantities.

The residual *R* and the Jacobian matrix *J* of the procedure are defined as:

$$R = \begin{pmatrix} \sigma^{n+1} - \sigma_{tr}^{n+1} + D^e(\sigma^{n+1})\Delta\lambda^{n+1}Q^{n+1} \\ p_c^{\,n+1} - p_{ctr}^{\,n+1} - \Delta\lambda^{n+1}h^{n+1} \\ f(\sigma^{n+1}, p_c^{\,n+1}) \end{pmatrix} \tag{3.5}$$

$$J = \begin{pmatrix} I_{4x4} + \Delta\lambda\dfrac{\partial}{\partial\sigma}D^eQ^{n+1} & \Delta\lambda\dfrac{\partial}{\partial p_c}D^eQ^{n+1} & D^eQ^{n+1} \\ -\Delta\lambda\dfrac{\partial}{\partial\sigma}h & 1-\Delta\lambda\dfrac{\partial}{\partial p_c}h & -h \\ \dfrac{\partial f}{\partial\sigma} & \dfrac{\partial f}{\partial p_c} & 0 \end{pmatrix} \tag{3.6}$$

The Jacobian matrix is here computed by means of a numerical approximation.

Namely, a centered difference scheme has been chosen, which has second order accuracy, and can be described as:

$$\frac{\partial R_i}{\partial x_j} = \frac{R_i(x_1,..,x_j+\vartheta,...x_n) - R_i(x_1,..,x_j-\vartheta,...x_n)}{2\vartheta} \tag{3.7}$$

the Jacobian matrix is therefore computed, element by element, as numerically approximated j^{th} derivative of the i^{th} component of the residual vector.

The stepsize ϑ chosen for the implementation is 10^{-7}, which is a reasonable value considering the machine precision (IEEE double) and the general assumptions (Pérez-Foguet et al. 2000) for the choice of the stepsize for the centered differentiation $\vartheta = (\text{macheps})^{1/3}$

3.1.2 Formulation F#2: integration in terms of strain

The second approach is based on a different formulation of the first equation of 3.5: stress vector is replaced by strain vector, while the unknowns remain σ^{n+1}, $p_c^{\,n+1}$ and $\Delta\lambda^{n+1}$.

Residual vector and Jacobian matrix, therefore, can be written as:

$$R = \begin{pmatrix} \varepsilon_{el}^{n+1} - \varepsilon_{el}^{n+1} + \Delta\lambda^{n+1}Q^{n+1} \\ p_c^{\,n+1} - p_{ctr}^{\,n+1} - \Delta\lambda^{n+1}h^{n+1} \\ f(\sigma^{n+1}, p_c^{\,n+1}) \end{pmatrix} \tag{3.8}$$

$$J = \begin{pmatrix} D^e(\sigma^{n+1}) + \Delta\lambda \dfrac{\partial}{\partial\sigma} Q^{n+1} & \Delta\lambda \dfrac{\partial}{\partial p_c} Q^{n+1} & Q^{n+1} \\ -\Delta\lambda \dfrac{\partial}{\partial\sigma} h & 1 - \Delta\lambda \dfrac{\partial}{\partial p_c} h & -h \\ \dfrac{\partial f}{\partial\sigma} & \dfrac{\partial f}{\partial p_c} & 0 \end{pmatrix} \qquad 3.9$$

The derivatives of *f*, *g*, and *h* are computed by mean of a symbolic manipulator (MATHEMATICA) in order to obtain a closed-form expression that can be used in the FORTRAN code to build the exact expression of the matrix J, thus allowing a further comparison possibility with the previous approach, in which the components of the matrix were numerically computed.

3.1.3 Consistent tangent operator

The resolution of boundary value problems by a FE code requires the design of a mesh of finite elements and the solution of a static equilibrium problem expressed by the weak form of the balance of momentum equation.

To this end, the definition of a consistent tangent matrix that allows the achievement of quadratic convergence in the global Newton-Raphson iteration is needed.

A crude approximation of the tangent matrix induces time-consuming analyses and a worse overall performance of the FE model.

It is worth noting, however, that the formulation of the consistent tangent matrix does not influence neither the final results of the analyses (if reached) nor the performance of the implementation at Gauss-point level.

In F#1 the matrix is evaluated by a rough approximation by perturbating the strain components with a small value of strain increment (order of magnitude: 10^{-8}) thus giving a slow rate of convergence in the global iterations.

On the contrary, in F#2, the different structure of the return mapping scheme allows to define the tangent matrix for an elastoplastic step in a more effective way (Lourenço, 1995):

$$\frac{\partial \Delta\sigma}{\partial \Delta\varepsilon} = J^{-1}{}_{4x4} \qquad 3.10$$

where the RHS is the upper left 4x4 matrix extracted from the Jacobian of the return mapping algorithm at the end of the converged local iteration. How these different approaches in the computation of the tangent matrix will be shown in the next section 3.1.4.

3.1.4 Simple 1-element analysis : simulation of triaxial tests

Following the two proposed schemes, in order to test the behavior of the routine at single Gauss-point level, a standalone FORTRAN routine has been written.

This first algorithm has been developed with debugging purposes only, because in order to solve even the simplest boundary value problem, the implementation of the routine within a FE code is needed.

To this end, a commercial FE code has been chosen, ABAQUS rel.6.4, and the original Fortran code has been "translated" into the subroutine *umat* to be passed to ABAQUS as user-defined material routine.

The time stepping control is splitted in two: a simple procedure in subroutine *umat* controls the maximum time increment, while the decision whether increase the time increment is assigned to ABAQUS. Inside *umat*, the maximum number of substeps is computed by:

$$subs = \frac{valD \cdot dtime}{tol} \tag{3.11}$$

where *valD* represents the Euclidean norm of the total strain increment vector at the beginning of the current increment, *tol* is a tolerance parameter ($tol = 10^{-5}$) and *dtime* is the current time increment.

If *subs* results greater of equal than the maximum number of substeps allowed, the analysis is restarted with a new time increment reduced to the 25%.

It is worth noting as a time stepping procedure should not be necessary, since the integration scheme is fully implicit, which is proven to be unconditionally stable. Such a procedure has however implemented in order to avoid a resulting trial stress state excessively far from the initial yield surface because of the exponential form of the elastic law, that would give serious numerical problems.

For checking the effectiveness of the two implementations some simple analyses have been carried out.

The single element chosen for the analyses is shown in Fig. 3.1: a 4 noded axisymmetric CPE4, isotropically consolidated and then subjected to triaxial tests simulated by applying a downward vertical displacement (total vertical strain of 20%) in correspondance of the top face of the element.

For all the calculations, the constitutive parameters of the model have been adopted as shown in Table 3.1.

For the simulation of the triaxial test (TXCID) on the normally consolidated soil, the finite element has been isotropically consolidated up to 100 kPa, value assumed for the confining pressure throughout the whole test.

To the same value has been set the preconsolidation parameter, so that the stress state initially lies on the initial yield surface. As far as the simulation of an overconsolidated soil is concerned, the initial isotropic pressure was 50 kPa, with an initial value for the hardening parameter of 500 kPa, thus resulting an initial OCR = 10.

In Fig.3.2 the results are presented, for both F#1 and F#2, in terms of deviatoric stress vs. mean stress, deviatoric stress vs. total vertical strain. In Fig. 3.3 the analysis results are given in terms of volumetric versus deviatoric strain.

M	B	$B_{e\backslash}$	L	β	ξ
1.33	0.0059	0.03	0.01	1.8	0.00

Table 3.1 Numerical values for the material parameters.

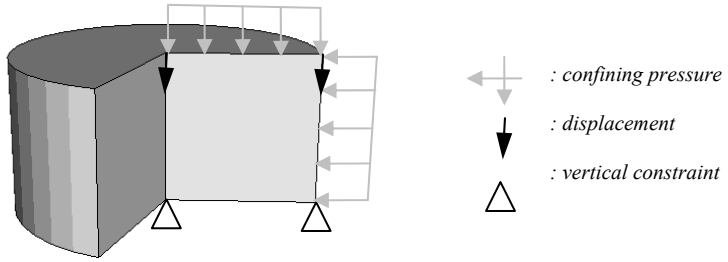

Fig. 3.1 Axisymmetric 4-noded element CAX4 for FE simulations of triaxial tests.

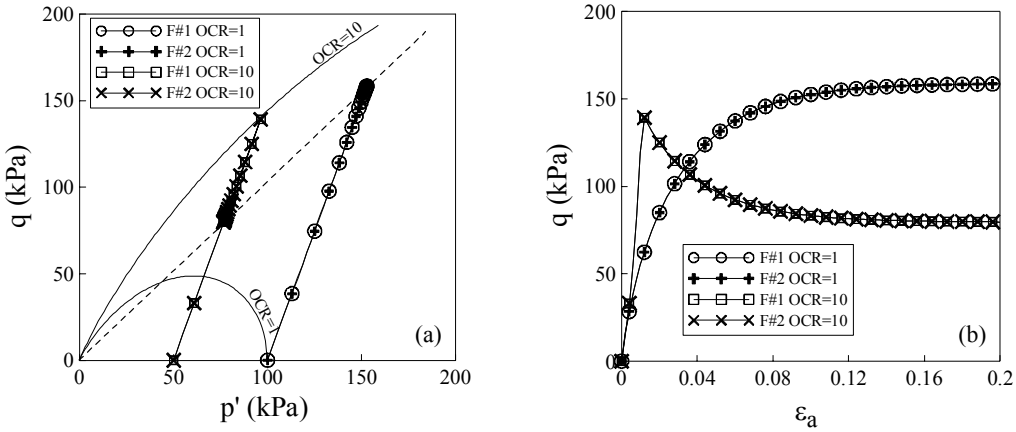

Fig. 3.2 F#1 and F#2, OCR=1 and OCR=10 TXCID tests: Stress path with initial yield surface and critical state line (a), deviatoric stress vs. axial strain (b).

For these simple tests the failure condition identifies the critical state, since the parameter ξ, which is related to dilatancy at failure through the 2.29, has been set to zero.

As expected, the curves shown in Fig. 3.3 asymptotically tend to an horizontal line, thus evidentiating null volumetric strain rate when the CSL is reached.

However, the choice of a suitable value for ξ will allow to take into account of a dilatancy angle different from zero.

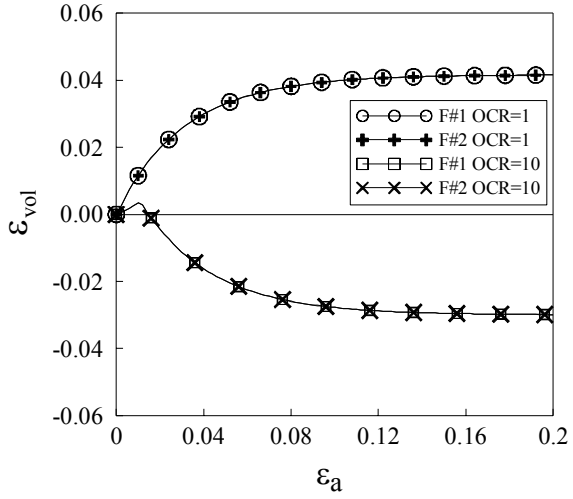

Fig. 3.3 F#1 and F#2, OCR=1 and OCR=10 TXCID tests: volumetric vs. deviatoric strain.

Moreover, an undrainded triaxial test has been simulated, whose results are presented in Fig. 3.4. In order to simulate the pore pressure, a different element type has been chosen: the 4-noded axysimmetric element with pore pressure CAX4P.

As it was expected, the total stress path (TSP), represented by the straight line in the left plot of Fig. 3.4 is different from the effective stress path (ESP, curved line), and the difference is given by the water pressure.

As for deviatoric stress vs. axial strain, the curve obtained well reproduces the exected real behaviour of NC soil subjected to a triaxial undrained test.

From the observation of the results, it is clearly apparent that the two formulations of the return mapping, F#1 and F#2, give almost exactly the same results, both in terms of stresses and volumetric strains vs. axial strains.

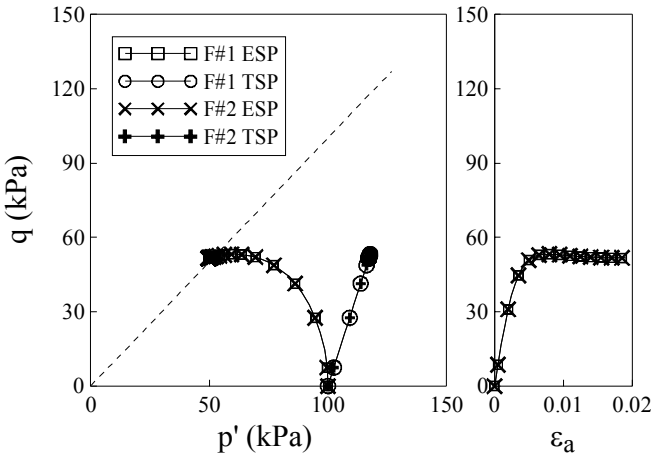

Fig. 3.4 F#1 and F#2, TXCIU test: TSP and ESP, deviatoric stress vs. axial strain.

In order to investigate about the computational time requested by the two routines, one among the aforementioned simulations has been chosen, i.e. the TXCID test on a NC soil.

In Table 3.2 the highest residual forces for the first time increment in which an axial strain of 2.10^{-4} are given: the analysis with F#1 converges after 7 iterations, while only 4 iterations are required for F#2.

Moreover, the convergence rate is faster in F#2, in which the material tangent matrix has been computed consistently with Newton's method starting from the Jacobian matrix of the return mapping algorithm.

However, it can be observed that the final total time is slightly higher than the time needed using F#1, this can be explained considering the different structure of the FORTRAN routines, requiring the evaluation of a greater number of equations in F#2. As a further remark, it is worth saying that for all the analyses the ABAQUS convergence criterion on the residual forces has been left unchanged, to the default value of $R_n^{\alpha} = 5 \cdot 10^{-3}$.

Iteration #	F#1 (CPU=60.2 s)	Iteration #	F#2 (CPU=72.1 s)
..4	-4.35	1	-35.2
5	-2.41	2	-6.40
6	-1.35	3	-0.935
7	-0.755	4	-0.129

Table 3.2 TXCID test, I increment: residual forces for F#1 and F#2.

As a further confirmation of the results, the efficiency of the operator has been tested for an analysis involving a larger set of elements; to this end a FE mesh composed of 120 axisymmetric 4-noded CAX4 elements, has been built.

The adopted numerical values for the parameters of the model are the same chosen for the preliminary tests (Table 3.1) and boundary conditions have been set as shown in Fig. 3.5: horizontal displacements are prevented along the right side, while vertical displacements are constrained to zero along the bottom side of the mesh. Along the centreline of the problem, i.e. the left side of the mesh, boundary conditions are consequent to the assumption of axisymmetric condition.

At this preliminary stage, the results of the simple boundary value problem, are of interest only as far as the CPU time needed for the computations, and they must be regarded as a benchmark for the constitutive routines.

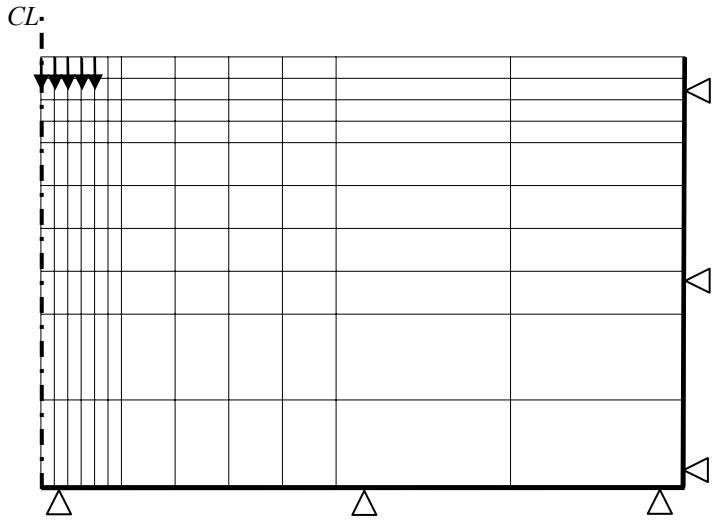

Fig. 3.5 FE mesh for an axisymmetric foundation.

The analysis has been performed in displacement control, constraining the downward movement of the first 5 nodes at the left-top corner of the mesh, thus simulating the behaviour of a circular foundation under a vertical centred load.

The foundation has not been modelled, and the loading phase has been modelled by simply applying a settlement to five adjacent nodes at the top right corner of the mesh.

The resulting required CPU time (in seconds) has been 3148.8 for F#1 versus 360.43 for F#2. In this case, the higher efficiency of F#2 is clearly evident.

3.2 Implementation of the CLoE model

The implementation of the CLoE hypoplastic model has been carried out within the framework suggested for the implementation of the K-hypoplasticity (Fellin and Ostermann, 2002). It has been proved how, for the integration of incrementally non-linear laws, the best approach is the explicit scheme (Tamagnini et al., 2000). Nevertheless, such a strategy requires the estimate of the error at each step and, possibly, a substep size automatic control.

As described in Section 2.2.1, the law is formulated in rate form as:

$$\dot{\sigma} = \mathbf{A}(\sigma, k)\dot{\boldsymbol{\varepsilon}} + \mathbf{b}(\sigma, k)\left|\dot{\varepsilon}\right| \tag{3.12}$$

The first problem to solve is the computation of the updated state of stress starting from an equilibrate state and given a strain increment passed by the FE code. Since in CLoE model it is impossible to formulate equation 3.12 in a closed form because of the structure of the mathematical model, this task has to be accomplished via an interpolation between the values assumed by tensors $\mathbf{A}(\sigma, k)$ and $\mathbf{b}(\sigma, k)$ in particular states of stress, the so-called *basic stress paths*, as described in Section 2.2.1.

Without going into details about the interpolation procedure, which is widely described in (Chambon et al., 1995), and defining $\mathbf{T}$ as the stress tensor $\boldsymbol{\sigma}$, let us consider the differential equation which is a way to represent equation 3.12:

$$\frac{\partial \mathbf{T}}{\partial t} = \mathbf{h}(\mathbf{T}, \mathbf{D}) \tag{3.13}$$

Let us define the temporal rate of the strain tensor as:

$$D = \frac{\partial \varepsilon}{\partial t} = \frac{\Delta \varepsilon}{\Delta t} \tag{3.14}$$

The transformation of the derivative in equation 3.14 in a discrete form is due to the particular nature of the computations: only the value of ε at the beginning and at the end of the time increment Δt is known, while we have no information about the state in the middle of the step.

In order to get the Jacobian matrix (see Section 1.12) needed for the resolution of BVPs, equation 3.13 has to be differentiated with respect to the strain increment, which yields the variational equation:

$$\frac{d}{dt}\frac{\partial \mathbf{T}}{\partial \mathbf{D}} = \frac{d}{d\mathbf{T}}\mathbf{h}(\mathbf{T}, \mathbf{D})\frac{\partial \mathbf{T}}{\partial \mathbf{D}} + \frac{d}{d\mathbf{D}}\mathbf{h}(\mathbf{T}, \mathbf{D})\frac{\partial \mathbf{D}}{\partial \mathbf{D}}, \qquad \frac{\partial \mathbf{T}}{\partial \mathbf{D}}(0) = 0 \tag{3.15}$$

Being $\Delta\sigma = \sigma(t_0 + \Delta t) - \sigma(t_0)$, in order to get:

$$\frac{\partial \Delta\sigma}{\partial \Delta\varepsilon} = \frac{\partial \sigma(t_0 + \Delta t)}{\partial t} = \frac{1}{\Delta t} \cdot \frac{\partial \mathbf{T}}{\partial \mathbf{D}}(\Delta t) \tag{3.16}$$

equation 3.15 has to be solved together with equation 3.13, which can be very difficult in closed form. A numerical approximation of equation 3.15 is therefore suggested:

$$\frac{d}{dt}\left(\frac{\partial \mathbf{T}}{\partial \mathbf{D}}\right)_{ij} = \frac{\partial \mathbf{h}}{\partial \mathbf{D}} = \frac{\mathbf{h}(\mathbf{D} + \vartheta) - \mathbf{h}(\mathbf{D})}{\vartheta} = \frac{\mathbf{h}(\mathbf{T}(\mathbf{D} + \vartheta), \mathbf{D} + \vartheta) - \mathbf{h}(\mathbf{T}, \mathbf{D})}{\vartheta} \tag{3.17}$$

but, from the definition of derivative:

$$\mathbf{T}(\mathbf{D} + \vartheta) = \frac{\partial \mathbf{T}}{\partial \mathbf{D}}\vartheta + \mathbf{T}, \quad \mathbf{D}(\mathbf{D} + \vartheta) = \mathbf{D} + \vartheta\mathbf{V} \tag{3.18}$$

where $\mathbf{V}$ is the standard basis tensor. Consequently, equation 3.17 reads:

$$\frac{d}{dt}\left(\frac{\partial \mathbf{T}}{\partial \mathbf{D}}\right)_{ij} = \frac{1}{\vartheta}\left(\mathbf{h}\left(\mathbf{T} + \vartheta\left(\frac{\partial \mathbf{T}}{\partial \mathbf{D}}\right)_{ij}, \mathbf{D} + \vartheta \cdot \mathbf{V}\right) - \mathbf{h}(\mathbf{T}, \mathbf{D})\right), \frac{\partial \mathbf{T}}{\partial \mathbf{D}}(0) = 0 \tag{3.19}$$

From the numerical point of view, the parameter ϑ has been chosen as:

$$\vartheta = \max(1, \|\mathbf{D}\|)\sqrt{macheps}) \tag{3.20}$$

where *macheps* denotes the machine precision, which is about 10^{-16} in IEEE double precision. Equations 3.13 and 3.19 are solved numerically and simultaneously following the procedure below described.

3.2.1 Adaptive explicit integration

The integration of the two differential equations whose solution will give the updated state of stress and the local Jacobian of the iteration, is performed through an explicit scheme which derives from the forward Euler method. The error and stepsize control is based on a Richardson extrapolation.

All the variables involved in the resolution of equations 3.13 and 3.19 are stored in a vector *y*, so that the equations can be written as:

$$y'(t) = F(y(t)), \quad y(0) = y_0 \tag{3.21}$$

An initial time step τ is chosen, so that $\tau \in [0, \Delta t]$, and two approximations are computed:

$$v = y_0 + \tau F(y_0) \tag{3.22}$$

$$w = y_0 + \frac{\tau}{2}F(y_0) + \frac{\tau}{2}F\left(y_0 + \frac{\tau}{2}F(y_0)\right) \tag{3.23}$$

v is the result of forward Euler method with stepsize τ, *w* is the result of two Euler steps of size $\tau/2$. Expanding the exact solution in Taylor series we get:

$$y(t) = y_0 + \tau y'(0) + \frac{\tau^2}{2}y''(0) + o(\tau^3) \tag{3.24}$$

which, thanks to the first of equations 3.21, becomes:

$$y(t) = y_0 + \tau F(y_0) + \frac{\tau^2}{2}F'(y_0)F(y_0) + o(\tau^3) \tag{3.25}$$

We can therefore write:

$$\begin{aligned} y(t) - v &= \frac{\tau^2}{2}F'(y_0)F(y_0) + o(\tau^3) \\ y(t) - w &= \frac{\tau^2}{4}F'(y_0)F(y_0) + o(\tau^3) \end{aligned} \tag{3.26}$$

As a consequence, the difference:

$$w - v = \frac{\tau^2}{4}F'(y_0)F(y_0) + o(\tau^3) \tag{3.27}$$

is an asymptotically correct estimate for the error. We set:

$$EST = \|w - v\| \tag{3.28}$$

If *EST* is below the tolerance set for the integration, the stepsize is accepted and the solution is the extrapolated value:

$$y = 2w - v \tag{3.29}$$

Further, we enlarge the stepsize in a standard way accordingly to

$$\tau_{n+1} = \tau \cdot \min\left(5, 0.9 \cdot \sqrt{\frac{tol}{EST}}\right) \tag{3.30}$$

If *EST* is greater than *tol*, the step is rejected and repeated with a smaller stepsize

$$\tau_{n+1} = \tau \cdot \max\left(0.2, 0.9 \cdot \sqrt{\frac{tol}{EST}}\right) \tag{3.31}$$

In the implementation into ABAQUS code, a more flexible strategy has been adopted for the estimate of the error in each iteration:

$$\|w-v\| = \sqrt{\sum_{i=1}^{6}\left(\frac{w_i - v_i}{s_i}\right)^2} \qquad 3.32$$

with the solution depending weights $s_i = \max(w_i, v_i) + ATOL$. The value for the threshold $ATOL$ can be supplied by the user.

3.2.2 Validation of the constitutive routine

As required before trying to solve complex BVPs, it is necessary to assess the reliability of the implementation.

In order to do that, the following procedure has been chosen: as already mentioned, in CLoE model some simple stress paths are given *a priori*, accordingly with the results of routine laboratory tests on the material.

Only two among the basic stress paths have been chosen for the validation: triaxial compression and extension.

The stress-strain and volumetric vs. axial strain curves have been computed in analytical way and by reproducing the same test through FE analyses.

The perfect matching between the two sets of tests is only a necessary condition for the effectiveness of the routine, but it would be a sufficient confirmation for the reliability of the implementation, since even the simple basic stress path in FE analyses has to be computed through the whole interpolation procedure.

The analytical equations of the CLoE model are given for triaxial compression:

$$\frac{\sigma_a}{\sigma_l} = 1 + \frac{a_{hc}\varepsilon_a}{c_{hc}\varepsilon_a + 1} \qquad 3.33$$

$$\varepsilon_v = a_{pc}\varepsilon_a{}^2 + b_{pc}\varepsilon_a \quad \text{for } \varepsilon_a < x_{pc} \qquad 3.34$$

$$\varepsilon_v = p_{fc}(\varepsilon_a - x_{pc}) \quad \text{for } \varepsilon_a > x_{pc} \qquad 3.35$$

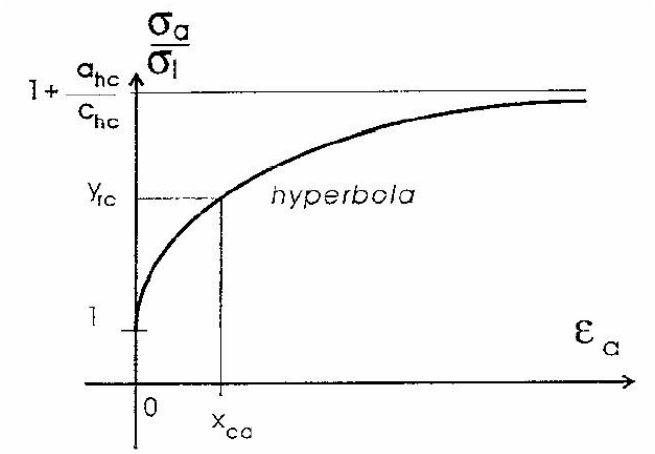

Fig. 3.6 Stress-strain relation in triaxial compression (Chambon et al., 1995).

where, in equation 3.33, the ratio of axial stress on lateral stress is related to the axial strain through two constitutive parameters, a_{hc} and c_{hc}. In equation 3.34 the volumetric strain is related to the axial strain through a_{pc} and b_{pc} via a parabola if the axial strain is less than another constitutive parameter x_{pc}. The second part of the curve is followed by the straight line of equation 3.35, and the whole curve is plotted in Fig. 3.7.

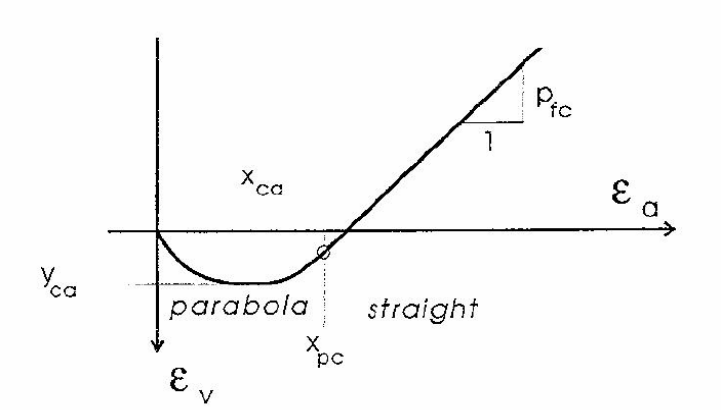

Fig. 3.7 Volumetric-axial strain for triaxial compression (Chambon et al., 1995).

As for triaxial extension, the stress-strain relation is given by:

$$\frac{\sigma_a}{\sigma_l} = 1 + \frac{a_{he}\varepsilon_a}{c_{he}\varepsilon_a + 1} \qquad 3.36$$

and shown in Fig. 3.8, while the volumetric-axial strain relation is given by the equations 3.37 to 3.39 and shown in Fig. 3.9.

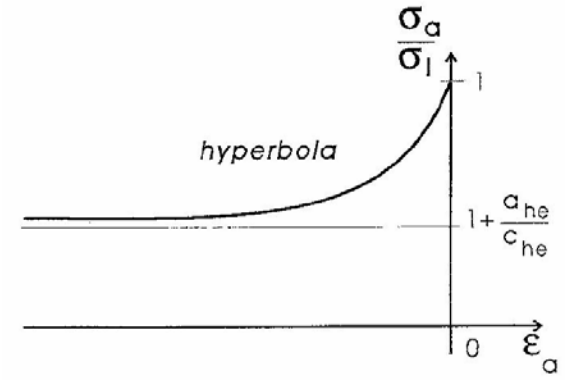

Fig. 3.8 Stress-strain relation for triaxial extension (Chambon et al., 1995).

$$\varepsilon_v = a_1\varepsilon_a^{\,3} + b_1\varepsilon_a^{\,2} + c_1\varepsilon_a \qquad \text{for } \varepsilon_a \in [x_{m2}, 0] \qquad 3.37$$

$$\varepsilon_v = y_e \qquad \text{for } \varepsilon_a \in [x_c, x_{m2}] \qquad 3.38$$

$$\varepsilon_v = a_b(\varepsilon_a - x_c)^4 + c_b \qquad \text{for } \varepsilon_a \in [x_{t2}, x_c] \qquad 3.39$$

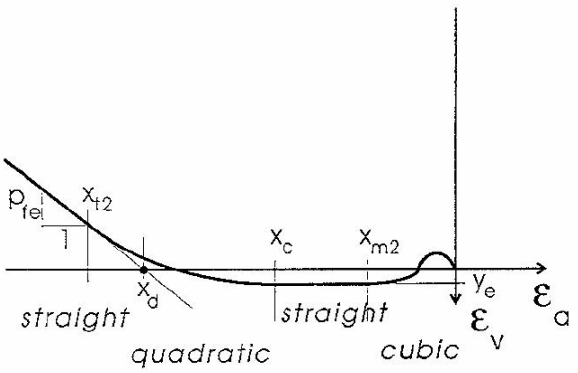

Fig. 3.9 Volumetric vs. axial strain for triaxial extension (Chambon et al., 1995).

The FE model used for validation purposes is the same described in Section 3.1.4 and shown in Fig. 3.1. The set of values for the internal variables shown below, coming from the calibration for a Hostun RF dense sand , was used:

parameter	basic path	value
a_{hc}	triaxial compression	445.573744711774200
c_{hc}	triaxial compression	92.281971097680380
a_{pc}	triaxial compression	-26.592670066879440
b_{pc}	triaxial compression	0.49462366506676613
p_{fc}	triaxial compression	-0.68
x_{pc}	triaxial compression	0.02208547824015395
a_{he}	triaxial extension	495.847845795075000
c_{he}	triaxial extension	-592.578517960124100
a_1	triaxial extension	56313.628540470840000
b_1	triaxial extension	218.496878737026900
c_1	triaxial extension	0.2119419723749161
x_{m2}	triaxial extension	-0.00194
x_c	triaxial extension	-0.002425
a_{bi}	triaxial extension	-98611.433621953980000
c_{bi}	triaxial extension	0.00
x_{t2}	triaxial extension	-0.012125
p_{fe}	triaxial extension	0.36
λ_c	isotropic compression	1200
λ_{co}	isotropic compression	37.405138519112920
λ_{ex}	isotropic compression	692.979577453249100
m_{co}	pseudo isotropic compression	1.224744871391589
m_{ex}	pseudo isotropic compression	0.00
a_{sl}	limit surface	0.6168456884322706
b_{sl}	limit surface	-0.8231301796912084
n_{sl}	limit surface (Van Eekelen, 1980)	-0.20
omcis	(Chambon et al., 1994)	0.36

Table 3.3 Parameters adopted in the validation tests.

The results of the comparison between the FE results and the analytical curves are shown in Fig. 3.10 and Fig. 3.11. The almost perfect agreement between the results obtained confirms the reliability of the implementation, and the constitutive routine is ready to be used for the resolution of more complex BVPs.

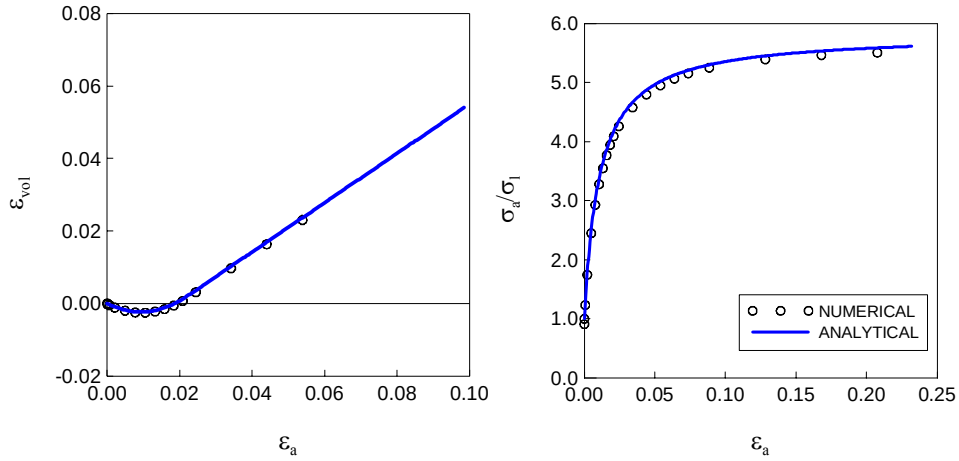

Fig. 3.10 Triaxial compression test: numerical/analytical comparison.

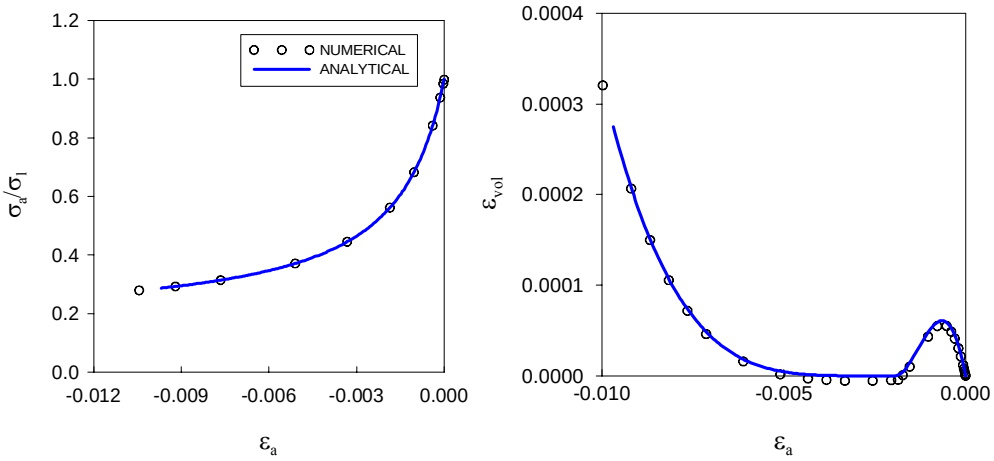

Fig. 3.11 Triaxial compression test: numerical/analytical comparison.

4 Finite element analyses

Main purpose of the implementation of different kinds of constitutive models has been the resolution of BVPs modelling the problem of shallow foundations on sand subjected to different loading schemes.

As previously pointed out, to this end a large set of experimental results was at disposal, so that a systemic comparison between experimental and numerical results was possible, thus allowing the assessment of the predictive capabilities of different constitutive assumptions. In particular, three different constitutive laws have been chosen: a model derived from the well-known Mohr-Coulomb failure criterion (EMC), already embedded in the library of constitutive models of the FE code chosen for the analyses (ABAQUS code), Simplified Sinfonietta Classica, an elastoplastic model modified in order to make easier the identification of the constitutive parameters, and a relatively recent model, belonging to the family of hypoplastic models, the CLoE model. The latter two models have been both implemented in ABAQUS by the Author.

The identification of the parameters has been carried out via back-analysis for EMC and SSC models, while a different approach has been followed for the calibration of CLoE's parameters, which will be widely described in Section 4.1.4.

After the identification, some of the laboratory tests have been reproduced, and results have been compared. In addition, an isoerror representation of the results has been proposed in order to have an overall sight of the reliability of the FE analysis results.

4.1 Description of the FE model

Due to the necessity of simplifying as much as possible the geometry of the model and to reduce the uncertainties in the computations which cannot to be clearly dependent on the constitutive assumptions, the geometry of the model has been modelled within the hypothesis of plane strain condition. This assumption appears to be suitable when the ratio between length and width of the foundation is equal to 3, while becomes slightly far from reality when such a ratio turns to 2 and 1.

However, since the calibration of the parameters is carried out through a back-analysis, as it will be pointed out in the next chapters, the effect of such a "strong" assumption should vanishes thanks to the particular values assumed by the parameters.

Obviously, the values of the parameters which can be putted in direct correlation with physical characteristics of the soil have been set *a priori*, and will not become object of identification.

Moreover, a simple *tied* contact assumption has been set for the interface between soil and foundation, thus allowing to decouple the results from the influence that the particular values assumed by the interface parameters would have.

Concerning this assumption, many researchers have studied the problem of a suitable modelling of the eccentric loads on shallow foundations. In particular it has been shown in (Hjiaj et al., 2003) how the footing remains in complete contact with the soil if the ratio between eccentricity and the width of the plate is less than 0.3, that is exactly the case studied in this work. However, in order to assure that such assumption is not far from the real behaviour of shallow foundations subjected to eccentric loads, a preliminary test has been carried out for verification purposes only.

Some doubts remain about the effect of such hypothesis when the role played by horizontal load components becomes relevant.

As far as the loading procedure is concerned, it has always been used a load-controlled mechanism, whose choice has been imposed by the particular loading schemes used in the experimental tests.

A scheme of the tests chosen for the numerical-experimental comparisons is shown in Table 4.1, with the following meaning for the symbols:

EMC (a=3)	CLoE(a=3)	SSC(a=3)	EMC (a=1)	EMC (a=2)
(CV)	CV	(CV)	(CV)	(CV)
VH3	VH3	VH3	VH3	VH3
VH8	VH8	VH8	VH8	VH8
VH14	VH14	VH14	VH14	VH14
V150H	V150H	V150H	V30H	V100H
e/B=0.125	-	e/B=0.125	e/B=0.125	e/B=0.125
e/B=0.25	-	e/B=0.25	-	e/B=0.25

Table 4.1 Tests for numerical-experimental comparisons

CV refers to centred vertical load, while VHn refers to a load inclined by a n degrees angle. VxxxH is a particular test in which a centred vertical load of xxx kN has been applied, followed by an horizontal load until breakage. e/B=0.125, being e the load eccentricity and B the width of the model foundation (0.08m), corresponds to an eccentric load with e=10mm, while e/B=0.25 refers to an eccentricity of 20mm. In Fig. 4.1a,b the different loading configurations are shown.

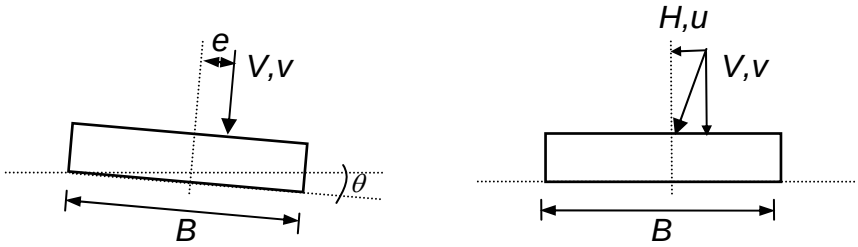

Fig. 4.1 Schemes of the different loading conditions: (a) eccentric loads, (b) inclined loads.

As for the presentation of the results, they are plotted in terms of generalized forces (vertical, horizontal, and momentum) versus generalized displacements (vertical, horizontal displacements and rotations) depending on the particular test considered.

4.1.1 FE model for numerical analyses

In this section a description of the FE model used for all the analyses is given. In Fig. 4.2 the FE mesh is shown. Vertical displacements are prevented along the sides, while both horizontal and vertical displacements are prevented along the bottom side of the mesh.

As for the soil, the finite elements CPE8, 8-noded elements in plane strain condition with parabolic shape function, are used. A unit weight of 16 kN/m^3 has been chosen, and the contribution of the self weight has been considered in all the analyses. As for the initial conditions, a geostatic situation has been set, with an initial value of $K_0 = 0.50$. All the analyses have been performed under the hypothesis of dry soil, which corresponds to the real situation in the laboratory tests.

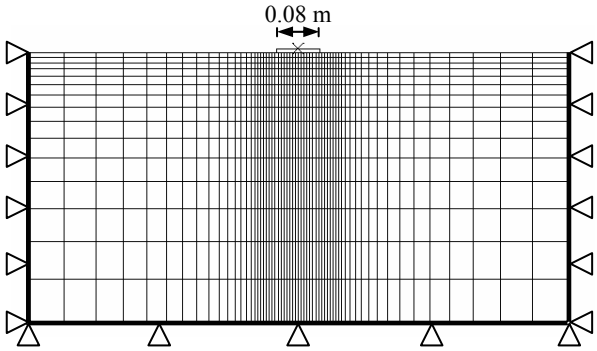

Fig. 4.2 FE mesh.

The 0.08 m wide foundation, on top of the mesh, has been modelled using rigid link elements R2D2, with a *tied* contact between footing and soil.

In order to verify the admissibility of such hypothesis, as anticipated in Section 4.1, a preliminary test has been performed and whose results are herein shown.

The *tied* contact has been replaced by a more realistic frictional one, with a friction angle assumed as 2/3 of the friction angle of the soil. So that, a rigid-perfectly plastic behaviour, as assumed in the theoretical frictional problem proposed by Mohr-Coulomb, has been chosen for this test.

The eccentric loading scheme of e/B=0.25 has been considered, and the final deformed configuration is shown in the contour plot in Fig. 4.3, with a scale factor equal to 2 for the displacements. As it can be easily observed, only a very limited amount of soil tends to loose contact with the footing, so that assuming that the footing remains in contact with the foundation can be considered a proper assumption.

Different variables have been plotted according to the different simulated tests: for vertical centred load tests, only the vertical load vs. vertical displacement is of interest, while for eccentric loading tests, in addition to the V-v plots, also momentum divided by B (M/B) versus rotation angle multiplied by B and vertical displacement versus rotation times B have been plotted and compared to the measurements. As for inclined loading tests, the results are presented in terms of V-v, horizontal load (H) versus horizontal displacement (u) and vertical (v) versus horizontal (u) displacement.

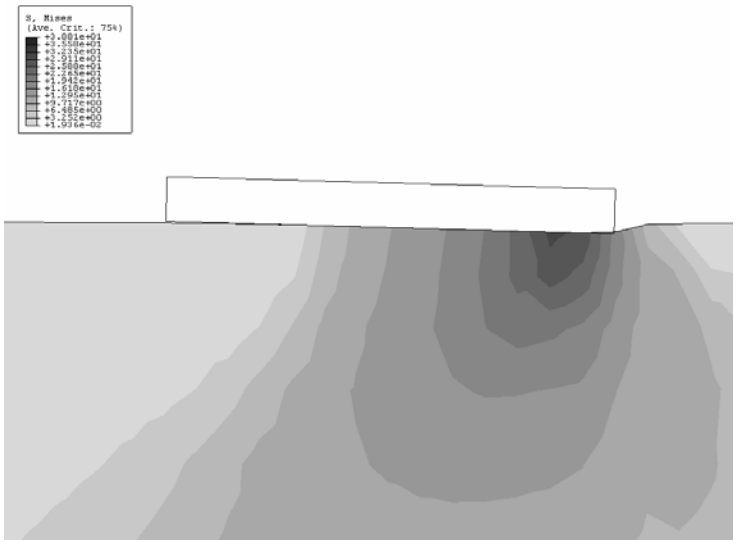

Fig. 4.3 e/B=0.2: deformed configuration (displacement scale = 2).

4.1.2 EMC parameters identification

Some of the constitutive parameters can be determined on the basis of the well-known mechanical characteristics of the dense Ticino sand used for the experimental tests: such parameters are the friction angle ϕ and the dilatancy ψ, which have been set to values of 40° and 20°, respectively for the first set of tests in which the depth of the foundation has been set to 0.24 m (a=3).

Considering a small value for the cohesion yield stress in correspondence to zero plastic strains ($c|_0$ = 0.05 kPa) only to ease the convergence of the FE analysis even at low stress levels, and 0.25 for the Poisson ratio ν, the remaining parameter to be calibrated is the Young modulus E, whose value has been identified through back-analysis on the basis of a centred vertical test.

Moreover, in addition to the comparison of the results obtained using CLoE, SSC and EMC models, a parametric study has been performed on the influence of the aspect ratio of the metallic plate used in the experimental tests on the reliability of the numerical predictions.

As for the FE model, all the different geometries have been modelled under the assumption of plane strain condition, thus requiring a different calibration for each test series.

The aim of such procedure is to verify the possibility to model as plane strain condition a even a geometry far from such theoretical assumption, as a square condition can be considered. This possibility allowing an important simplification from the computational point of view since the only way to properly model such a geometry would be a three-dimensional analysis, more expensive from a computational point of view.

In conclusion, throughout all the tests, for aspect ratios equal to 1 to 3, corresponding to the 0.08m x 0.08m square situation to a 0.08m x 0.24m foundation, respectively, the geometry of the FE model has been left unchanged, and only the parameters E and ϕ have been changed in order to match the experimental data for the centred vertical load test.

The resulting set of constitutive parameters is shown in Table 4.2 and the calibration curve are plotted in Fig. 4.4 and Fig. 4.5 in terms of vertical force versus downward displacements, for the different aspect ratios of a=1, a=2 and a=3, respectively.

E (kPa)	ν	ψ (°)	ϕ (°)	$c\|_0$ (kPa)
1400 (a=1)			29 (a=1)	
2600 (a=2)	0.25	20	37 (a=2)	0.05
3700 (a=3)			40 (a=3)	

Table 4.2 Constitutive parameters for the EMC model.

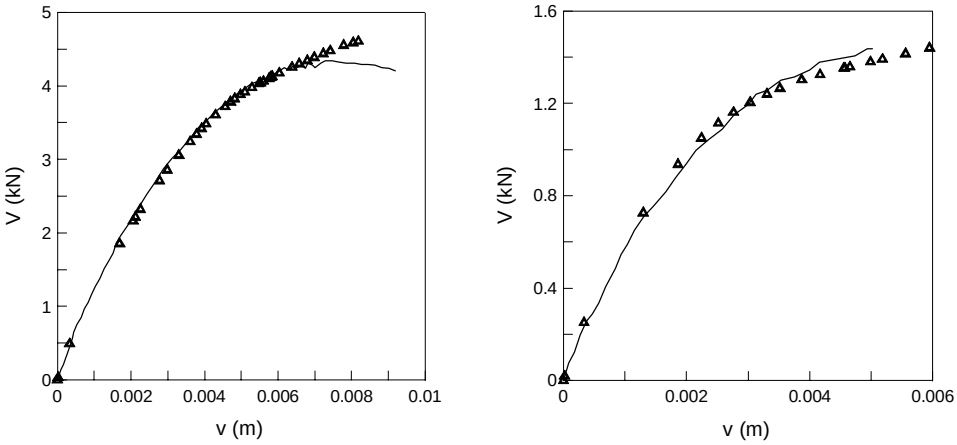

Fig. 4.4 EMC model. Calibration curves (a=1,2).

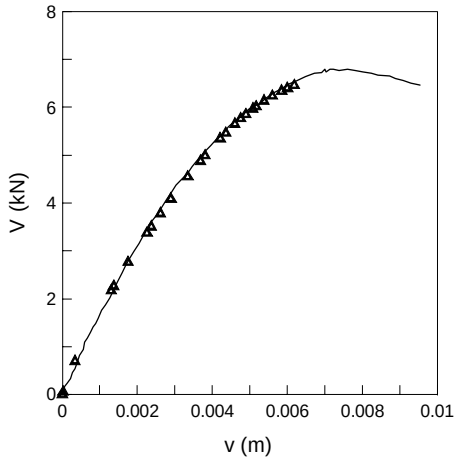

Fig. 4.5 EMC model. Calibration curves (a=3).

4.1.3 SSC parameters identification

Like for the EMC model, also for SSC model some of the parameters have been determined on the basis of the physical and mechanical characteristics of Ticino sand. Without specifying the meaning of all the parameters, whose description has already been carried out in Section 2.1.2, in Table 4.3 the set of constitutive parameters, resulting from the identification test presented in Fig. 4.6, is shown. In addition, the initial value for the hardening parameter, p_{c0}, was set to 5 kPa.

It is worth noting how the numerical values were chosen in order to reproduce the best fitting to the experimental data, through a trial-and-error procedure on the parameters which have been calibrated via back-analysis. It can be observed, however, that the ultimate load computed via numerical analyses is less than a half of the ultimate experimental vertical load. The initial upward concavity of the numerical curve is due to the small elastic nucleus created at the beginning of the analysis by imposing the value of p_{c0} = 5kPa: such an assumption has been imposed in order to avoid convergence problems when the state of stress addresses the critical state line with low confining pressures.

M	B	B_e	L	β	ξ
1.42	0.0009	0.0195	0.001	1.7	0.297

Table 4.3 Constitutive parameters for the SSC model.

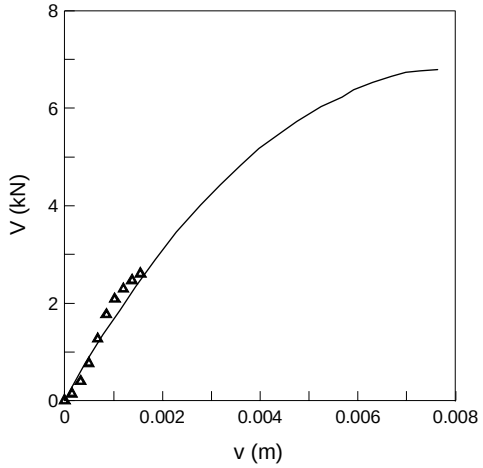

Fig. 4.6 SSC model. Calibration curves.

4.1.4 CLoE parameters identification

The identification of the parameters of the CLoE model is not straightforward: as shown in Section 2.2.1, the parameters have to be calibrated starting from the so called *basic stress paths*. Moreover, in order to simplify the identification procedure, it has been introduced a redundancy for some of the parameters, so that their values are often constrained each other. Therefore, one must be careful when determining the numerical values of such parameters, in order to avoid the violation of the mathematical constraints on them. A simple Excel spreadsheet has been developed (Desrues, 2004), giving the numerical values for the relevant parameters on the basis of the results of a triaxial compression and triaxial extension tests.

Since our main objective is the evaluation of the capability of different constitutive models to well capture the experimental behaviour, such triaxial tests have been simulated using the SSC model. In this way, the calibration of the parameters of the CLoE model is the only one which has not been carried out through a back analysis, since such a procedure is completely ineffective due to the large number of constitutive parameters of the hypoplastic model. The final set of calibration curves is shown in Fig. 4.7 and Fig. 4.8, and the corresponding parameters are listed in Table 4.4

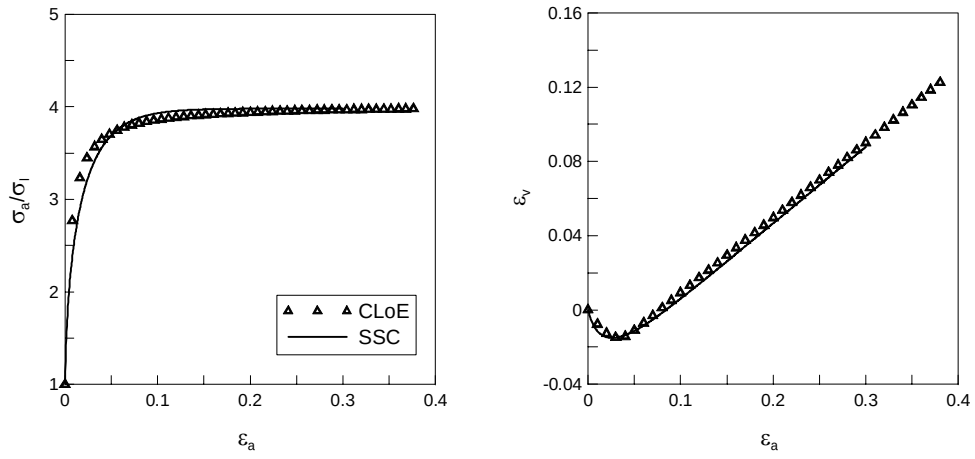

Fig. 4.7 CLoE model. Calibration curves for triaxial compression.

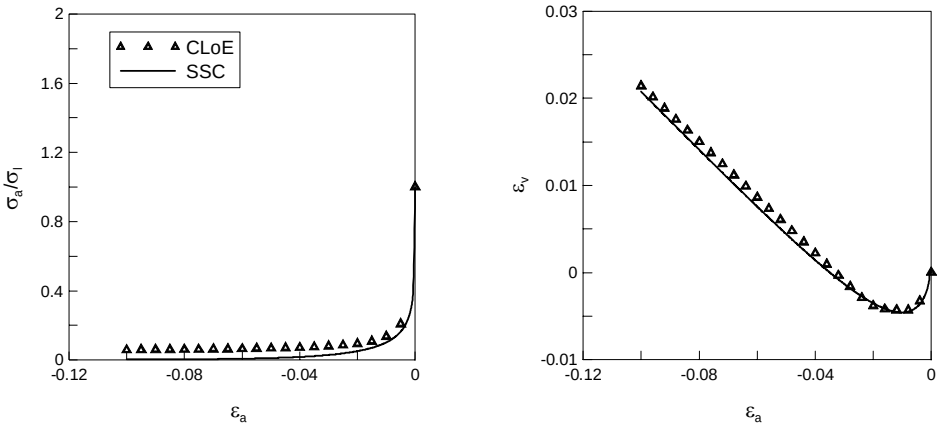

Fig. 4.8 CLoE model. Calibration curves for triaxial extension.

parameter	basic path	value
a_{hc}	triaxial compression	533.7217843
c_{hc}	triaxial compression	176.5658784
a_{pc}	triaxial compression	-13.7741047
b_{pc}	triaxial compression	0.9090909
p_{fc}	triaxial compression	-0.4050000
x_{pc}	triaxial compression	0.0477015
a_{he}	triaxial extension	947.5645496
c_{he}	triaxial extension	-996.5431752
a_1	triaxial extension	13633.6228294
b_1	triaxial extension	81.0198360
c_1	triaxial extension	-0.7121800
x_{m2}	triaxial extension	-0.0066000
x_c	triaxial extension	-0.0072600
a_{bi}	triaxial extension	-18264.4822307
c_{bi}	triaxial extension	0.0043100
x_{t2}	triaxial extension	-0.0236217
p_{fe}	triaxial extension	0.3200000
λ_c	isotropic compression	1500.0000000
λ_{co}	isotropic compression	151.1933019
λ_{ex}	isotropic compression	748.1742853
m_{co}	pseudo isotropic compression	1.2200000
m_{ex}	pseudo isotropic compression	1.0000000
a_{sl}	limit surface	0.6803909
b_{sl}	limit surface	-0.1556271
n_{sl}	limit surface (Van Eekelen, 1980)	-0.2500000
omcis	(Chambon et al., 1994)	0.35

Table 4.4 Constitutive parameters for the CLoE model.

Due to the procedure above described for the calibration of the numerical values of the constitutive parameters, even the simple centred vertical load tests are predictions, but for completeness of presentation, such results are given in this section, mainly devoted to back-analysis calibration, and they are shown in Fig. 4.9.

As it can be observed, the CLoE model, which has shown excellent results when large unloading stress paths are followed, e.g. in case of deep excavation problems (Leoni et al., 2003; Viggiani and Tamagnini, 2000), is much far from the experimental results from both the qualitative and quantitative point of view, when modelling the relatively simple loading paths involved in the case of shallow foundations.

A further study, which goes beyond the scope of this work, should be carried out in order to investigate on the reasons of such a poor quality of the predictions.

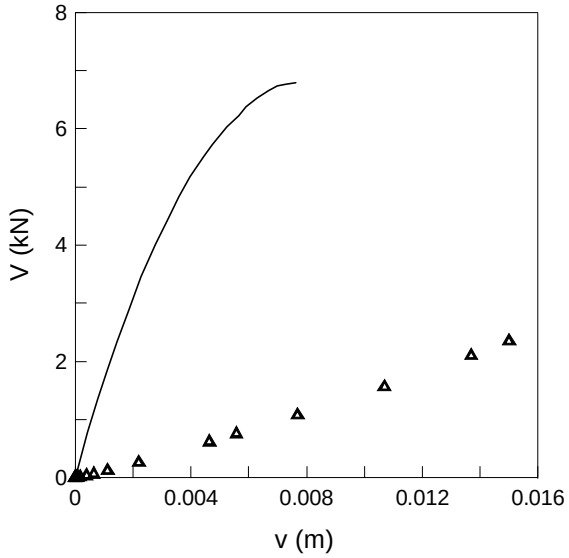

Fig. 4.9 CLoE model. Centred vertical load test.

4.2 Analysis results

In this section the numerical-experimental comparisons are presented. The results are shown depending on the particular loading scheme, separately for each constitutive model: CLoE, SSC and EMC.

Due to the procedure adopted for the identification of the numerical values of the constitutive parameters, tests performed with EMC and SSC can be regarded as “class B1” predictions, according to the definition given in (Lambe, 1973).

Such a procedure requires the execution of a preliminary test, in this case a centred vertical load test, that will be the basis for the calibration of some of the parameters.

On the other side, for the CLoE model, the classical procedure for “class A” predictions has been followed, since the calibration of the constitutive parameters has been carried out on the basis of triaxial compression and extension tests.

As a concluding comparison, a parametric study has been performed by analysing the reliability of the predictions evaluated on the basis of a relative error, defined as difference between measurements and numerical results varying the aspect ratio of the metallic plates, for different load inclinations and at different load levels.

Throughout all the plots shown in this Section, the solid line represents the reference measurements, while the symbols are the numerical predictions.

4.2.1 Inclined load VH3, VH8, VH14

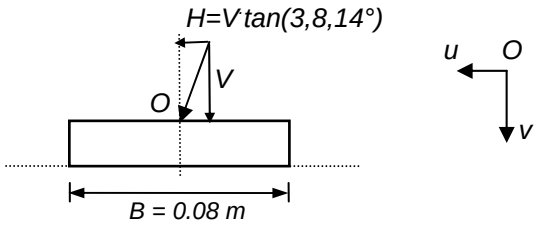

Fig. 4.10 Load scheme and variables.

The first set of loading scheme that has been considered, apart from the centred vertical load which has been used for calibrating the constitutive parameters, is a set of inclined loads.

The inclination angle has been set according to the real disposition of the experimental inclinations, say 3, 8 and 14 degrees. In this first set of tests it has been focused only on the situation of aspect ratio a=3, corresponding to an out-of-plane depth of the metallic plate of 0.24 m. This situation, among the three considered in the experiments (a=1,2,3) is the closest to the assumption of plane strain condition for the numerical analyses.

For this set of comparisons, the results are presented in terms of vertical load versus vertical displacement (V-v), horizontal component versus horizontal displacement (H-u), and vertical versus horizontal displacement (v-u).

In Fig. 4.11 and Fig. 4.12 the results obtained with the hypoplastic CLoE model are shown: as expected due to the difficulties in modelling even a simple centred vertical test, this model gives predictions far from the experimental measurements.

In particular, the behaviour of the soil appears to be mainly elastic and collapse is reached without a significant approach to an asymptotic value.

Such a shortcoming is evident in almost all the plots, for all the different inclinations. It is worth noting how this different behaviour stems from an almost identical behaviour for triaxial tests at single Gauss point level, as shown in the calibration curves (Fig. 4.7 and Fig. 4.8).

Going deeper into the analysis of the results, it can be observed that the V-v curves (A1, B1 and C1) in Fig. 4.11 and Fig. 4.12, show how the response predicted using the CLoE model is only slightly influenced by the load inclination.

Moreover, the H-u curves (A2,B2 and C2) are more sensitive to the inclination, even though they are still far away the experimental measurements. However, in both sets of curves, the concavity remains upward directed, thus in contrast with the experimental curves.

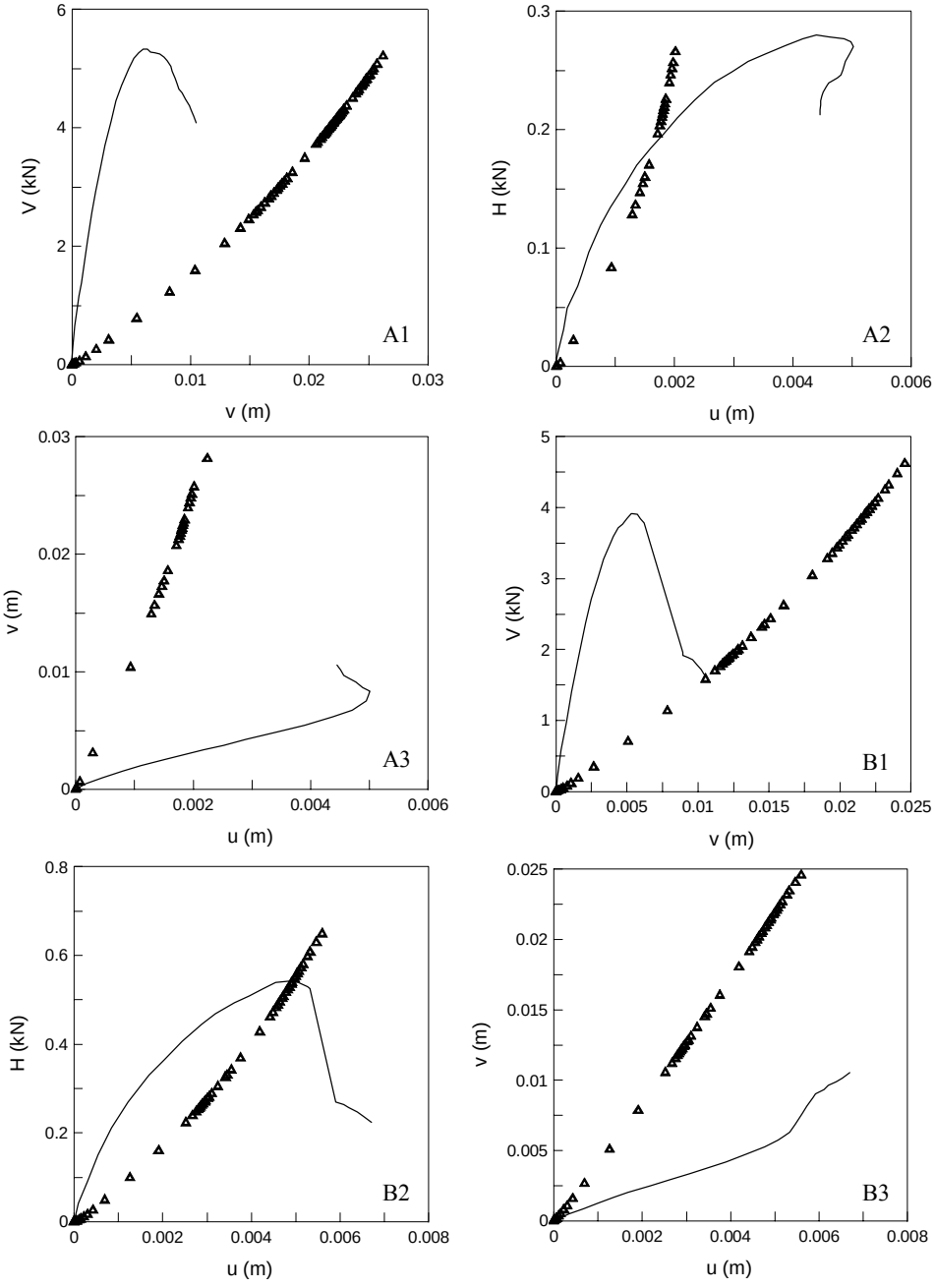

Fig. 4.11 CLoE model A1-A3: VH3, B1-B3: VH8.

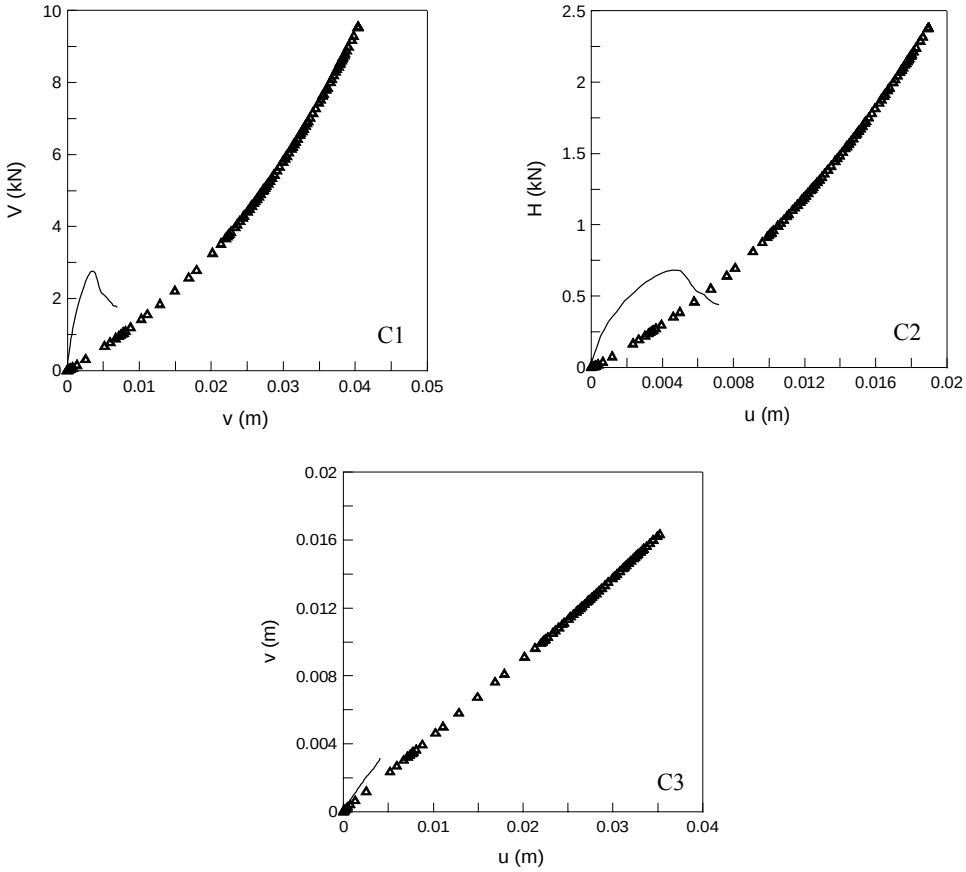

Fig. 4.12 CLoE model. C1-C3: VH14.

From the observation of the displacement curves u-v (A3,B3 and C3) a progressive improvement of the predictions is shown: the analysis results are more consistent with the measurements at least from a qualitative point of view, since they are both shaped as a straight line.

The inclination of such lines is far from the experimental one when load is almost vertical, while tends to approach the measurements with as much as the inclination increases.

However, this seems to be an incidental result and not really due to the effectiveness of the model in capturing the behaviour of the system soil-structure.

Considering the large differences both from a qualitative and quantitative point of view, it seems to be useless to dwell upon further details.

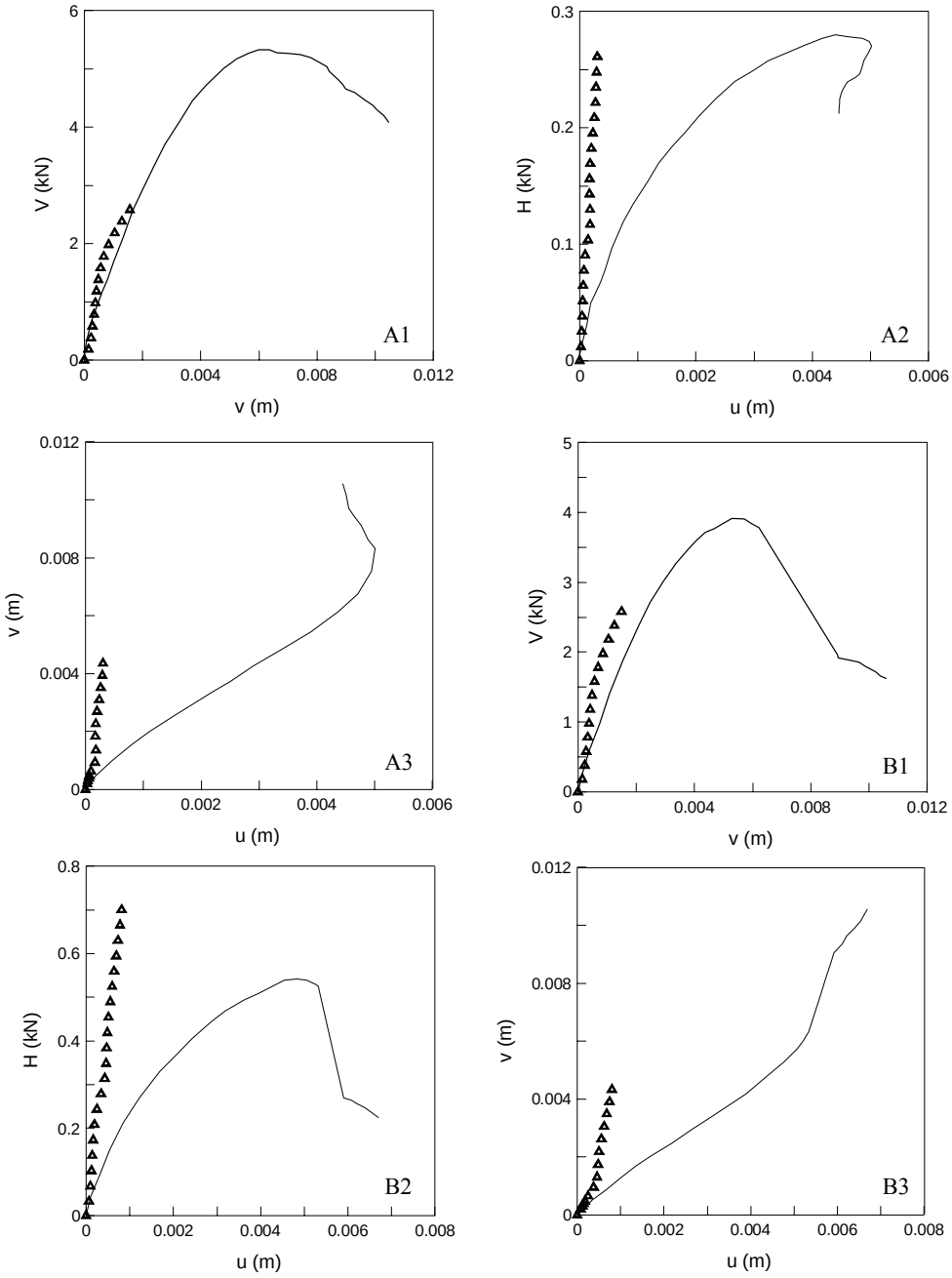

Fig. 4.14 SSC model. A1-A3: VH3, B1-B3: VH8.

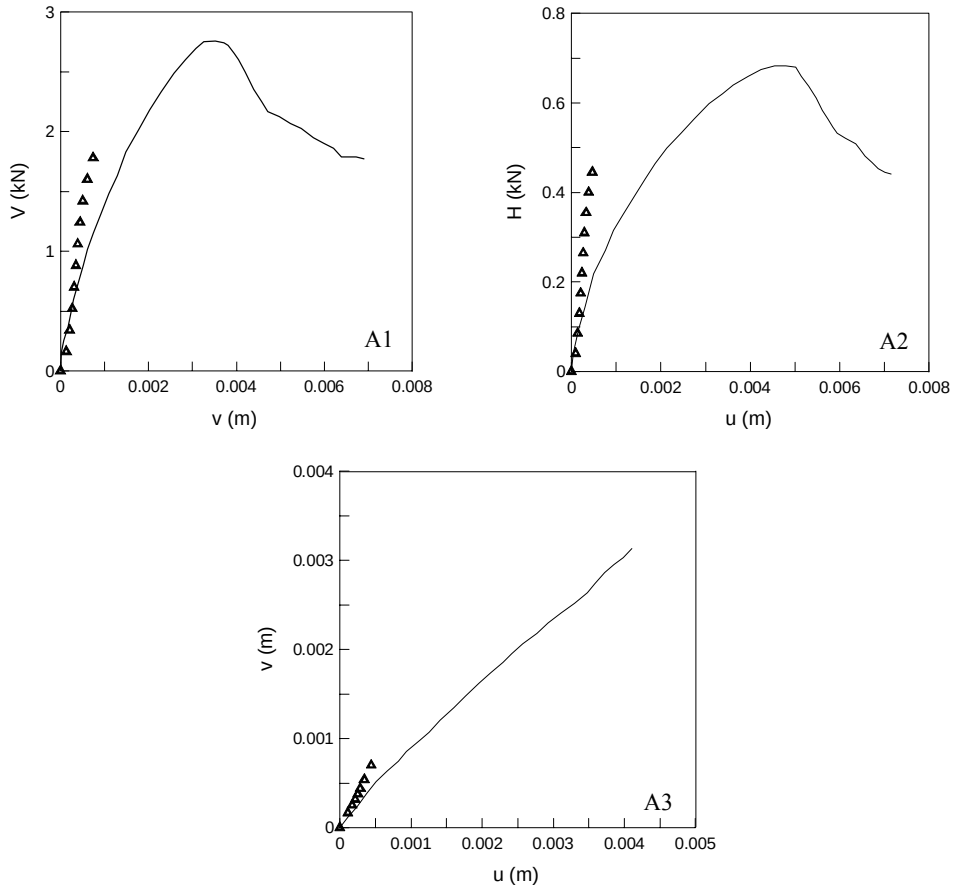

Fig. 4.15 SSC model. A1-A3: VH14.

As for the SSC model is concerned, results are plotted in Fig. 4.14 and Fig. 4.15. In terms of V-v curves (A1, B1 and C1), FE results are not far from the measurements, even if only a percentage of the experimental limit load is reached.

However, a deterioration in the predictions is observed with the increase of the load inclination, as it can be observed by comparing A1 with B1 and C1, which can be explained considering that the identification has been carried out starting from a centred vertical test.

H-u results (A2, B2, and C2), are undoubtedly far from the measurements thus reflecting also on the u-v predictions (A3, B3 and C3).

In particular, the problems encountered in the calibration tests, in which only a small part of the ultimate load was mobilized, negatively influences all the further predictions.

As compared to the results obtained with the CLoE model, however, provided that large differences are still present in the predictions, such discrepancies are less eminent and mostly limited to the quantitative point of view.

Moreover, it is worth noting how the predictions in terms of horizontal displacements are strongly influenced by the assumption of perfectly rough (*tied*) contact between footing and soil. The role played by this simplifying hypothesis is less substantial when the horizontal load component becomes less important.

To conclude the comparisons about the case of inclined loads, the results concerning the EMC model are presented.

It is evident a good agreement between computed displacements and measurements, not only for the V-v curves shown in A1, B1 and C1 (Fig. 4.16), but also for the more "difficult" H-u curves A2, B2 and C2.

In particular, as for v-u plot A3, the qualitative result is consistent with the measurements, while a limited quantitative difference appears: thus can be explained observing graph A2, in which horizontal displacements are slightly underestimated, thus reflecting on the higher slope of curve in A3. Similar observations can be drawn about the other v-u plots (B2 and C2).

As it can be easily observed, the quality of the predictions is barely influenced by the load inclination, since with this constitutive model, the results of the FE analyses are particularly close to the experimental results throughout all the tests.

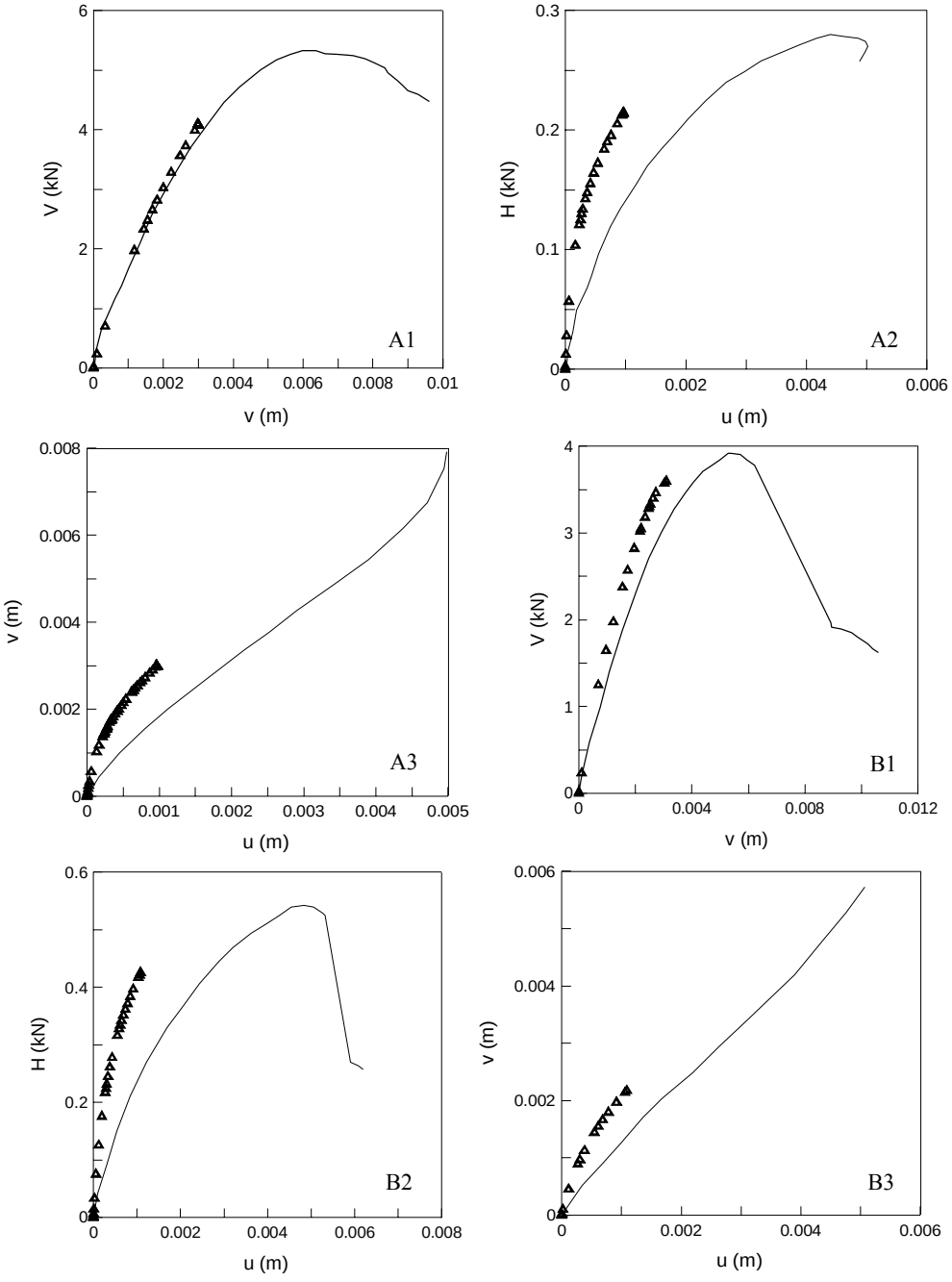

Fig. 4.16 EMC model. A1-A3: VH3, B1-B3: VH8.

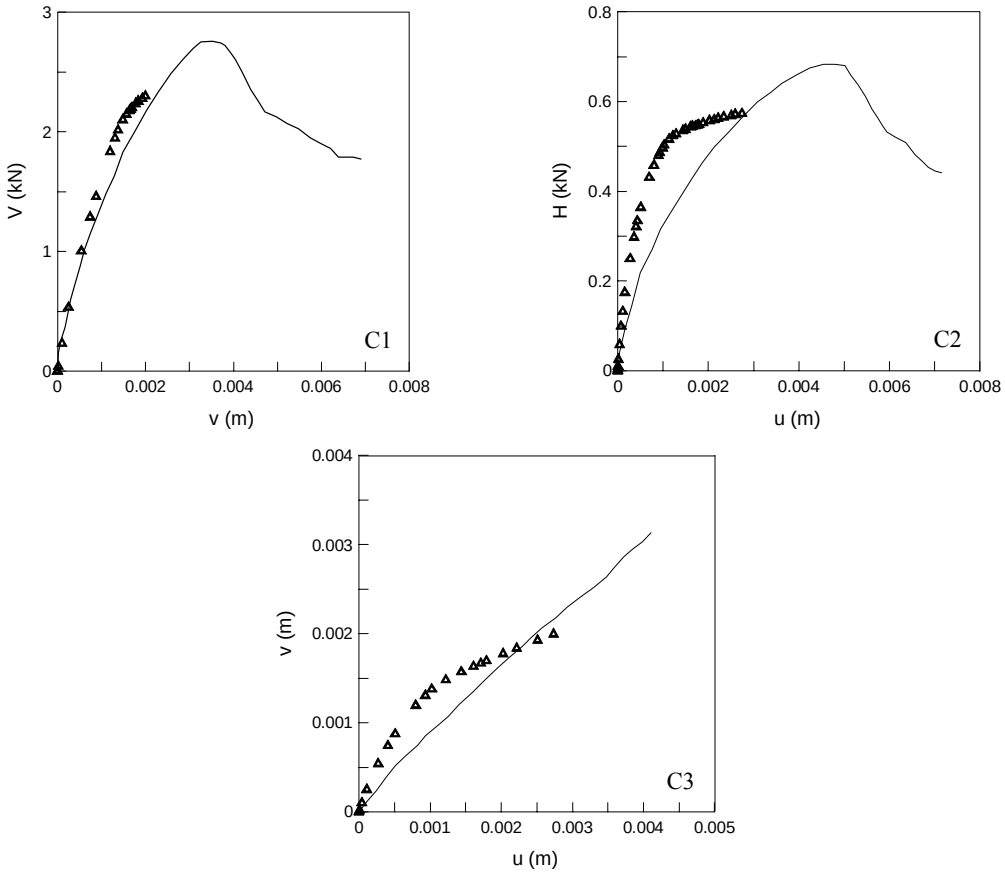

Fig. 4.17 EMC model. C1-C3: VH14.

4.2.2 Vertical-Horizontal load V150H

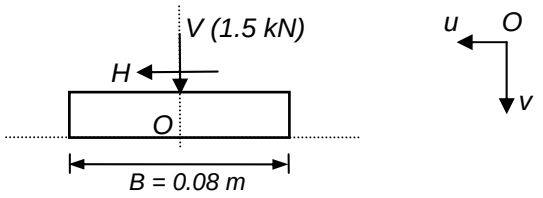

Fig. 4.18 Load scheme and variables

Another loading scheme modelled through FE analyses is the V150H: a centred vertical load is applied, in this case until an overall force of 1.5 kN is reached, followed by the application of an horizontal force until failure while the vertical component is kept constant (Fig. 4.18).

The out-of-plane depth of the foundation for the experimental tests considered in these comparisons is again 0.24 m, thus giving an aspect ratio a=3.

This particular loading scheme should follow the V-v calibration curves, shown in Section 4.1, until the vertical load chosen for each test series, apart from some minor differences due to the uncertainties involved in each laboratory test.

The coupling between vertical and horizontal forces and the corresponding displacements, provokes an increase in vertical displacements during the application of horizontal load even if the vertical load is kept constant.

For the sake of clarity the comparisons are shown in separate figures (Fig. 4.19, Fig. 4.20 and Fig. 4.21) for each considered constitutive model.

The analysis performed using the CLoE model shows a behaviour that reproduces the shapes of the experimental results, but the numerical values are still far the measurements.

In particular, in Fig. 4.19 A1 the additional vertical displacement due to the vertical load is well captured, but the displacement predicted for the initial loading phase is much larger than the measured one. Not far from reality is the H-u graph (Fig. 4.19 A2): a good prediction of the shape of the experimental curve is shown, even if this comes with an overestimated displacement.

As expected, all these problems can be retrieved in the last chart (Fig. 4.19 A3) where vertical displacement is plotted versus the horizontal one: it is worth noting, however, how, as for the shape, the predictions are not far from the experimental results.

As far as the SSC model is concerned, in Fig. 4.20 A1 the initial part of the numerical curve shows a clear elastic behaviour due to the initial value of the hardening parameter p_{c0}. Such effect, however, tends to disappear even for very low values of vertical load.

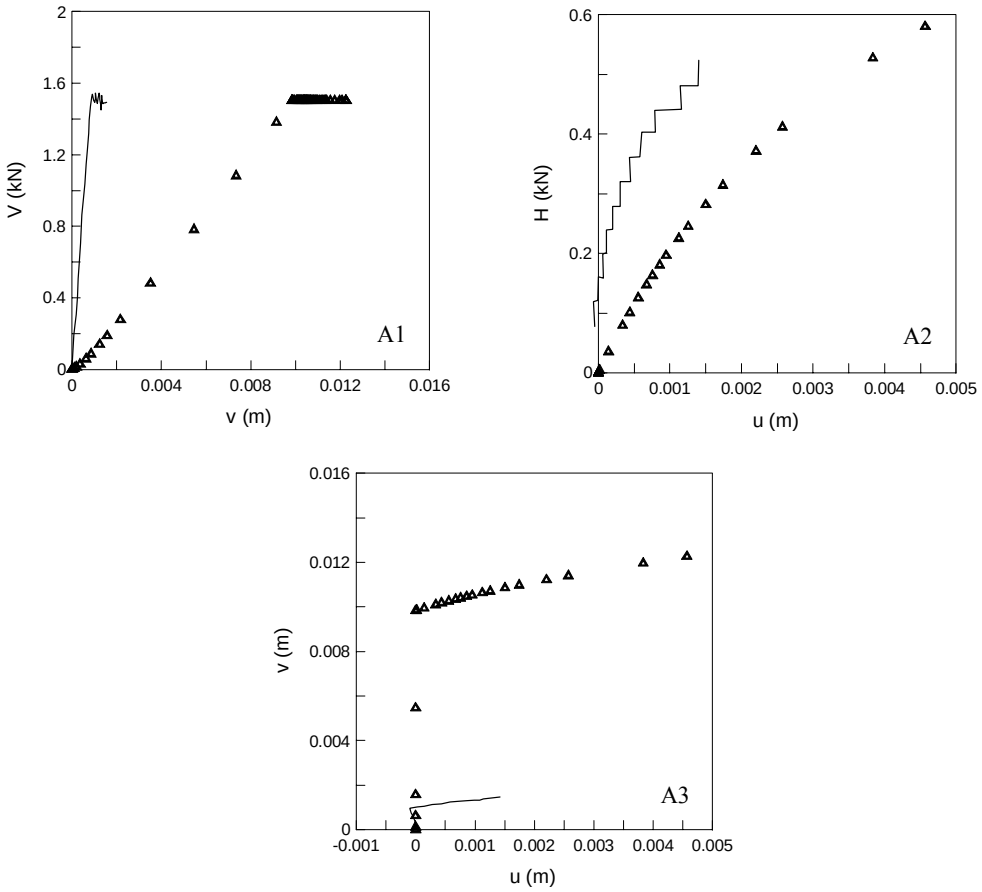

Fig. 4.19 CLoE model. A1-A3: V150H.

The further comparison, concerning the H-u curves (Fig. 4.20 A2) shows an acceptable agreement: the concavity of the numerical curve is less pronounced, however the predicted values are close enough to the measurements if values of horizontal load far from the failure load.

A further comment can be made about the capability of the model to capture the limit horizontal load in this test, even if the corresponding horizontal displacements are less that a half of the measured ones, thus negatively influencing the v-h curve shown in Fig. 4.20 A3.

As observed for the previous set of tests, the EMC model gives the more satisfactory results, as shown in Fig. 4.21 A1-A3.

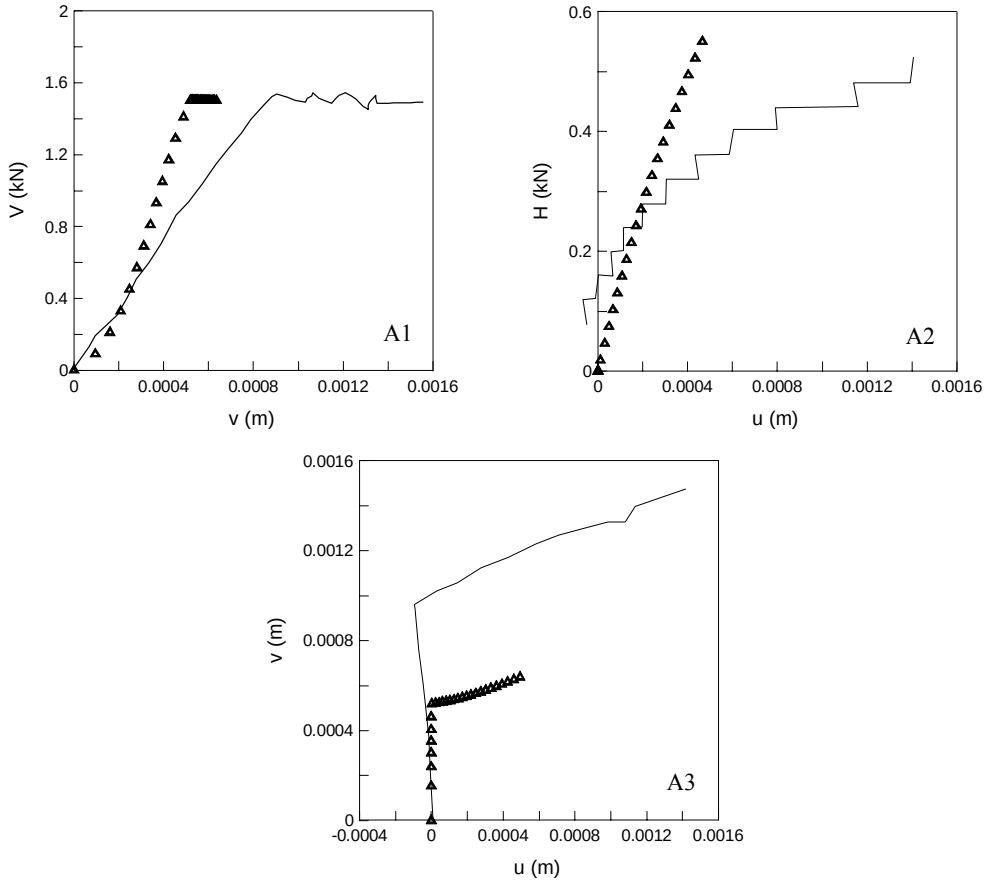

Fig. 4.20 SSC model. A1-A3: V150H.

In particular, the settlement computed with the vertical load applied in the first step of the test is in almost perfect agreement with the experimental measurements.

In the further step, when the horizontal component is added to the vertical part, which is kept constant once the final value is reached at the end of the previous step, the horizontal displacement of the foundation is again in excellent agreement with the measured one.

It can be observed, moreover, the more than satisfactory prediction of the vertical settlement due to the application of the vertical component (Fig. 4.21 A1)

Such a good prediction is summarized in Fig. 4.21 A3, in which the vertical settlement is related to the horizontal displacement of the foundation: in this case, an overall excellent result can be observed from both qualitative and quantitative point of view.

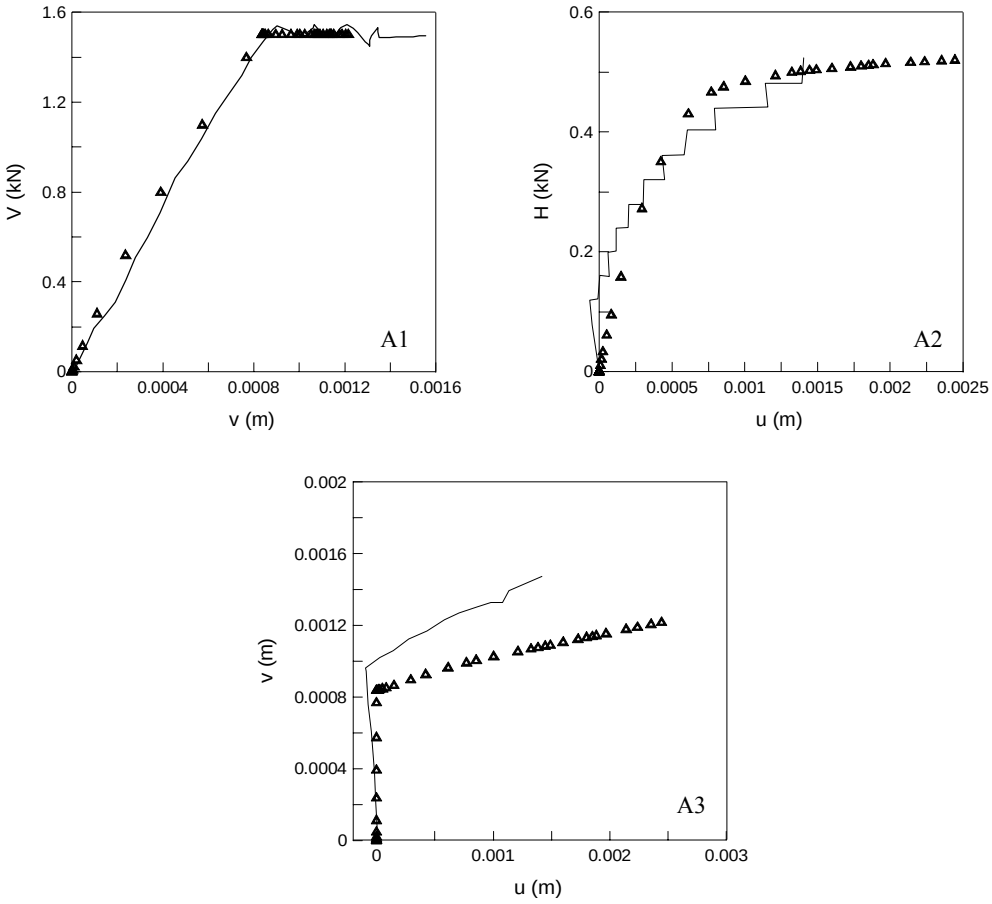

Fig. 4.21 EMC model. A1-A3: V150H.

4.2.3 Eccentric load e/B=0.125, e/B=0.25

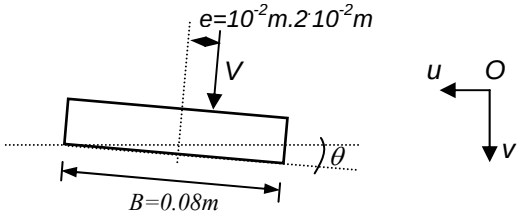

Fig. 4.22 Load scheme and variables.

In this section the FE analysis results obtained from the modelling of the application of an eccentric load on the metallic plate are shown.

Considering the results of the previous tests, the CLoE model has been excluded from the comparison, since it has shown strong limitation in capturing the experimental behaviour even in simple centred vertical load tests.

Therefore, only the results obtained with SSC and EMC model will be presented. As a result, the quality of the predictions shown using SSC model are good but they are still underestimating as far as the prediction of the limit load is concerned, while predictions of the settlements far from the limit load are good in relation to the measurements.

It is worth noting, that the shape described by the numerical plots is not always smooth as expected, thus showing fast changes in slope.

The results concerning the small eccentricity, e/B=0.125, shown in Fig. 4.23 A1-A3 are in a better agreement with the experimental measurements than series B1-B3, showing the same loading scheme of eccentric load, but this time with a larger eccentricity (e/B=0.25).

Also for this set of comparisons, the best result is the one given by the EMC model. Fig. 4.23 A1-A3 and B1-B3 undoubtedly reveal the effectiveness of such a model in capturing the experimental displacements and rotations.

In particular, Fig. 4.23 A2 shows how the FE analysis is perfectly matching the experimental curve in terms of vertical displacements versus angle of rotation of the foundation multiplied by the width B.

With the increase of the eccentricity, whose corresponding tests are shown in Fig. 4.23 B1 to B3, the apparent major differences in Fig. 4.23 become less important considering the initial shape of the experimental curve, which has been probably affected by a measurement error.

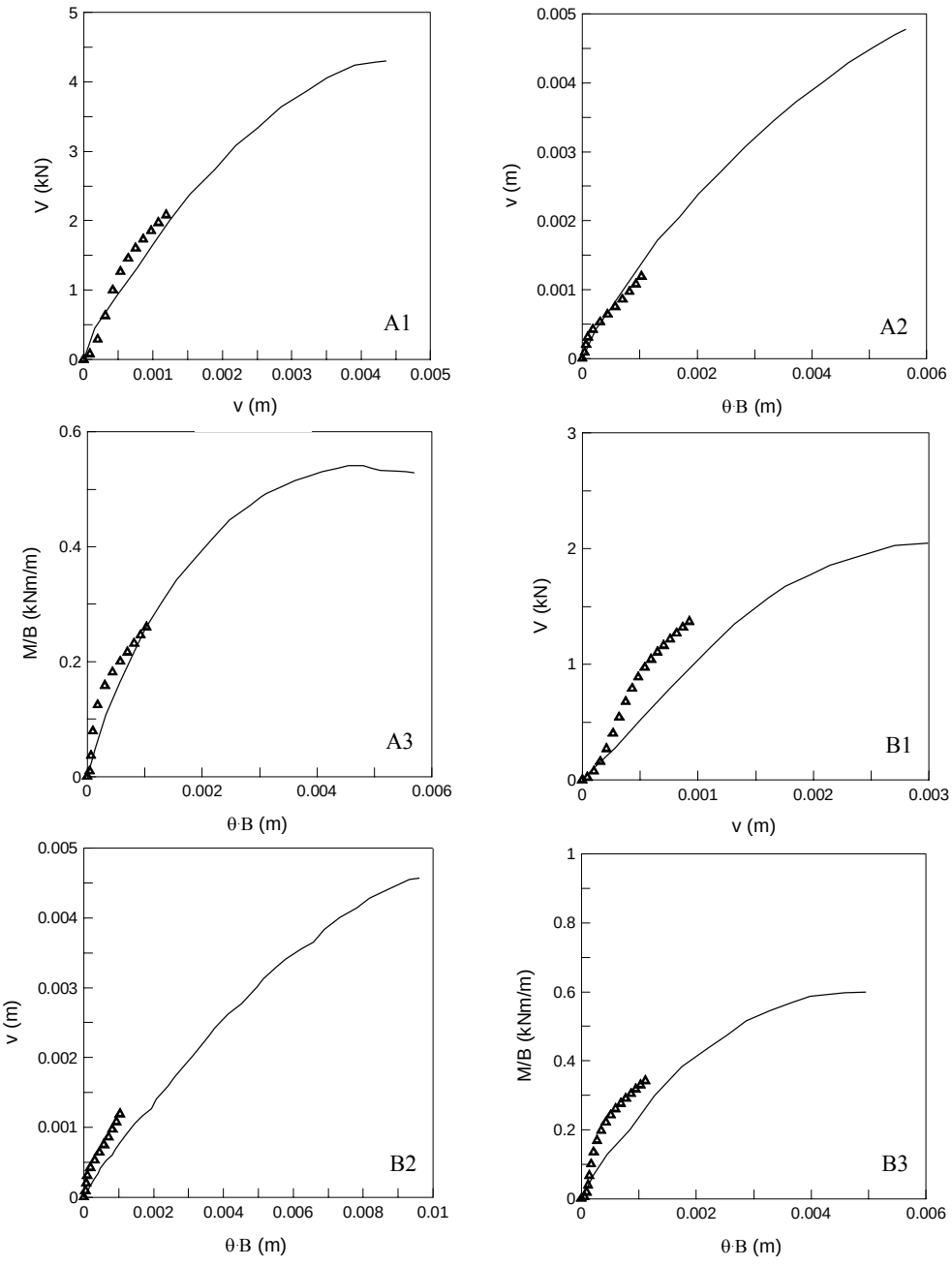

Fig. 4.23 SSC model. A1-A3: e/B=0.125 B1-B3: e/B=0.25.

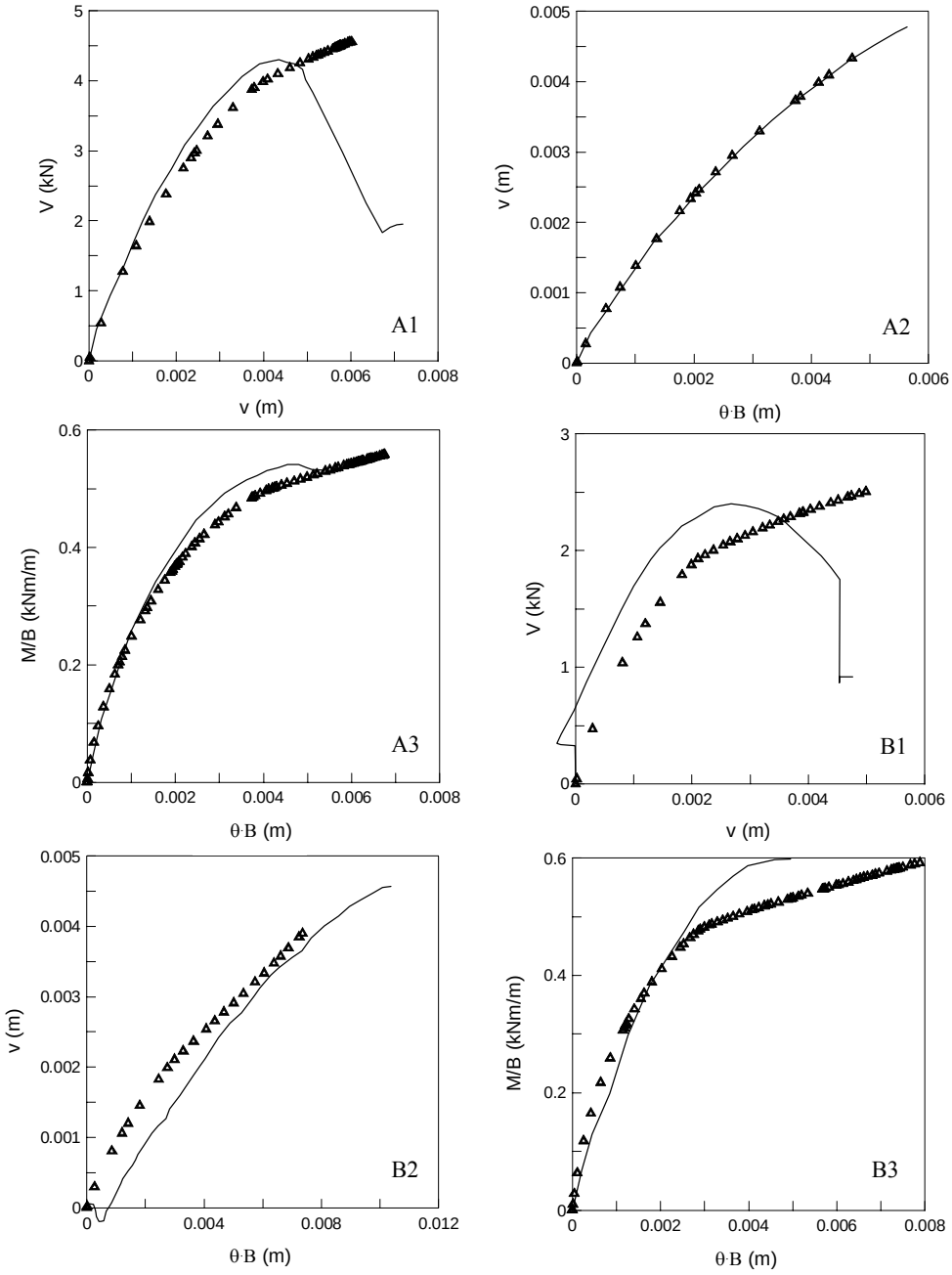

Fig. 4.24 EMC model. A1-A3: e/B=0.125 B1-B3: e/B=0.25.

4.2.4 Parametric comparison for EMC model

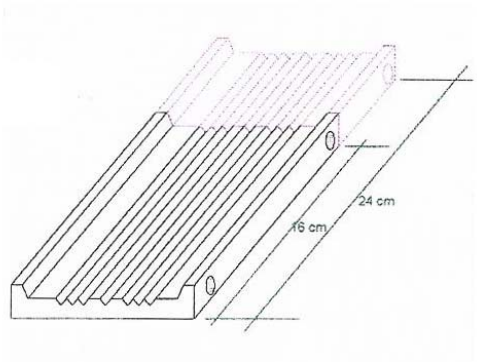

Fig. 4.25 Shapes of metallic plates.

As shown in the previous Sections, as of this point only the experimental measurements concerning a rectangular 0.08x0.24 m foundation has been taken as a reference, being such a geometry the closest to a plane strain condition.

Considering the good performance of the EMC model, as shown by the results presented in this Chapter, it has been explored the possibility, as sketched in Section 4.1.2, to model even different geometries with an aspect ratio a=1 and a=2, corresponding to the out-of-plane depths of 0.08 m and 0.16 m, respectively, which were involved in the laboratory tests.

In these further tests, the same plane strain assumption for the FE analyses, but a different set of values of constitutive parameters has been used, whose calibration has been carried out as explained in Section 4.1.2.

This further set of tests is mainly focused on an evaluation of the possibility to use a simple constitutive model, like the EMC already embedded in the library of constitutive models of the ABAQUS code, with a simple 2D FE model representing the real three-dimensional problem.

As shown in Table 4.1 and recalled in Table 4.5, the numerical analyses have been performed according to the availability of experimental measurements, so that a systematic comparison can be performed only on the results of the tests performed with the same loading scheme when varying the only aspect ratio.

Let us focus first on the inclined load tests: such a large set of data requires an easy way to represent the results in order to have a clear information about the quality of the predictions.

To this end only the V-v tests have been taken into account, and a relative error has been defined as shown in 4.1, where v_{FE} is the vertical displacement as predicted in the FE analyses corresponding to a given percentage of the limit load as evaluated in the laboratory,

EMC (a=1)	EMC (a=2)	EMC (a=3)
(CV)	(CV)	(CV)
VH3	VH3	VH3
VH8	VH8	VH8
VH14	VH14	VH14
V30H	V100H	V150H
e/B=0.125	e/B=0.125	e/B=0.125
-	e/B=0.25	e/B=0.25

Table 4.5 EMC mode: Set of FE analyses performed.

$$err\% = \frac{\left|v_{FE} - v_{LAB}\right|}{v_{LAB}} \cdot 100 \qquad 4.1$$

and v_{LAB} is the vertical settlement of the foundation measured during the test in correspondence of the same load level. The absolute value of their difference is therefore divided by v_{LAB} in order to make $err\%$ a dimensionless quantity.

The resulting set of data has been plot as shown in Fig. 4.29 to Fig. 4.31, for the three different load inclination which has been considered, namely 3, 8 and 14 degrees: the x values are represented by the different aspect ratios considered, that is a=1, 2 and 3. On the y axis the experimental limit load percentages are considered, and the lines contoured in the plots correspond to *isoerror* lines.

As it can be observed, when the load inclination is small, namely 3 degrees, there is a wide area of the plot in which the $err\%$ is less than the 25%, while the $err\%$ becomes higher when around a 10% or over 90% of the limit load is considered.

When increasing load inclination (8°, Fig. 4.30), such an area narrows, so that the high reliability area is restricted between 25% and 85% of the limit load.

When the load inclination is set to a value of 14 degrees (Fig. 4.31), the trend observed in the two previous contour plots is confirmed: the best area is now limited from 20% to less than 60% of the limit load, and it is more evident the influence of the aspect ratio on the quality of the predictions, since it is increasing with increasing abscissa, which corresponds to a higher value for the aspect ratio.

For the same tests, also a different representation is proposed: in Fig. 4.32, while the data represented on the vertical axis are the percentages of limit load, in the abscissa the load inclinations are plotted.

Summing up, in the first set of contour plots the load inclination has been considered as a parameter, while in this last set of plots the parameter was the aspect ratio.

Thus allowing to investigate, in the former case, the influence of the aspect ratio being constant the load inclination, while, in the latter, the influence of the load inclination with fixed aspect ratio has been studied.

The plot refers to the situation of an aspect ratio a=3, while in Fig. 4.33 and Fig. 4.34, the different situations in which a=2 and a=1 were respectively taken into account.

Considering an aspect ratio of a=3, as shown in Fig. 4.32, the per cent error is below 25% within a range o 20%-80% of the limit load with an evident worsening of the predictions when the load inclination increases to 14 degrees.

Such a behaviour is confirmed in Fig. 4.33 and Fig. 4.34, where the influence of the load inclination is more accentuated.

As a concluding remark, it can be observed how the influence of both the geometry of the foundation and the load inclination play a similar role on the quality of the predictions: indeed, their appropriate variation induce a similar effect on the isoerror maps.

As stated before, only the inclined load tests have been used for such a comparison, while the VxxxH and the eccentric load test results are shown only as a further confirmation of the effectiveness of the EMC model, and they are plotted in figures from Fig. 4.35 to Fig. 4.37

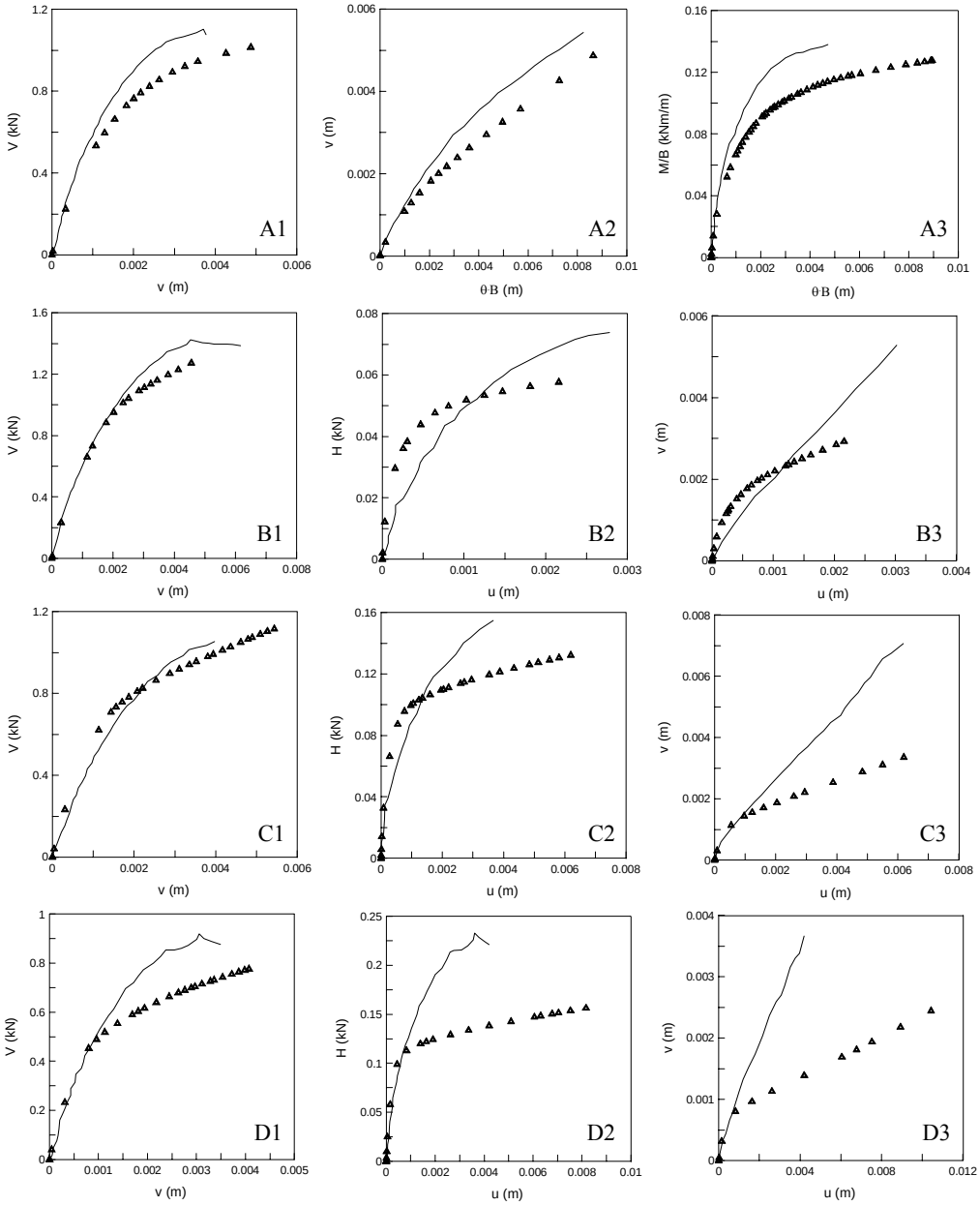

Fig. 4.26 EMC model, **a=1**. A1-A3: e/B=0.125 B1-B3: VH3 C1-C3: VH8 D1-D3: VH14.

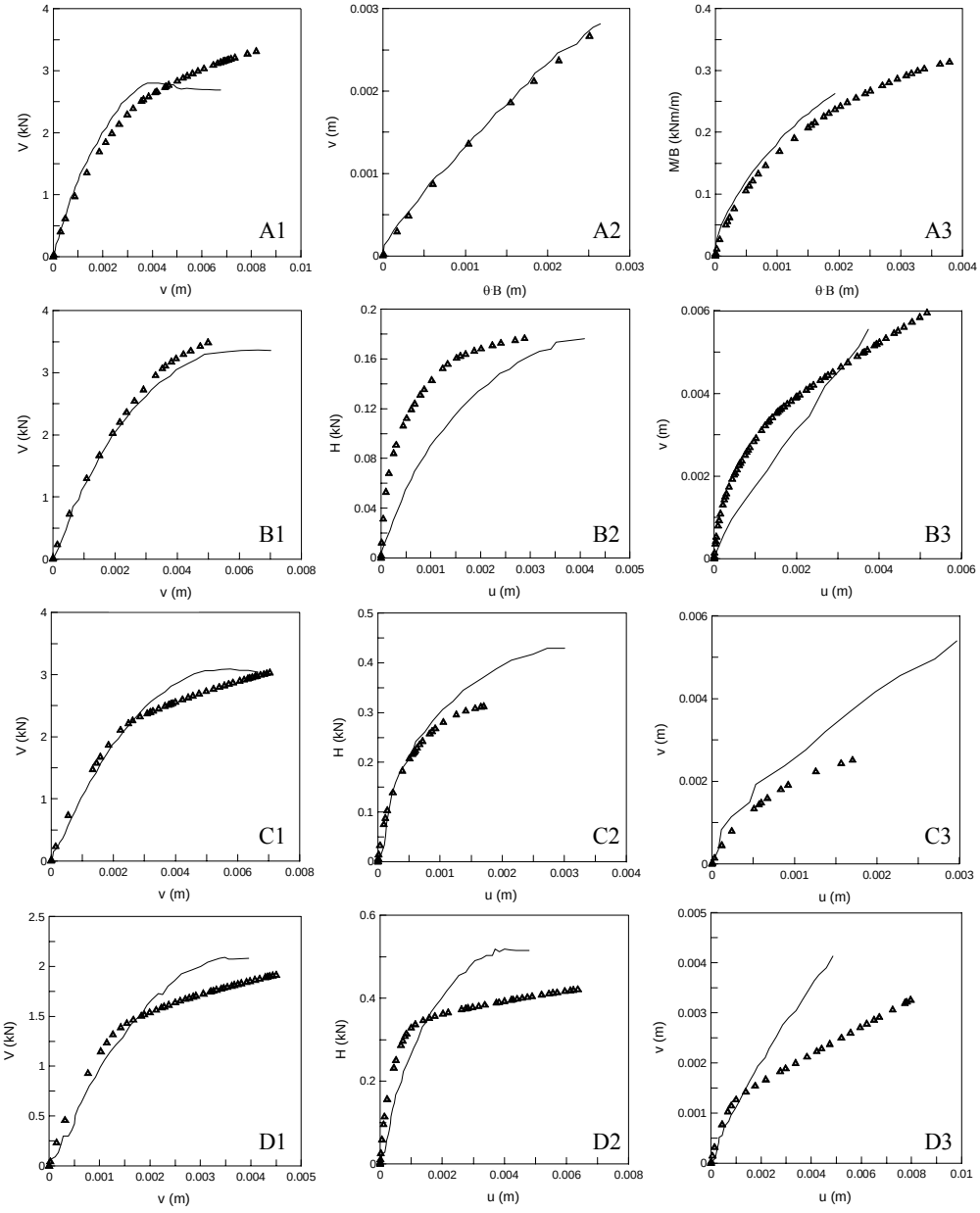

Fig. 4.27 EMC model, **a=2**. A1-A3: e/B=0.125 B1-B3: VH3 C1-C3: VH8 D1-D3: VH14.

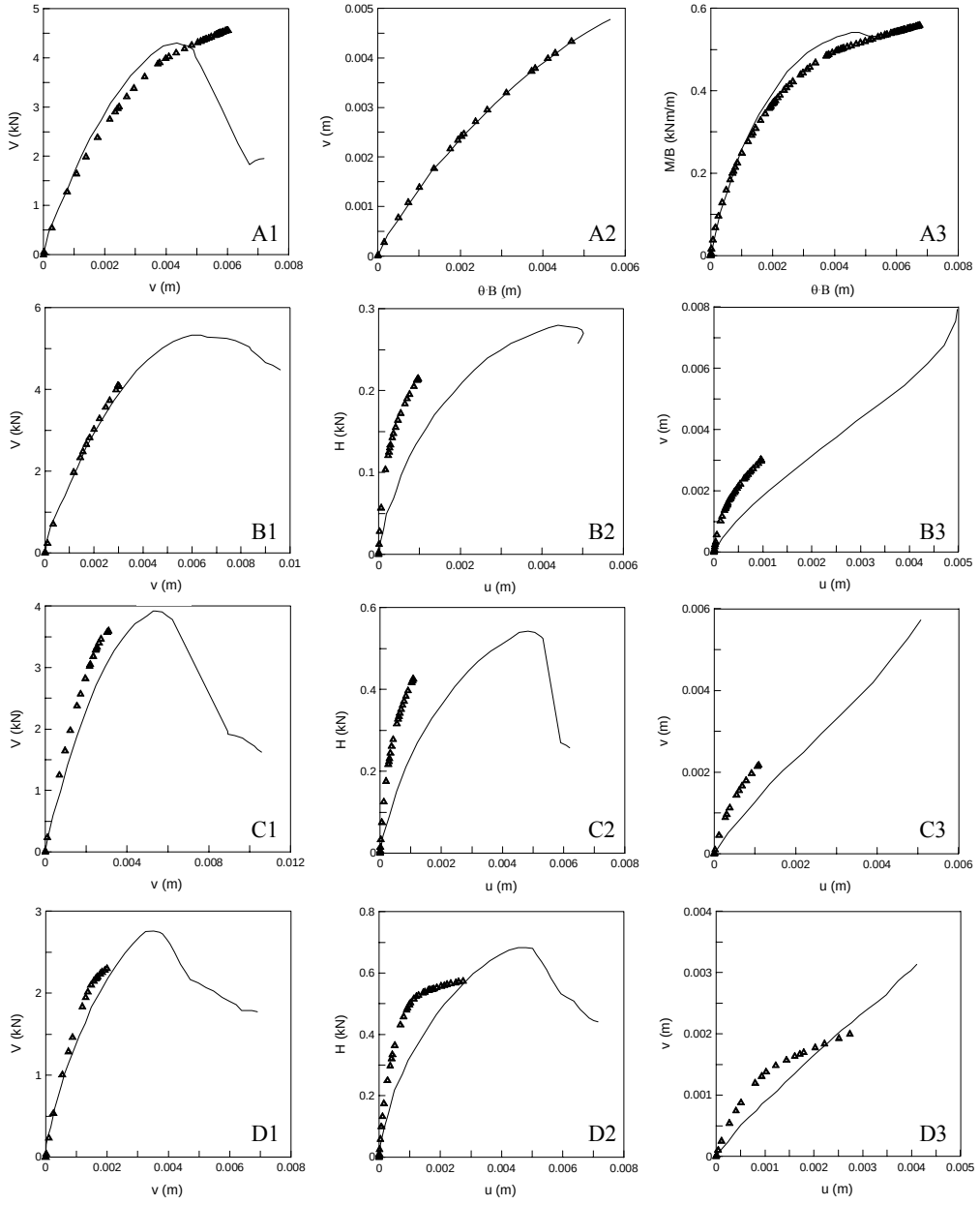

Fig. 4.28 EMC model, **a=3**. A1-A3: e/B=0.125 B1-B3: VH3 C1-C3: VH8 D1-D3: VH14.

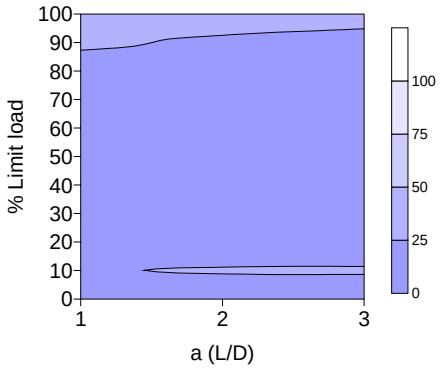

Fig. 4.29 EMC model. VH3.

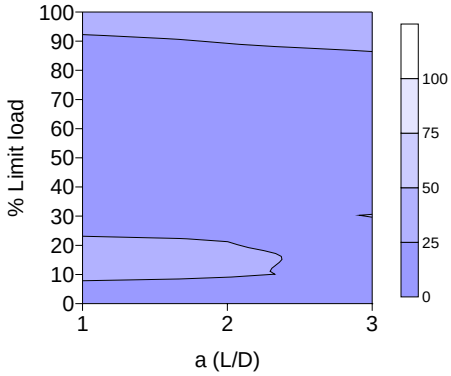

Fig. 4.30 EMC model. VH8.

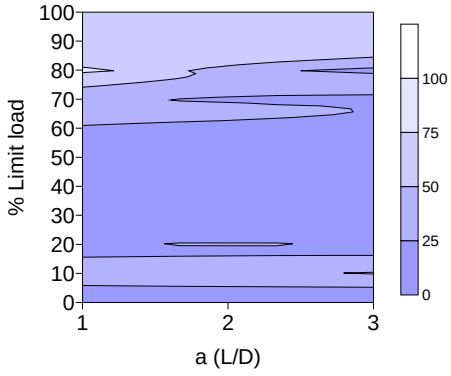

Fig. 4.31 EMC model. VH14.

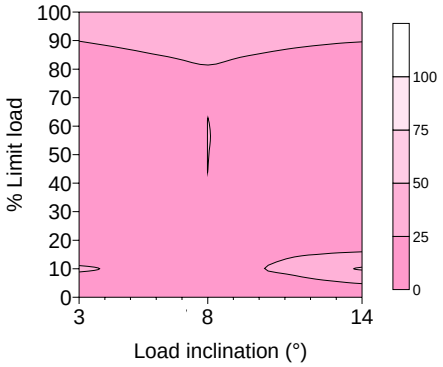

Fig. 4.32 EMC model: a=3.

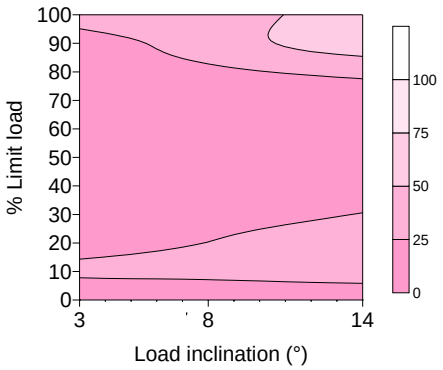

Fig. 4.33 EMC model: a=2.

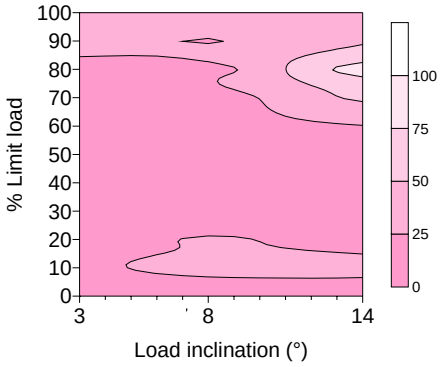

Fig. 4.34 EMC model: a=1.

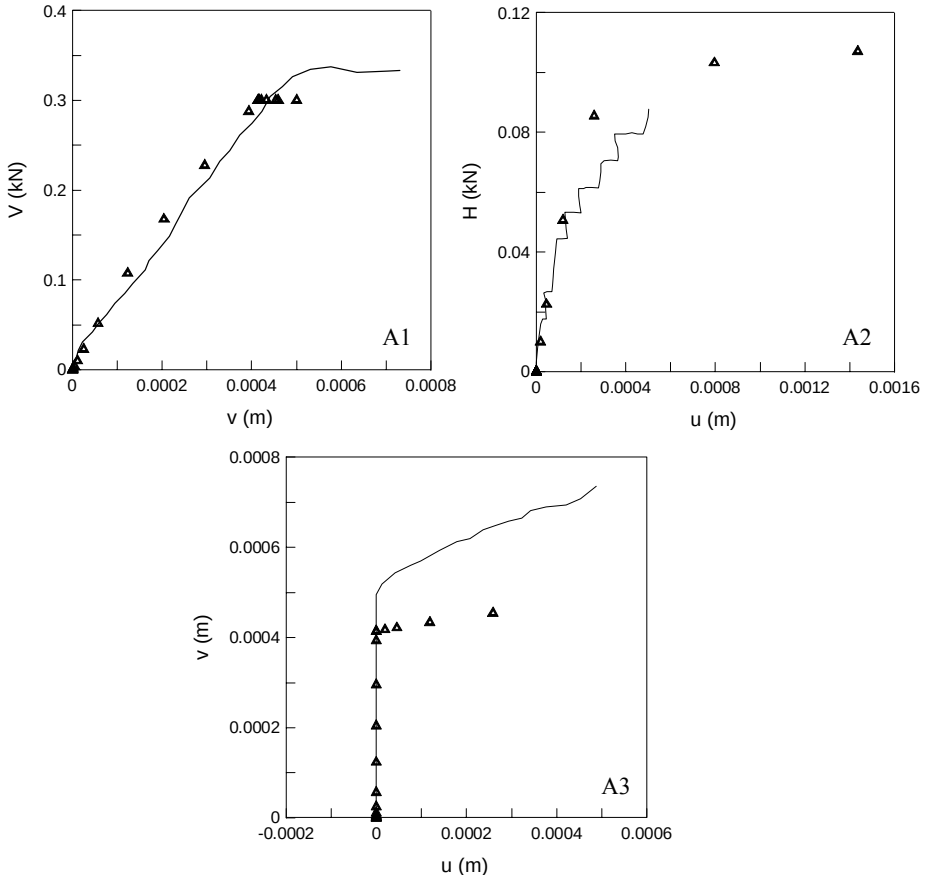

Fig. 4.35 EMC model, **a=1**. V30H.

Starting with the analysis of the result obtained from the numerical-experimental comparison in the case of square 0.08 m x 0.08 m foundation (a=1) for a V30H test, shown in Fig. 4.35, the numerical results are again in good agreement with the measurements, both from a qualitative and quantitative point of view. In this test, the shape of the foundation seems to have a minor influence on the quality of the results.

In Fig. 4.36 the results concerning the a=2 configuration are shown. The choice of the tests has been conditioned by the availability of laboratory measurements, and a comparison with the previous case of a=1 (and with the next a=3) is therefore impossible.

We just observe the good agreement of the numerical predictions with the experiments, both for the e/B=0.25 test (A1, A2 and A3) and for the V100H test (B1, B2 and B3), and will not be dwelt on Fig. 4.37, in which some results with a=3 are shown.

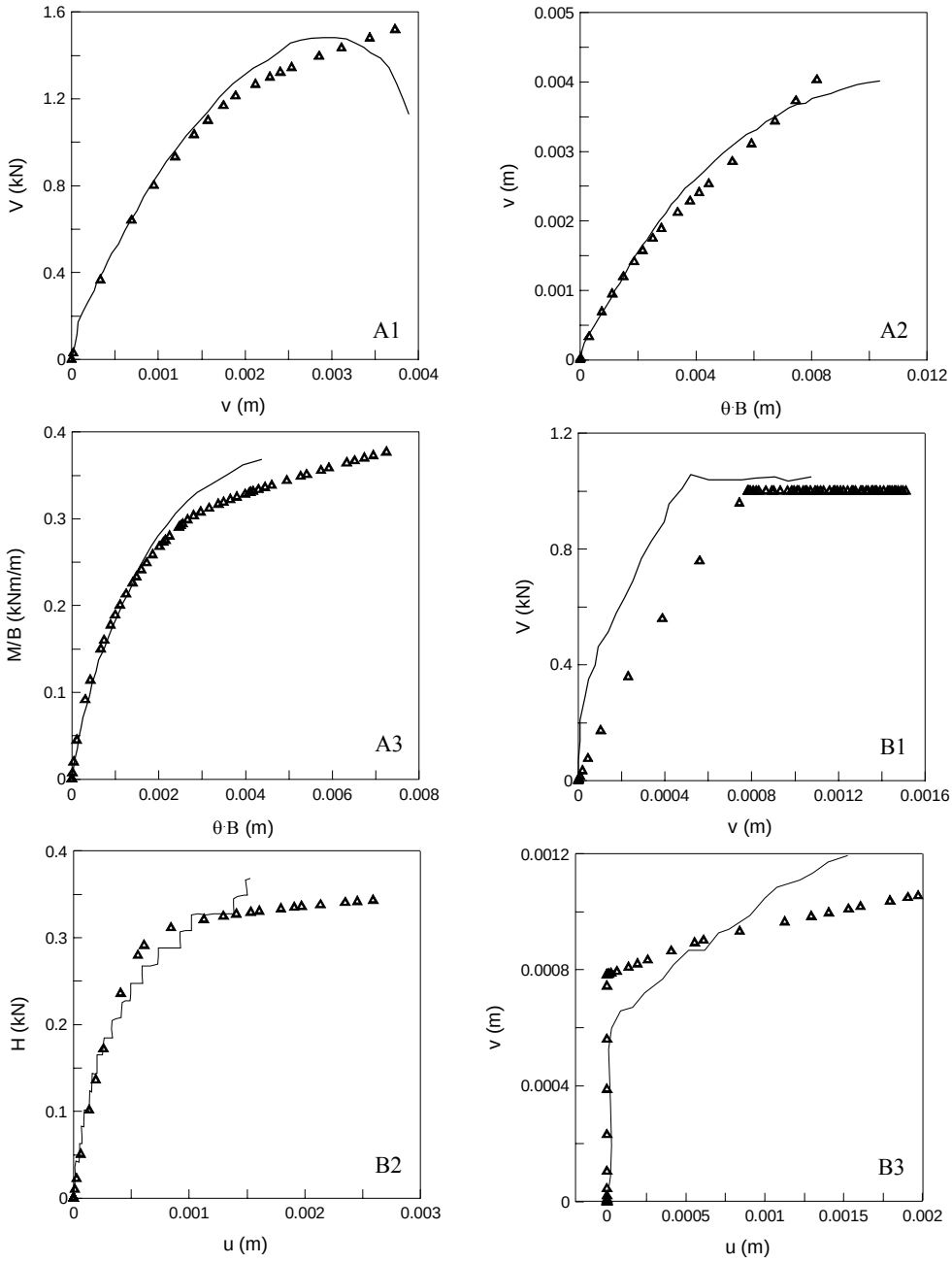

Fig. 4.36 EMC model, **a=2**. A1-A3: e/B=0.25 B1-B3: V100H.

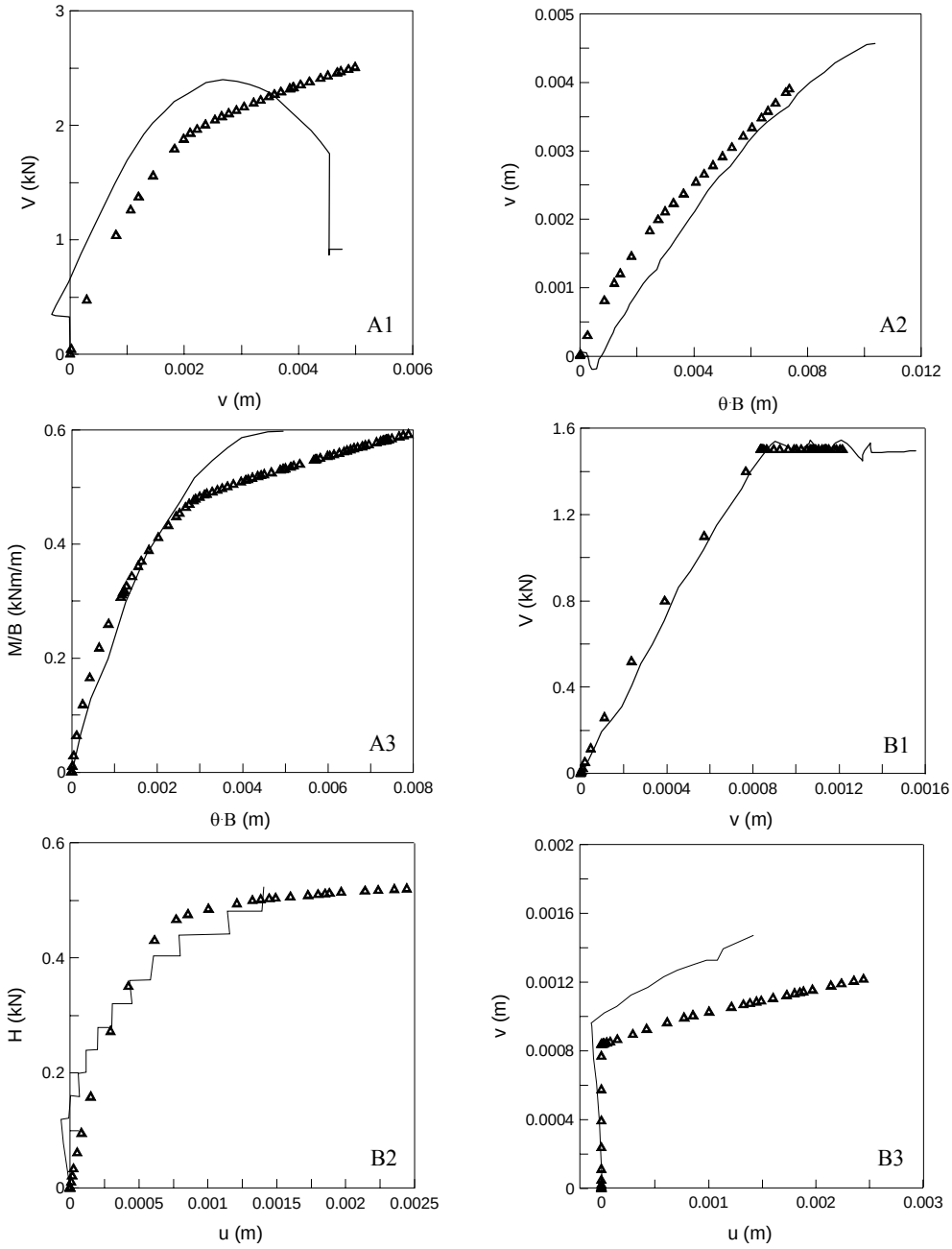

Fig. 4.37 EMC model, **a=3**. A1-A3: e/B=0.25 B1-B3: V150H.

It is worth noting how such results have already been discussed in the Sections focused on the specific tests, and they are here proposed again in order to have an overall idea of the effectiveness of the EMC model when modelling the different loading situations considered.

5 Conclusions

Since powerful computers have become accessible to the common user, a great interest has been devoted to the methods of resolution of engineering problems, and particularly to the finite element method (FEM).

The resolution of a boundary value problem through FE analyses requires the assumption of a constitutive model for the material involved. In particular, for the soil, many constitutive laws have been proposed in the past, starting from the original work of the Cambridge group which, in the '60s, developed the Cam-Clay model within the framework of elastoplasticity.

The constitutive models are often built aiming to model some laboratory tests following simple stress paths, like triaxial compression or extension and oedometric paths, but the best confirmation of the capability of a constitutive assumption to capture the behaviour of soils involved in a geotechnical construction comes from the comparison of the results of FE analyses with the measurements on real structures.

Among the classes of geotechnical engineering problems which are nowadays easily studied through FE analyses, the case of shallow foundations is one of greatest interest, since it involves very common structures relatively easily reproducible in laboratory tests in reduced or true scale, in order to assure the availability of a database of measurements useful for the validation of the models.

In this work a large series of laboratory tests on rigid shallow foundations on sand (Montrasio, 1994) has been used as "benchmark" for the evaluation of the predictive capabilities of the constitutive models considered: the Simplified Sinfonietta Classica (SSC) model, CLoE hypoplastic model, and the Extended Mohr Coulomb (EMC) model already embedded in the library of constitutive routines of ABAQUS, the FE code chosen for all the numerical analyses herein presented.

The numerical-experimental comparisons were carried out in terms of generalized forces (forces and moments) versus generalized displacements (settlement and rotations) instead of a stress/strain approach, in the light of the definition of a macro-element behaviour.

Due to the hypothesis of *rigid* footing, there is no need to choose a constitutive law for the metallic plate on which the loads were applied, thus allowing to focus on the effects of the constitutive assumptions for the soil. To model the footing, a *rigid link* element has been used.

For the SSC and CLoE models the implementation into the FE code was necessary and the two constitutive routines were developed using the Fortran code.

The theoretical validation of the constitutive models was already carried out by the respective Authors, even if the SSC differs from the original Sinfonietta Classica in some points, as widely explained in Chapter 1.

However, in this work the capability of the models to capture the behaviour of soils has been assumed *a priori*, at least for the stress paths typically followed in simple laboratory tests, and it has mainly been focused on the effectiveness and reliability of the implementations.

For the implementation of the SSC model, two different formulations have been proposed, both within the framework of *elastic predictor* and *plastic corrector*: the former formulation has been built in terms of stress components, the latter in terms of strains. The advantages in a formulation in terms of stresses are mainly in the easier formulation of the of the residual vector's derivatives required by Newton's algorithm, while with a formulation in terms of strains the computation of the consistent tangent operator is straightforward.

A simple axisymmetric test has been performed in order to evaluate the effectiveness of the two routines: provided that the results obtained are coincident, as expected, some important differences occur as far as the computational cost is concerned.

The formulation in terms of strain components and analytical construction of the consistent tangent operator, reveals to be more efficient than a formulation in terms of stress components in which a numerical approximation of the tangent operator is given.

The explicit algorithm used for the implementation of the CLoE model has not been subjected to performance tests since already used by other Authors for the implementation of the K-hypoplasticity (Fellin and Ostermann, 2002), but only some tests on the *basic stress paths* have been performed, in order to assess the reliability of the implementation.

Some simplifications have been imposed on the FE model reproducing the real situation of the laboratory tests: a plane strain condition model was built, and the hypothesis of a perfectly rough behaviour between the metallic plate and the soil was assumed.

The need of such simplification is due to the necessity of limiting the uncertainties of the model, since specific tests should be performed to properly determine the most suitable interface model and its parameters.

It is worth noting, however, that it has been widely demonstrated how such an assumption does not influence the analysis results, as regards contact pressures, if the eccentricity is less then 0.3 times the width of the foundation.

After the design of the FE model, with suitable boundary and initially geostatic conditions the calibration of the constitutive parameters via back-analysis on the basis of a simple centred vertical load test was carried out.

The analysis results obtained have shown strong limitations of the CLoE model in reproducing the experimental results, even if the calibration, based on a triaxial compression and extension tests, has given quite satisfactory results.

The shape of the obtained curves shows a monotonic upward orientation that is in contrast with the experimental measurements. Only in some particular cases, the shape of the numerical simulation roughly reproduces the experimental behaviour.

Such limitations should be explained carrying out a theoretical study on the formulation of the law, thus going beyond the scope of this work, which mainly focuses on the evaluation of the predictive capability of different constitutive models.

As far as the predictive capability of the SSC model is concerned, some good results are obtained: even if the limit load predicted through FE analysis is always underestimated with respect to the experimental one, the displacement prediction is almost always consistent with the measurements.

The simplified version of the original Sinfonietta Classica shows its major limitation in the prediction of the shape of the load displacements curves, since the concavity of the first part of the curves is directed upward, thus showing a prevailing elastic behaviour.

This fact is undoubtedly due to the value assumed for the initial value of the hardening parameter, which has been set to 5 kPa, a considerable value if compared to the confining pressures involved in the real problem.

Unfortunately, due to convergence problem in correspondence to a low confining pressure, the value of p_{c0} cannot be reduced without compromising the stability of the computations.

The problem could be solved by substituting the structure of the yield function and the plastic potential proposed by Nova with another formulation, as for instance the one suggested in (Lagioia et al., 1996), which has already been successfully used by many Authors.

Another improvement that would increase the efficiency of the proposed model, is the substitution of the hypoelastic form for the elastic behaviour, that could be conveniently replaced by hyperelasticity, for instance in the form proposed in (Borja et al., 1997) thus allowing to skip the integration of the elastic predictor. The elastic problem would be solved in closed form only knowing the elastic strain components by simple evaluation of an energy function.

These observation are the basis for a further development of the implementation and would permit the modelling of a cyclic behaviour of the soil thanks to the assumption of a free energy function.

The best predictions are obtained with the simplest EMC model: the results are quite satisfactory both from a qualitative and a quantitative point of view.

A wide set of tests has been performed, and the capability of the model to capture the experimental behaviour is clearly shown in Chapter 4.

Moreover, the influence on the reliability of the numerical analysis has been investigated by the editing of *isoerror maps*, in which the difference between numerical and experimental results is put in relation to the per cent amount of the measured limit load, the load inclination and the out-of-plane depth of the footing, thus allowing to conclude that the best performances of the model are achieved when the applied load is within a range far from the initial loading steps and the ultimate load.

In conclusion, the numerical-experimental comparisons are suggesting that the CLoE model, which has been proven to give satisfactory results when applied for the resolution of geotechnical engineering problems like deep excavations or tunnel excavations, shows strong limitations in the modelling of the relatively simple case of a shallow foundation.

Moreover, the identification of the parameters of the hypoplastic model in not straightforward, and requires, at least, a triaxial compression test, that is a routine laboratory test, but also a triaxial extension, which is decisively a less common test.

All these shortcomings raise some doubts on the practical applicability of such a model for the resolution of a simple geotechnical problem.

The SSC model gives better results, even still far from the experimental results, but the overall response can be considered as satisfactory, even taking into account the easy calibration of the constitutive parameters herein carried out through back-analysis, but that could be performed starting from the results of a triaxial compression and an oedometric test.

Among the three models chosen for the mechanical behaviour of the soil, the EMC model gives the best results. Despite its relatively simple mathematical structure, as compared with the other models chosen for the comparisons, the results are extremely good for almost all the tests reproduced via FE analyses.

The calibration test, a simple centred vertical load test, revealed the capability of the model of capturing the behaviour of the experimental model only by operating on the values of Young modulus E and the shear strength ϕ even if the important assumption of plane strain condition was chosen .

The reliability of the predictions was shown for inclined and eccentric load test for more complex loading paths as well, all giving a good agreement between computed and measured displacements and rotations.

References

ALLERSMA G. B. (2003) "Centrifuge research on bearing capacity of suction caissons." *FONDSUP*, Paris, 29-36.

BELLOTTI R., CRIPPA V., MORABITO P., PEDRONI S., BALDI G., FRETTI C., OSTRICATI D., GHIONNA V., JAMIOLKOWSKI M., and PASQUALINI E. (1985) "Laboratory validation of in situ tests." *AGI Jubilee Volume XI ICSMFE*, San Francisco.

BORJA R. I., LIN C.-H., and MONTANS F. J. (2001). "Cam-Clay plasticity, Part IV: Implicit integration of anisotropic bounding surface model with nonlinear hyperelasticity and ellipsoidal loading function." *Computer Methods in Applied Mechanics and Engineering*, 190, 3293-3323.

BORJA R. I., and TAMAGNINI C. (1998). "Cam-Clay plasticity Part III: Extension of the infinitesimal model to include finite strains." *Computer Methods in Applied Mechanics and Engineering*, 155, 73-95.

BORJA R. I., TAMAGNINI C., and AMOROSI A. (1997). "Coupling Plasticity and Energy-Conserving Elasticity. Models for Clays." *Journal of Geotechnical and Geoenvironmental Engineering*, 948-957.

BOUSSINESQ J. (1885). *Application des potentiels à l'étude de l'équilibre et du mouvement des solides élastiques*, Goutier-Villard, Paris.

BRINCH HANSEN J. (1967) "The philosophy of foundation design criteria safety factors and settlement limits." *Symposium on bearing capacity and settlement of foundations*, Duke University, 9-13.

BUTTERFIELD R., and GOTTARDI G. (2003) "Determination of yield curves for shallow foundations by "swipe" testing." *FONDSUP*, Paris, 111-118.

CHAMBON R., and DESRUES J. (1985) "Bifurcation par localisation et non linéarité incrémentale: un example heuristique d'analyse complète." *Plastic Instability*, Aussois, 101-113.

CHAMBON R., DESRUES J., HAMMAD W., and CHARLIER R. (1994). "CLoE, a new rate-type constitutive model for geomaterials: theoretical basis and implementation." *International Journal for Numerical and Analytical Methods in Geomechanics*, 18, 253-278.

CHAMBON R., DESRUES J., HAMMAD W., and CHARLIER R. (1995). "CLoE Consistance et Localisation Explicite, une loi incrémentale non lineaire."

CHAMBON R., DESRUES J., and TILLARD D. (1994) "Shear moduli identification versus experimental localisation data." *Localisation and Bifurcation Theory for Soils and Rocks*, Aussois, 101-111.

CHEN W.-F., and HAN D. J. (1988). *Plasticity for Structural Engineers*, Springer Verlag, New York.

COLOMBI A. (2005). "Physical modelling of an isolated pile in coarse grained soils," PhD thesis.

CREMER C., PECKER A., and DAVENNE L. (2001). "Cyclic macro-element for soil-structure interaction: material and geometrical non-linearities." *International journal for numerical and analytical methods in geomechanics*, 1257 - 1284.

CREMER C., PECKER A., and DAVENNE L. (2002). "Modelling of nonlinear dynamic behaviour of a shallow foundation with macro-element." *Journal of earthquake engineering*, 6(2), 175 - 211.

CUNDALL P. A., and STRACK O. D. L. (1979). "A discrete numerical model for granular assemblies." *Géotechnique*, 29(1), 47-65.

DESRUES J. (1984). "La localisation de la déformation dans le matériaux granulaires," PhD Thesis, Université de Grenoble.

DESRUES J. (2004). *Personal Communication.*

DESRUES J., and CHAMBON R. (1989). "Shear band analysis for granular materials: the question of incremental non linearity." *Ingénieur*, Archive 59, 187-196.

FELLIN W., and OSTERMANN A. (2002). "Consistent tangent operators for constitutive rate equations." *International Journal for Numerical and Analytical Methods in Geomechanics*, 26(1213-1233).

GUDEHUS. (1979) "A comparison of some constitutive laws for soils under radially symmetric loading and unloading." *3rd International Conference for Numerical Modelling in Geomechanics*, Aachen, 1309-1324.

HAIRER E., and WANNER G. (1991). *Solving Ordinary Differential Equations. II: Stiff and Differential-Algebraic Problems*, Berlin.

HIBBITT, KARLSSON, and SORENSEN. (2003). *ABAQUS Theory Manual*.

HJIAJ M., LYAMIN A. V., and SLOAN S. W. (2003) "Bearing capacity of a shallow foundation subjected to an eccentric load using numerical limit analysis." *FONDSUP*, Paris, 311 - 318.

KOLYMBAS D. (1991). "An outline of hypoplasticity." *Archives of Applied Mechanics*, 61, 143-151.

KOLYMBAS D., and WU W. (1993). "Introduction to hypoplasticity." Modern Approaches to Plasticity, Kolymbas, ed., Elsevier, 213-224.

LADE P. V. (1977). "Elasto-plastic stress–strain theory for cohesionless soil with curved yield surfaces." *International Journal for Solids and Structures*, 13, 1019-1035.

LAGIOIA R., PUZRIN A. M., and POTTS D. M. (1996). "A New Versatile Expression for Yield and Plastic Potential Surfaces." *Computers and Geotechnics*, 19(3), 171-191.

LAMBE T. W. (1973). "Prediction in soil engineering." *Géotechnique*, 23(2), 149-202.

LEONI M. (2004) "Two different strategies for the implementation of an elastoplastic constitutive model." *NUMOG IX*, Ottawa, 229-235.

LEONI M., MIRIANO C., TAMAGNINI C., and VIGGIANI G. (2003) "Ground movements induced by excavations in sand: a comparison between different hypoplastic models." *3X4 Workshop: Constitutive modelling and analysis of boundary value problems in geotechnical engineering*, Napoli, 375-412.

LEONI M., and MONTRASIO L. (2003) "A numerical investigation on shallow foundations on sand." *FONDSUP*, Paris, 335-344.

LOURENÇO P. B. (1995). "An orthotropic continuum model for the analysis of masonry structures." *TNO-95-NM-R0712*, University of Technology, Delft.

MÉNETREY P., and WILLAM K. J. (1995). "Triaxial failure criterion for concrete and its generalization." *ACI Structural Journal*, 92, 311-318.

MONTRASIO L. (1994). "Un metodo per il calcolo dei cedimenti di fondazioni su sabbia soggette a carichi eccentrici e inclinati," PhD thesis, Politecnico di Milano.

MONTRASIO L., and NOVA R. (1997). "Settlements of shallow foundations on sand: geometrical effects." *Géotechnique*, 47(1), 49-60.

NOVA R. (1977). "On the hardening of soils." *arch mech stos*, 29(3), 445-458.

NOVA R. (1988) ""Sinfonietta classica": an exercise on classical soil modelling." *Constitutive equations for granular non-cohesive soils*, Cleveland, 239-257.

NOVA R., CASTELLANZA R., and TAMAGNINI C. (2003). "A constitutive model for bonded geomaterials subject to mechanical and/or chemical degradation." *International Journal for Numerical and Analytical Methods in Geomechanics*, 27, 705-732.

NOVA R., and DI PRISCO C. (2003) "The macro-element concept and its application in geotechnical engineering." *FONDSUP*, Paris, 389 - 396.

POULOS H. G., and DAVIS E. H. (1974). *Elastic solution for soils and rock mechanics*, John Wiley & Sons, New-York.

SCHOFIELD A., and WROTH P. (1967). *Critical State Soil Mechanics*, Mc-Graw Hill, New York.

SIMO J. C., and GOVINDJEE S. (1986). "B-Stability and symmetry preserving return mapping algorithms for plasticity and viscoplasticity." *International Journal for Numerical Methods in Engineering*, 31, 151-176.

SIMO J. C., and HUGHES T. J. R. (1997). *Computational Inelasticity*, Springer Verlag, New York.

TAMAGNINI C., CASTELLANZA R., and NOVA R. (2002). "A Generalized Backward Euler algorithm for the numerical integration of an isotropic hardening elastoplastic model for mechanical and chemical degradation of bonded geomaterials." *International Journal for Numerical and Analytical Methods in Geomechanics*, 26, 963-1004.

TAMAGNINI C., CASTELLANZA R., and NOVA R. (2002). "Implicit integration of constitutive equations in computational plasticity." *Révue Française de Génie Civil*, 6, 1051-1067.

TAMAGNINI C., VIGGIANI G., and CHAMBON R. (2000). "A review of two different approaches to hypoplasticity." Constitutive Modelling of Granular Materials, Springer, Berlin.

TAMAGNINI C., VIGGIANI G., CHAMBON R., and DESRUES J. (2000). "Evaluation of different strategies for the integration of hypoplastic constitutive equations. application to the CLoE model." *Mechanics of Cohesive-Frictional Materials*, 5(4), 263-289.

TEJCHMAN J., and HERLE I. (1999). "A class "A" prediction of the bearing capacity of plane strain footings on sand." *Soils and Foundations*, 39(5), 47-60.

TERZAGHI K. (1943). *Theoretical soil mechanics*, John Wiley & Sons, New-York.

TRUESDELL C. A. (1956). "Hypo-elastic shear." *Journal of Applied Physics*, 27, 441-447.

VAN EEKELEN H. A. M. (1980). "Isotropic yield surfaces in three dimensions for use in soil mechanics." *International Journal for Numerical and Analytical Methods in Geomechanics*, 4, 98-101.

VESIC A. S. (1975). "Bearing capacity of shallow foundations." Foundation Engineering Handbook, Van Nostrand Reinhold Company, 121-147.

VIGGIANI G., and TAMAGNINI C. (2000). "Ground movements around excavations in granular soils: a few remarks on the influence of the constitutive assumptions on FE predictions." *Mechanics of Cohesive-Frictional Materials*, 5(5), 399-423.

WU W., and KOLYMBAS D. (1999). "Hypoplasticity then and now." Constitutive Modelling of Granular Materials, Springer, Berlin.

ZIENKIEVICZ O. C., and TAYLOR R. L. (2000). *The Finite Element Method (5th edition)*.